Quantifying morphologic changes of a coastal foredune using a low-cost remotely piloted aerial system (RPAS)

Julia G. Moloney

A thesis submitted in partial fulfilment of the degree of

Master of Science in Environmental Management

University of Otago, Dunedin, New Zealand

January 31st, 2017

Abstract

Mid-latitude sandy coasts are dynamic environments. Monitoring coastal morphodynamics is important for understanding the response of coasts to short-term storm events, for understanding the response of coasts to long-term environmental change, and for managing beach-dune systems. Remotely piloted aerial systems (RPAS) (or drones) present new opportunities for coastal monitoring. This type of platform is inexpensive, efficient, requires minimal expertise, and also provides high resolution aerial imagery. Photogrammetry can be used to derive digital surface models (DSMs) or digital terrain models (DTMs) from RPAS imagery.

This thesis assesses the efficacy of low-cost RPAS for describing the morphology and morphodynamics of coastal foredunes. The first objective is to compare DSMs produced by RPAS surveying with DTMs derived using conventional survey methods. Objective two assesses the accuracy and precision of RPAS surveying to quantify morphologic changes of a coastal foredune. The third objective is to examine the influence of vegetation on RPAS-derived DSMs.

Comparisons are made between total station, RTK-GPS, terrestrial laser scanner and RPAS surveys conducted on the St. Kilda beach foredune, Dunedin. The surveying methods are compared based on survey efficiency, cost, accuracy of the DTM/DSM, and their sensitivity to atmospheric and environmental limitations. RPAS photogrammetry is used to develop a time series of DSMs, which describe short-term patterns of sedimentation and morphological changes in the lee of this foredune. Vegetation surveys were conducted on the foredune at Mason Bay, Stewart Island, and the areas are classified as uniform and dense, variable, and sparse vegetation, or bare sand. Plots containing each class were surveyed with RPAS and RTK-GPS, to produce a DTM and a DSM that are compared to determine the elevation difference.

The RPAS survey was the most efficient method for developing DSMs, even when considering the set-up and data processing time (Objective 1). The RPAS produced the second most precise surface, with a RMSE of 8 cm. The RPAS is more sensitive to environmental and atmospheric conditions; however, this method is very rapid, and undesirable weather conditions can be avoided. The results show there is un-modelled systematic error in the DSM caused by lens distortion, which increases outside the GCP network – areas outside the network were not used for subsequent analysis.

Vegetation presence can prevent the derivation of accurate DTMs. The RPAS did not accurately quantify sand deposition due to the presence of vegetation (Objective 2). The sand dampened the vegetation, causing a decrease in elevation in the change model. The sensitivity of the RPAS to vegetation is insignificant in areas with bare or sparse vegetation, or when quantifying large-scale changes (for example, foredune erosion).

Vegetation height, vegetation cover/density, GSD, the structural properties of the plant, and the surface spectral properties, were identified as factors causing an elevational offset in the DSM (Objective 3). The elevation of the areas with bare sand were statistically equal in the DTM and DSM, however, the dense, variable and sparsely vegetated areas were statistically different. The elevation difference between the DSM and DTM is the largest in the densely vegetated areas (30 cm).

Low-cost RPAS are capable of achieving high-quality morphologic surveys of coastal foredunes. The method affords the advantages of efficiency and flexibility. However, due to the sensitivity of the method to vegetation, low-cost RGB RPAS are more suited to quantifying the morphology of bare sand or sparsely vegetated areas, quantifying large-scale changes, or for long-term morphologic monitoring. Low-cost RPAS are not capable of accurately quantifying small-scale changes in areas with dense vegetation. However, as RPAS platforms develop, it is expected that sensors capable of penetrating vegetation will become more accessible for low-cost platforms.

Acknowledgements

Firstly, I would like to thank my supervisors Mike and Pascal. Mike, thanks for all of the encouragement over the last two years, the challenges you've helped me overcome, and helping me through my inability to 'omit needless words'. Pascal, thanks for your patience through our four hour long meetings, and agreeing to co-supervise half-way through; your photogrammetry knowledge has made all the difference.

To my colleague, Tom. Even though there were times I wanted to push you off the top of the dune, I couldn't have gotten through the last couple of years without your help. Thanks for all of the support, the long hours spent conducting fieldwork, and for proof reading my work.

A massive thanks to all of my field assistants, who volunteered their own time to help collect my data; Claire, Dave, Louis, Alice, Ryan, and Adelaine, I really appreciate your hard work. Thanks to Sarah and Zoe from the surveying department for conducting the TLS surveys.

To Teresa, for the positive words, the support, and the inspiration to do a master's degree in the first place. To Chris, for all of the hours you've spent helping me with my GIS issues. To Scott, for your help with the drone, even though you crashed it on the first day.

Thank you to Alastair and Mike from the surveying department, for all of the equipment you let me borrow, answering all of my annoying surveying questions, and helping me salvage stuffed-up data. To Nigel and Dave from the geography department, thank you for the help with the gear, and putting up with our last minute fieldwork expeditions.

Thanks to Jeff from the Dunedin Model Aero Club, for your help gaining the Wings Badge. To the Dunedin City Council for allowing us to conduct our work at St. Kilda, and to the St. Kilda community (and the dogs on John Wilson Drive) for your interest and support in mine and Tom's projects.

To my office mates; Adelaine, Kenzie, and Seta. Thanks for the endless coffee breaks, the support, and for last-minute proof reading.

To Jamal, for all of your support, encouragement, and motivation to keep going. Thanks to Mum, Dad, Daniel and Bridget, for your kind words, and for supporting me through the last couple of years. A big thanks to Daniel for proof reading some of my work, I can only imagine how boring it must've been for you.

Table of Contents

List of Figures

List of Tables

List of Abbreviations

A. arenaria	*Ammophila arenaria*
ALS	Aerial laser scanner
ATC	Air traffic control
ATV	All-terrain vehicle
BBA	Bundle block adjustment
C. repens	*Coprosma repens*
CAA	Civil aviation authority
CASA	Civil aviation and safety authority
CI	Confidence intervals
DEM	Digital elevation model
DoD	DEM of difference
DSM	Digital surface model
ECS	Elevation change surface
EOPs	Exterior orientation parameters
EXIF	Exchangeable image file
FAA	Federal aviation administration
GIS	Geographic information systems
GNSS	Global navigation satellite system
GPS	Global positioning system
GRS80	Geodetic reference system 1980
GSD	Ground sampling distance
IDW	Inverse distance weighting
INS	Inertial navigation system
IOPs	Interior orientation parameters
L. arboreus	*Lupinus arboreus*
LiDAR	Light detection and ranging

LINZ	Land information New Zealand
LOOCV	Leave one out cross validation
ME	Mean error
MfNZ	Model flying New Zealand
MSL	Mean sea level
NDVI	Normalized difference vegetation index
NIR	Near infrared
NZD	New Zealand dollar
PD	Principal distance
PDOP	Position dilution of precision
PPA	Principal point of autocollimation
RGB	Red, green, blue
RMSE	Root mean square error
RPAS	Remotely piloted aerial system
RTK-GPS	Real time kinematic global positioning system
TBC	Trimble Business Centre
TLS	Terrestrial laser scanner
UAV	Unmanned aerial vehicle
VCS	Volumetric change surface

Chapter 1

Introduction

1.1 Introduction

Sandy coasts are dynamic environments and understanding the morphological characteristics of such systems is of interest to coastal geomorphologists (Saye *et al.*, 2005). Specifically, foredune morphology influences a number of coastal processes, including the exchange of sediment between the beach and hinterland environments (Hesp, 2002). Foredune morphology is determined by a number of factors such as sand supply, vegetation presence, vulnerability to erosion, and human interference (Hesp, 2002).

Monitoring morphologic changes in coastal foredunes is important for understanding trends in the response of coasts to environmental change, and aiding the management of beach-dune systems (O'Shea and Murphy, 2013). Short to medium term changes, over days, weeks and months, are typically caused by erosion and scarping, forced by storm events (Dissanayake *et al.*, 2015). Quantifying short-medium term changes, therefore, requires the ability to conduct short-notice and efficient surveys to capture event-scale changes.

Digital terrain models (DTMs) and digital surface models (DSMs) can be used to describe coastal morphologies (Papakonstantinou *et al.*, 2016). DTMs/DSMs are virtual 3D surfaces, created by interpolating point-based elevation data (Bhattacharya *et al.*, 2013). DTMs are surfaces that describe the ground topography; DSMs, are surfaces that describe the elevation of the visible surface (Whitehead and Hugenholtz, 2014), for example, the vegetation canopy. DTMs/DSMs can be used to describe the morphology of a dune system, and the temporal changes in elevation and volume (Mathew *et al.*, 2010).

DTMs/DSMs are derived from elevation surveys. Coastal surveys can be conducted by a range of methods, from traditional optical-based methods such as total stations (Castelle *et*

al., 2008), to laser-based methods (Feagin *et al.*, 2014), and more recently, photography collected by drone platforms (Gonçalves and Henriques, 2015). Each surveying method has advantages and disadvantages, however, there is often a trade-off between the survey cost, efficiency, and accuracy (Bangen *et al.*, 2014). The method used is also dependent on a number of factors; the size of the study area, topography, vegetation present, climate, resources available, skill level of the operator, purpose of the study, and the timeframe.

Aerial photography is one of the earliest methods, whereby elevation data is extracted from a series of overlapping photographs, using the process of photogrammetry. Aerial photographs can be collected from a number of platforms, such as satellites, piloted aircrafts, and more recently, 'remotely piloted aerial systems' (RPAS) (UAV or Unmanned Aerial Vehicles, or 'drones') (Remondino *et al.*, 2011). RPAS technology is useful for collecting aerial photographs because of their mobility, surveying efficiency, and quality of data. RPAS platforms have an advantage of flying at low-altitudes, which provides detailed imagery of the study area. A range of RPAS models are available. The cost of this technology ranges between < $1,000 to $100,000 NZD. Low-cost, off-the-shelf models require less expertise than high-cost RPAS, and have the potential to provide DSMs with sub-metre accuracy (Whitehead and Hugenholtz, 2014). The accessibility of low-cost RPAS, the potential for high accuracy data, and the efficiency of RPAS surveying, provides an opportunity for this technology to be used more widely in the coastal geomorphology field.

1.2 Monitoring foredune morphology

Coastal foredunes offer a range of ecological and social services on sandy coastlines where they adjoin metropolitan development (Taylor *et al.*, 2015). They are a natural coastal defence, protecting the hinterland from inundation and erosion (Bochev-van der Burgh *et al.*, 2011). Foredunes are one of the most seaward features of beach-dune systems, and consequently absorb direct wind and wave energy (Taylor *et al.*, 2015). They are especially important when anthropogenic features are located directly landward of the features (Taylor *et al.*, 2015). Due to the dynamic nature of sandy coasts, coastal managers routinely monitor coastal foredunes and beaches (Morton *et al.*, 1993).

Surveying foredune morphology, and quantifying morphologic changes can be useful for identifying trends and patterns, and hence aid in the management of such systems (Morton *et al.*, 1993; Saye *et al.*, 2005). Morphologic changes of coastal foredunes are indicative of other coastal processes, such as the establishment of vegetation in a dune system (Rozé and

Lemauviel, 2004); erosion caused by storm waves (Ierodiaconou *et al.*, 2016); or anthropogenic influences (Martinez *et al.*, 2006).

Historically, coastal morphology was described using aerial photography (Whitlow, 1986; Kidson *et al.*, 1989), or by surveying profiles across the dune with a dumpy level (Higgins, 1933; Thom and Hall, 1991). As technology has advanced, more methods are available for surveying coastal dune morphology. Total stations and real-time kinematic GPS (RTK-GPS) are useful ground-based instruments for surveying profile lines over foredunes (Castelle *et al.*, 2008; Armaroli *et al.*, 2013). Both methods can also be used to derive 3D digital elevation models of small areas. Light detection and ranging (LiDAR) is useful for large-scale surveys, and this technology can be mounted on either aerial or terrestrial platforms. RPAS is becoming more common for monitoring coastal morphology and feature mapping (Scarelli *et al.*, 2016; Papakonstantinou *et al.*, 2016).

1.3 Remotely piloted aerial systems (RPAS)

Remotely piloted aerial systems (RPAS) can provide low-level aerial photography and can also be equipped with different sensors (such as multi-spectral cameras or LiDAR) to survey morphology (Whitehead and Hugenholtz, 2014). RPAS are available in a range of models that have developed from kites and blimps, to multi-rotor and fixed-wing aircrafts (Aber *et al.*, 2010c). RPAS flights are generally restricted to altitudes lower than piloted aircrafts; in New Zealand, United Kingdom, Australia, and America, the maximum flying height for RPAS is 400 ft.

The components of an RPAS include the aircraft, the ground control station and the communication data link (Colomina and Molina, 2014). Typically, an aircraft includes the platform, a sensor, a Global Navigation Satellite System (GNSS) and an Inertial Navigation System (INS). RPAS can be equipped with different types of sensors, including, RGB cameras, hyperspectral cameras, multispectral cameras, LiDAR, and infrared sensors (Colomina and Molina, 2014). GNSS enables the aircraft to determine its location, so that coordinates of each image are recorded in the metadata. The INS is used to track the aircraft's orientation and velocity. The ground control station is the technology on the ground that controls the aircraft, i.e. the remote control (Colomina and Molina, 2014). The communication data link is the connection between the aircraft and ground control station, and ensures the operator is in control of the RPAS.

RPAS surveying employs photogrammetry; the process of obtaining accurate measurements of objects within imagery (Mikhail *et al.*, 2001). Prior to the evolution of RPAS, aerial photography was typically obtained by satellites and piloted aircrafts (Andrews *et al.*, 2002). However, recent advances in RPAS technology has made this type of technology less expensive and more accessible. RPAS surveying is efficient, and therefore, is useful for environmental research. RPAS technology is typically employed in coastal settings to survey morphology (Mathew *et al.*, 2010; Mancini *et al.*, 2013) and characterize vegetation (Dandois and Ellis, 2010; Li *et al.*, 2016). RPAS is considerably less expensive than conventional surveying methods, and requires less expertise.

Conducting accurate surveys of foredune morphology can be difficult with low-cost RPAS. Low-cost RPAS surveys generally employ an RGB (red, green, blue) digital camera. RGB cameras capture photographs in the visible spectrum, i.e. the colours the human eye can see, and hence, they cannot penetrate vegetation. Consequently, low-cost RPAS produce digital surface models, which depict the elevation of the top surface, and not necessarily the ground surface (Whitehead and Hugenholtz, 2014).

1.4 Study justification

Most coastal surveying methods are expensive and/or time consuming (Hugenholtz *et al.*, 2013). This is especially true when large areas are surveyed, or when the topography is steep and inconsistent. The purpose of this study is to evaluate the effectiveness and efficiency of a small RPAS in such circumstances. The RPAS used in this study is inexpensive ($2,000) compared to larger RPAS models, and does not require extensive training. Unlike total stations and GPS units, RPAS provides photographs in addition to elevation data. Imagery is useful for supplementing elevation and volumetric data. RPAS are developing constantly, and RPAS suitable for photogrammetry are becoming less expensive. If low-cost, off-the-shelf RPAS can be used to derive high accuracy morphological data, there is potential for this technology to be employed more widely for coastal geomorphology research, and by local authorities for monitoring and managing coastal environments.

1.5 Research aims and questions

The aim of this study is to assess the efficacy of low-cost RPAS for surveying coastal foredunes. The objectives are (i) to compare surveying with a low-cost RPAS to conventional coastal surveying methods (a total station, RTK-GPS, and terrestrial laser scanner); (ii) to

quantify elevation and volumetric changes in a coastal foredune in the short-medium term; and (iii) to assess the influence of vegetation on RPAS derived DSMs.

The research is based on field surveys conducted at St. Kilda beach, Dunedin and Mason Bay, Stewart Island, and data processing using photogrammetric and GIS. To complete this study, the following three research questions will be addressed:

1. How does the accuracy and cost of data collected by low-cost RPAS compare to other coastal surveying methods?
2. Can data recorded by a low-cost RPAS be used to quantify morphologic change in a coastal foredune?
3. To what degree, and how does vegetation affect the development of digital terrain models from RPAS photogrammetry?

1.6 Study sites

1.6.1 Introduction

The experiments described in this study involved coastal foredune surveys using RPAS and other methods at two locations in southern New Zealand. The two study sites are the St. Kilda beach foredune, Dunedin, and the Mason Bay foredune, Stewart Island (Figure 1.1). The St. Kilda foredune was selected because it provided an opportunity to evaluate sediment deposition in the lee of excavated notches designed for sediment transport. Therefore, morphologic changes in this area were expected, which provided an opportunity for the RPAS to quantify change. This foredune has also been eroded in the past, which indicated the possibility of quantifying erosion in this study.

Figure 1.1: The St. Kilda and Mason Bay study sites.

The Mason Bay foredune exhibits a variety of vegetation densities and cover, which provided an opportunity to test the ability of the RPAS for deriving a DTM of vegetated areas. This section will describe each study site in detail, and provide justification for conducting the study at the St. Kilda beach and Mason Bay.

1.6.2 St. Kilda beach, Dunedin

St. Kilda beach is located on the southern coast of the Otago Peninsula, approximately 45.9˚S, 170.5˚E. St. Kilda is characterized by a continuous, alongshore foredune, approximately 1 km long, 20 m wide, and 12 m high (above mean sea level). The foredune developed seaward of John Wilson Drive after the deliberate introduction of *Ammophila arenaria* (marram grass) (Figure 1.2a and b).

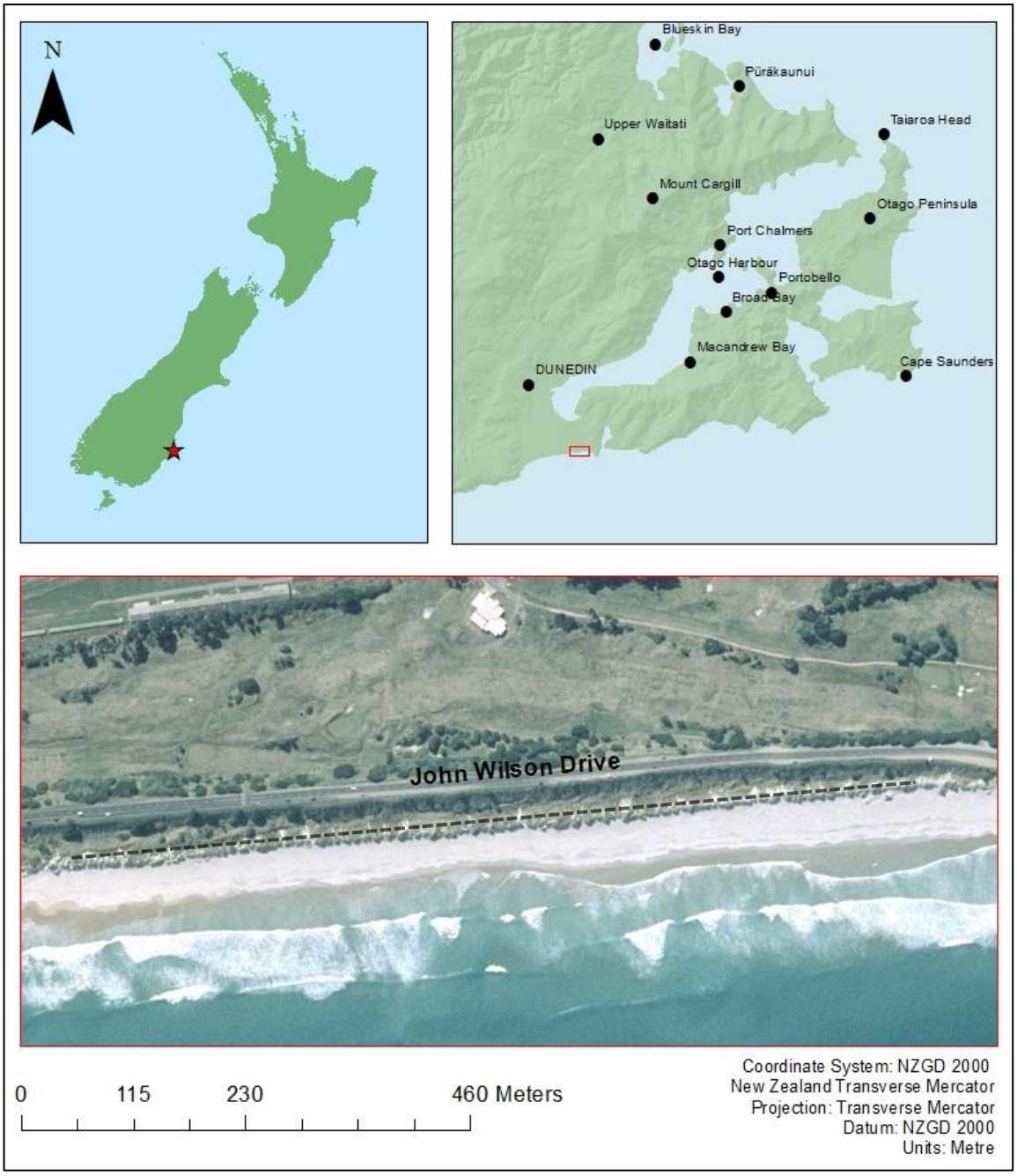

Figure 1.2a: St. Kilda beach and foredune, Dunedin, New Zealand. The black dotted line represents the foredune crest.

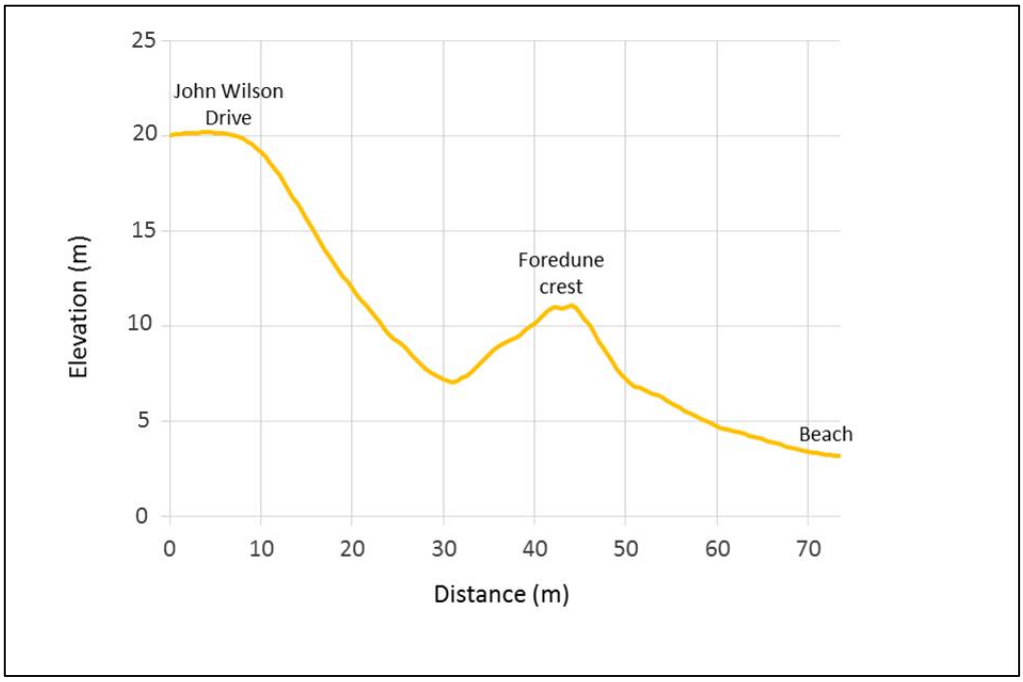

Figure 1.2b: A cross section of the St. Kilda, Dunedin foredune from John Wilson Drive to the beach. The elevation is measured in metres above the GRS80 ellipsoid.

The prevailing wind at St. Kilda is south-west (Figure 1.3), due to the orientation of the coast, this causes a pattern of alongshore sedimentation (Hilton, 2010). The north-westerly wind has a smaller effect on sediment movement as a result of the shelter provided by the Otago Peninsula.

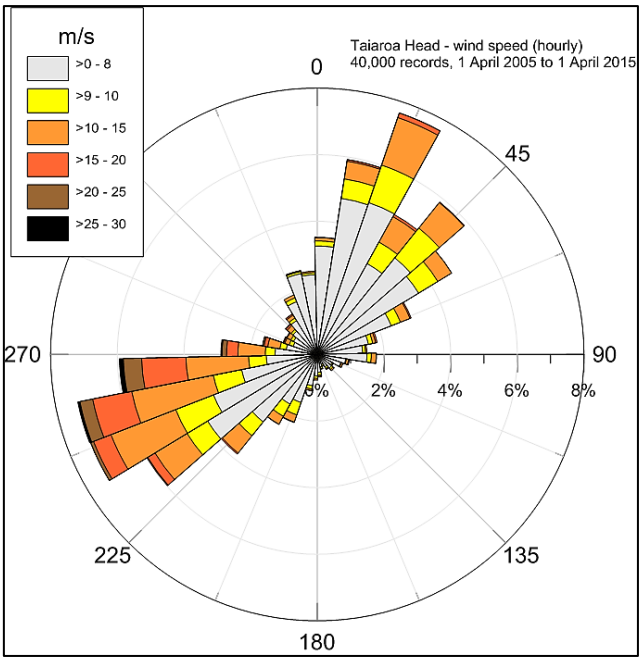

Figure 1.3: The wind rose for St. Kilda, Dunedin. Measurements are from Taiaroa Head on the Otago Peninsula (Hilton *et al.*, 2016).

This site was chosen because of the history of storm-induced erosion, and hence, the potential to quantify foredune erosion using the RPAS. The foredune has been scarped on a number of occasions; storm events in 1978 and 2009 caused erosion of John Wilson Drive, revealing the waste buried beneath. Prior to 2009, the foredune continued to accrete and prograde. However, between 2009 and 2014 the foredune growth as halted, and now remains at a relatively consistent height (Hilton *et al.*, 2016) (Figure 1.4).

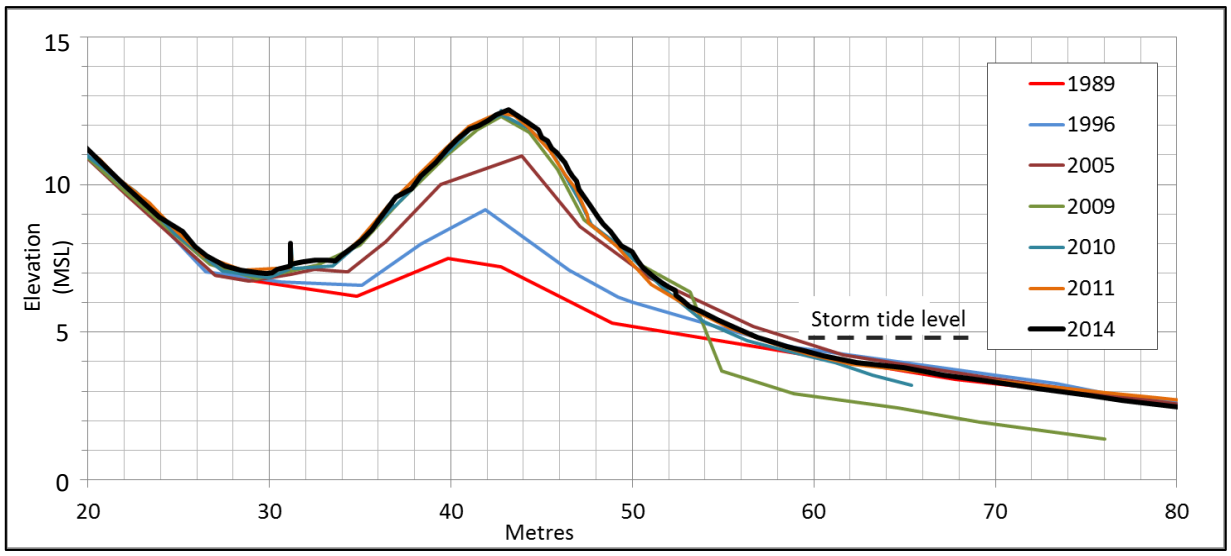

Figure 1.4: A time series of profiles line along *Section 17* on the St. Kilda foredune (Hilton, 2010).

The general field site (Area A) is a section of the St. Kilda foredune, approximately 400 m × 85 m. This site is divided into two subsections; Area B and Area C (Figure 1.5). Area B is approximately 85 m × 65 m and was selected for two main reasons. Firstly, St. Kilda is accessible, and was, therefore, suitable for the multiple surveys required to address Research Question One. Secondly, the site includes a variety of surfaces; areas of flat bare sand, areas with hummocky topography and sparse vegetation, steep topography, densely vegetated topography, and asphalt. Therefore, each surveying method could be tested on a variety of surface types and topography.

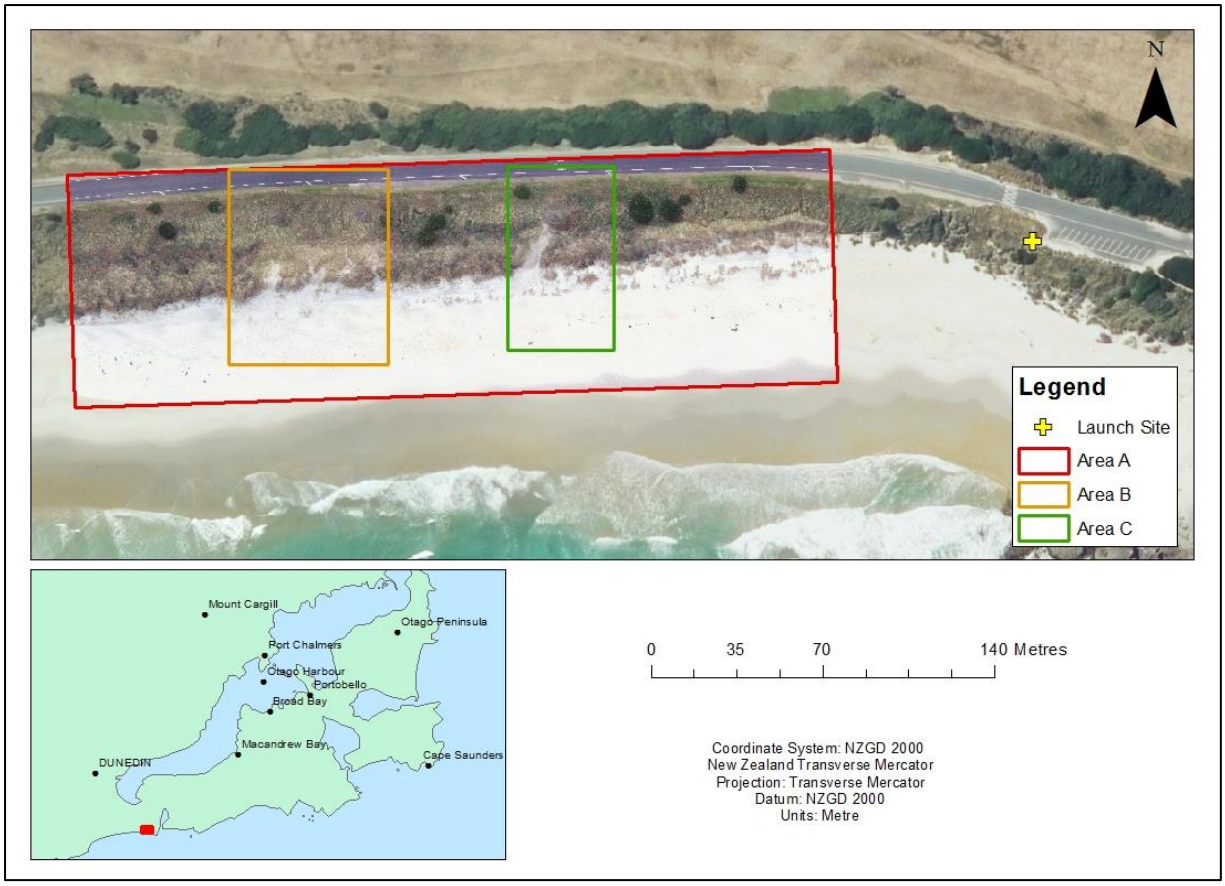

Figure 1.5: The St. Kilda beach study site, Dunedin – Area A, B and C.

Area A was initially selected to conduct the fieldwork for Research Question 2. Sections of this foredune have been eroded during storm events in the past, hence, this area was selected to capture any potential erosion or sand deposition that might occur during the study period. Research Question 2 was focussed on Area B and Area C which encompasses three constructed 'notches'. The relationship between the prevailing onshore winds and the morphology of the foredune provided an opportunity for another Masters' student's project. The aim of this project was to examine the effectiveness of 'notches' cut in the foredune to facilitate sediment transport and deposition behind the foredune (the area between the foredune and John Wilson Drive) (Figure 1.6). This project provided an opportunity to test the RPAS for quantifying changes in morphology due to storm events and manipulations in foredune morphology.

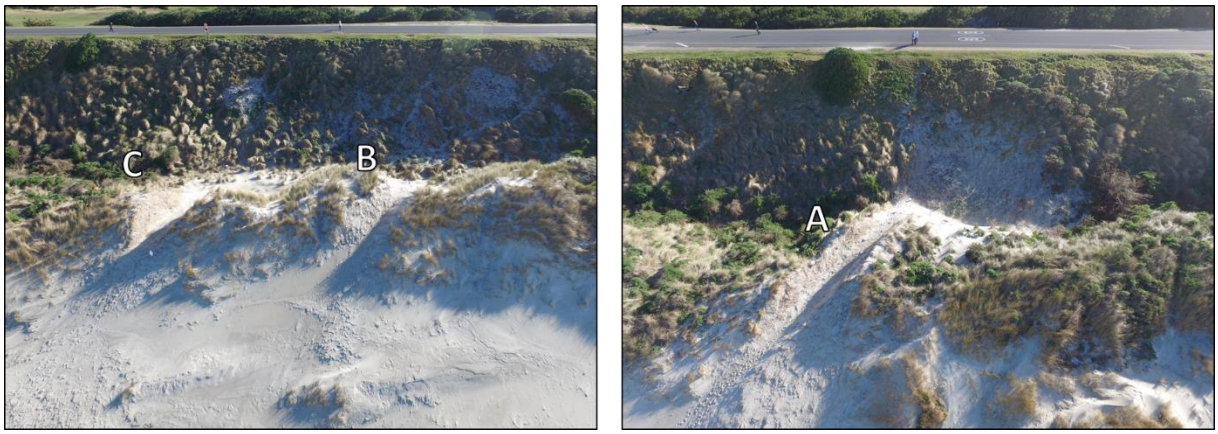

Figure 1.6: Aerial photographs of the three excavated notches (A, B and C) located at St. Kilda beach, Dunedin. Photographs captured on the 10th of September, 2016. Note: pedestrians for scale.

1.6.3 Mason Bay, Stewart Island

The fieldwork for the final research question was conducted on a section of the Mason Bay foredune, located on the west coast of Stewart Island, New Zealand. Mason Bay is a transgressive dune system located on the west coast of Stewart Island, New Zealand, at approximately 46.9˚S, 167.7˚E. The foredune is approximately 120 m wide and the dune system stretches approximately 3 km inland, in the direction of the prevailing westerly wind (Figure 1.7).

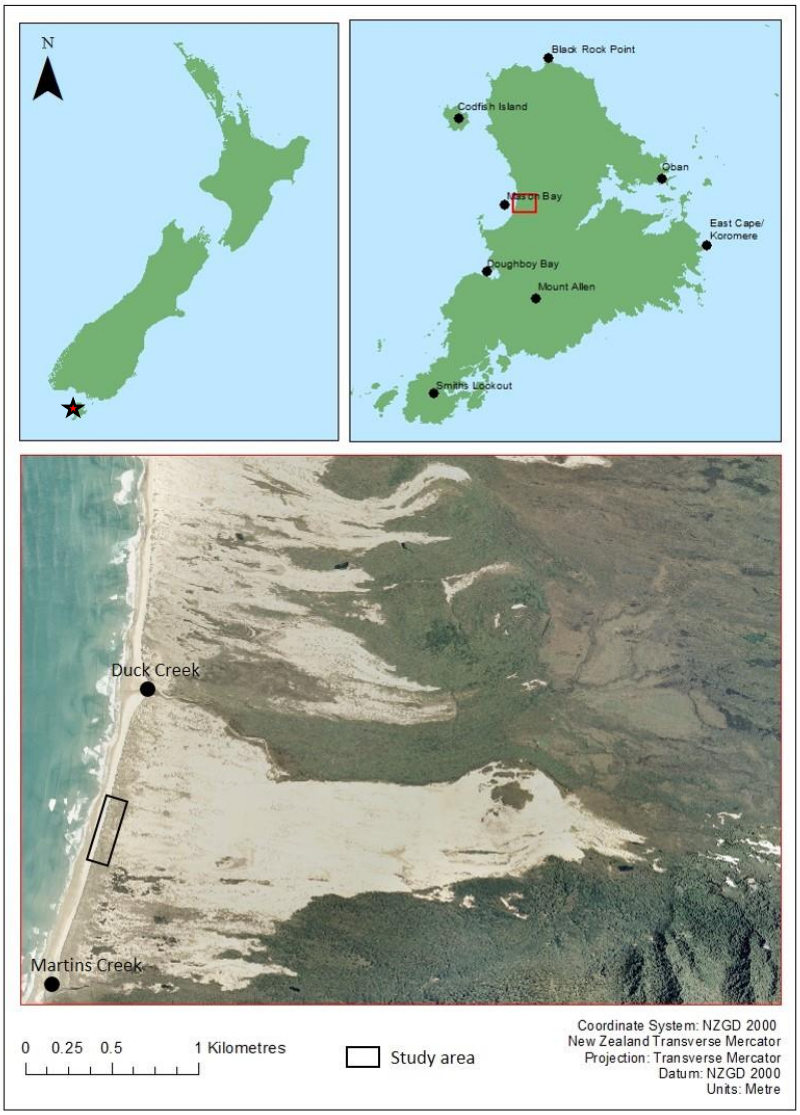

Figure 1.7: The northern and central (southern-most) sections of the Mason Bay dune system, Stewart Island, New Zealand.

Prior to the 1930s, the dune system consisted of native grass species such as *Ficinia spiralis* (pingao). *A. arenaria* was introduced to Kilbride sheep farm in the 1930s, at the southern end of Mason Bay, to stabilise the dune system (Hilton *et al.*, 2005). It subsequently spread by natural processes, eventually invading the northern sections of the bay. By 1989 it had established a large, continuous foredune between Martin and Duck Creeks. In 2001 the Department of Conservation began an *A. arenaria* eradication programme at Mason Bay to remove *A. arenaria* from the entire dune system (Hilton and Konlechner, 2010).

The eradication of *A. arenaria* has created variations in cover and density of the species. There is a clear boundary of the areas of the foredune that have been sprayed on one occasion (March, 2016), and the areas that have been sprayed on five occasions (Figure 1.8).

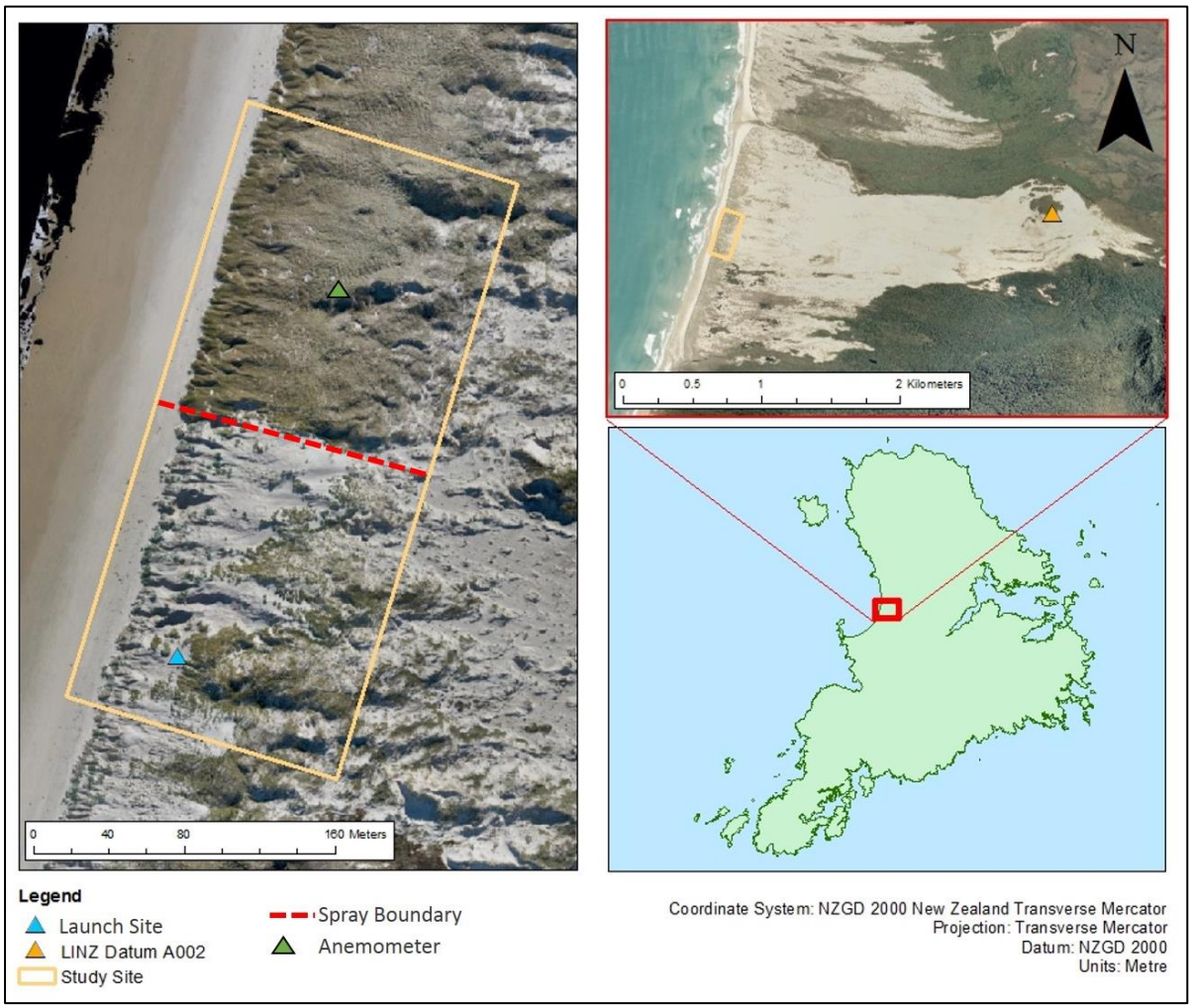

Figure 1.8: The Mason Bay study site. Photo source: Pascal Sirguey, 2014.

The Mason Bay foredune provided a good test for the ability of the RPAS to detect the ground surface through different vegetation covers and densities, to produce a DTM. The northern section of the study area primarily consists of thrifty *A. arenaria* densely covering the area. The southern section has a sparse vegetation cover, which is predominantly dead *A. arenaria*. The western section of the foredune has a more varied cover comprised of different dune species such as *Gentiana, Sonchus, Pimelea, Isolepis* and *Coprosma.*

1.7 Thesis structure

This thesis is divided into six chapters. Chapters 1 and 2 introduce the topic, and provide the research context for this study. Chapters 3, 4 and 5 address each of the three research question outlined in Section 1.3.

Chapter 2 describes and explains different coastal surveying methods, and the theory behind these methods. Specifically, a review of low-cost RPAS suitable for photogrammetry is conducted. The difference between digital terrain models and digital surface models is explained, as well as the relevance of such models for coastal geomorphology research. Lastly, the relationship between vegetation and deriving DTMs from RGB photography is explored.

Chapter 3 is focused on coastal surveying methods, to address Research Question 1. The purpose of this chapter is to compare conventional coastal surveying methods with a low-cost RPAS, and assess the differences between the methods. This chapter concludes with a discussion on the findings, and the advantages and disadvantages of employing low-cost RPAS surveying.

Chapter 4 examines the ability of a low-cost RPAS to quantify changes coastal foredune morphology using RPAS photogrammetry. This chapter assesses the accuracy of RPAS photogrammetry, and the insight gained from the accuracy assessment is used to minimalize the error associated with quantifying changes in foredune morphology. The downfalls of RPAS photogrammetry are discussed, in conjunction with the ability of the method to quantify morphologic changes.

Chapter 5 is dedicated to the third research question, and investigates the impact of vegetation on RPAS surveying. The role of vegetation height and cover is assessed. The surfaces produced by the RPAS are compared with surfaces produced by an RTK-GPS, over areas with different vegetation covers and densities, to determine the differences in elevation recorded by the methods.

The sixth and final chapter is a synthesis of the findings from this thesis. The key findings from each chapter are collated and discussed to address each research question. This chapter will end with the overall conclusions drawn from this thesis.

Chapter 2

Research context

2.1 Introduction

The topography of coastal dune systems can indicate processes (such as sedimentation, erosion and accretion) occurring within that environment (Zhou and Xie, 2009). Surveying and monitoring the topography of coastal landscapes can, therefore, provide an insight into these coastal processes. Surveys can be accomplished using a range of methods, including total stations (Eamer and Walker, 2013); GPS units (Armaroli *et al.*, 2013); aerial photography (Hugenholtz *et al.*, 2008); and laser scanners (Zhou and Xie, 2009). Historically, coastal morphology has been described with beach-dune profiles along established transects or with area based-surveys involving multiple x, y and z observations (El-Ashmawy, 2015). Recently, small, relatively cheap (compared to some traditional survey methods, such as total stations or RTK-GPS), off-the-shelf remotely piloted aircraft systems (RPAS) are available for surveying coastal environments (Aber *et al.*, 2010a).

Coastal surveys are used to create digital terrain models (DTMs) and digital surface models (DSMs) (Baptista *et al.*, 2011). DTMs/DSMs are raster representations of an area using elevation data (Bhattacharya *et al.*, 2013). DTMs/DSMs are used to represent the morphology of a landscape, to quantify temporal changes, to extract profiles, or to calculate sand volume (Mathew *et al.*, 2010). DTMs are created from elevation measurements of the ground, whereas DSMs are created from elevation measurements of the top surface (for example, the top of the vegetation canopy) (Whitehead and Hugenholtz, 2014).

Volumetric calculations are important for quantifying morphologic changes within dune systems (Eamer and Walker, 2013). This can be achieved by analysing DTMs/DSMs of the same area at different periods in time (Mathew *et al.*, 2010). Understanding the dynamic

storage of sand can give insight into the rate of change, and the potential causes for that change (Arbogast *et al.*, 2009). Morphologic changes can be influenced by a number of factors. For example, the formation of blowouts (gaps in a dune initiated by aeolian processes) can provide pathways for sediment transport from the beach to the hinterland, a result of changes in wind speed, wind direction, and vegetation cover (Gares and Nordstrom, 1995). A scarped face on the windward side of a foredune can indicate an erosional event (or series of events) (Dissanayake *et al.*, 2015). Accretion in the hinterland may suggest the establishment of sand-binding vegetation (such as *Ammophila arenaria*) in the backdune (Rozé and Lemauviel, 2004). Conversely, a loss of sediment in the hinterland could indicate establishment of vegetation on the foredune (Konlechner *et al.*, 2016).

Advances in surveying technology have provided affordable and relatively simple methods for collecting elevation data (Smith and Bryan, 2007). RPAS - also referred to as drones or unmanned aerial vehicles (UAVs) - are becoming more common in the coastal geomorphology field (Klemas, 2015). RPAS can be equipped with multiple sensors, providing a cheaper, low-altitude alternative to conventional aerial photography platforms (Pereira *et al.*, 2009). Typically, RPAS are equipped with cameras; the images are used within photogrammetry software to extract a point cloud, a DSM and/or orthomosaic (Remondino *et al.*, 2011).

As RPAS technology has evolved, specialised RPAS photogrammetry software has developed. There is a range of photogrammetry software available, including Pix4D Mapper, Agisoft Photoscan, Correlator3D, ERDAS Imagine UAV, Menci Software APS, Inpho UAS Master, MicMac, and OpenDroneMap. The aforementioned software have packages specific for processing RPAS photography. This type of software largely automates image processing to create DSMs and orthomosaics. Software prices are variable, and differ depending on the package and the supplier.

The modern photogrammetry method employed for processing RPAS imagery can produce systematic errors in the photogrammetric model, that are not quantified in the photogrammetry software (Sirguey *et al.*, 2016). Modern photogrammetry attempts to solve the sensor's interior orientation parameters (IOPs) and exterior orientations parameters (EOPs) simultaneously within a triangulation. In traditional photogrammetry, the IOPs were solved prior to conducting the triangulation, and only the EOPs were solved using triangulation. A study conducted by Sirguey *et al.* (2016) found that this process potentially creates systematic

errors in the output surface that are not reported by the photogrammetry software. Hence, the error reported by the software can be deceptive, and needs to be investigated further.

RPAS can capture low-altitude photographs and videos (Tahar *et al.*, 2012). This imagery presents coastal features in relatively high detail, for example, the high tide mark (Vousdoukas *et al.*, 2011). The photographs also provide a close-range birds-eye perspective, which can reveal aspects of features that cannot be seen from the ground (Kaneko and Nohara, 2014). This is useful for recognising the spatial relativity of features (Kaneko and Nohara, 2014). Capturing low-altitude photography is unique to this sort of platform, and can be advantageous over other platforms. Certain RPAS models (typically multi-rotors) allow the camera to be oriented at different angles in the vertical plane. Low-altitude oblique photographs can be captured, providing a unique perspective and breadth of view. This is especially useful when assessing the details of the landscape after a survey has taken place.

The aim of this chapter is to provide the research context of this thesis. The structure of this chapter is based on the three research questions described in Chapter 1, and will examine the theory behind each question. This chapter begins by investigating the methods currently employed to survey coastal dune systems, their associated limitations and introduce RPAS surveying. Issues associated with "modern" photogrammetry will be discussed. The use of DTMs/DSMs for monitoring and quantifying changes in coastal dune systems will be explained. Lastly, the influence of vegetation on RPAS derived DSMs will be explored.

2.2 Coastal surveying methods

Researchers have surveyed coasts using total stations (Castelle *et al.*, 2008), GPS (conventional and real-time kinematic) (Morton *et al.*, 1993; Pardo-Pascual *et al.*, 2005), laser scanners (aerial and terrestrial platforms) (Hilary *et al.*, 2002; Feagin *et al.*, 2014), and aerial imagery (Mathew *et al.*, 2010).The cost and availability of technology largely influences which method is used, however, the timeframe, the desired accuracy, the skill level of the operator, survey area, vegetation, topography and climate also need to be considered.

This section will assess coastal surveying using total stations, RTK-GPS, laser scanners, and aerial photography for producing DTMs/DSMs, and the associated limitations. DTM/DSM accuracy is dependent on the density and accuracy of points collected by the surveying instrument (Gallay *et al.*, 2013). It is, therefore, important to understand the efficiency (the rate of point acquisition) and accuracy of each surveying method.

2.2.1 Total stations

Total stations are a laser-based surveying method, comprised of an electronic theodolite and an electronic distance meter (High, 2006). A total station emits a laser aimed at a target (usually a prism, unless the total station is 'reflectorless') which reflects the laser back to the total station (Nelson *et al.*, 2009). The time it takes for the laser to return to the total station determines the distance between the target and the total station. The total station stores this data, and calculates the elevation and coordinates of the point using trigonometry (Nelson *et al.*, 2009). The data can then be uploaded into software to interpolate points and create a DTM (El-Ashmawy, 2015). This type of surveying requires a minimum of two people – one to operate the total station and the other to hold the reflector (unless the total station is 'reflectorless') (El-Ashmawy, 2015).

In the coastal context, total stations are generally used to establish ground control points (GCPs) (for example, Danzi *et al.*, 2012; Darwin *et al.*, 2014), or to produce profiles lines (for example, Castelle *et al.*, 2008), due to the potential for millimetre accuracy (Nelson *et al.*, 2009). A dense point cloud is required to produce an accurate DTM (El-Ashmawy, 2015), especially for areas with hummocky topography. Total station surveys over large areas can be time consuming, and hence inefficient for surveying a dense array of points (Baily *et al.*, 2003). On the other hand, smaller areas, with relatively consistent topography can be efficiently surveyed with a total station, and provide high accuracy data suitable for producing DTMs.

Although some surveying methods are generally more efficient than others, the duration of the survey is largely dependent on the terrain. Bangen *et al.* (2014) compared surveying methods in rivers and streams. The total station survey recorded points at a rate of 176 points/hour, whereas the RTK-GPS survey of the same area collected 336 points/hour. These results are not necessarily representative of surveying with these two methods. Theoretically, surveying with a total station might be slower than an RTK-GPS, due to the repositioning of the total station telescope after each point is taken. This is typically true over areas with undulating terrain, however, over flat terrain it is possible that the movement of the total station prism takes less time than recording a point with an RTK-GPS (depending on the "occupation time" of the RTK-GPS).

2.2.2 Real-time kinematic global positioning system

Real-time kinematic GPS (RTK-GPS) is a point-based, high accuracy GPS surveying method, often used for coastal surveys. RTK-GPS consists of a static receiver (the base station), a moving receiver (the rover), and a communication device (for example, a radio or cell phone) that connects the rover and base station (Pardo-Pascual *et al.*, 2005).The base station is established over a point with known coordinates, and receives constant location information from satellites in the vicinity. As the roving receiver moves, it receives information via radio communication with the base station; the location of the point is determined, and corrected for atmospheric errors (Pardo-Pascual *et al.*, 2005). RTK-GPS surveys can be operated by one person – an advantage in some situations. RTK-GPS is often used for beach profiles (Armaroli *et al.*, 2013) and surveying ground control points (Gonçalves and Henriques, 2015), but the data provided is also useful for creating DTMs (Harley *et al.*, 2011).

Theuerkauf and Rodriguez (2012) and Bangen *et al.* (2014) found surveying with RTK-GPS more efficient than surveying with a total station. This is possibly because after a point is recorded by the total station and the prism is moved to a new location, the telescope has to be refocussed on the new prism position. In situations where the total station does not have line-of-sight to the entire study area, the total station is moved and set-up at a different location. When the RTK-GPS records a point, the rover is held over the point for a certain amount of time (the "occupation time"), and then moved to the next point without altering any of the equipment. The longer the "occupation time" the more accurate the point (Stewart and Rizos, 2002). The RTK-GPS can also be an advantage because it can record points directly into a coordinate system, based on the point that the base station is set up over. To orientate a total station survey, the coordinates of at least two points are required.

In a study conducted by Harley *et al.* (2011), an RTK-GPS was mounted onto an all-terrain vehicle (ATV) to collect point coordinates on a 3.6 km long beach. 10,000 points were collected over eight hours. However, mounting the RTK-GPS to an ATV has some limitations; the ATV was limited to areas with flat topography, and the ATV is subject to sinking, tilting and shaking in the sand, which influenced the point accuracy.

The accuracy of points recorded by an RTK-GPS unit is largely dependent on the Position Dilution of Precision (PDOP) value (Lemmon and Gerdan, 1999). The PDOP value represents the geometry of satellites in the area (Han *et al.*, 2014). Ideally, satellites are spread

widely and evenly across the sky in the given area, which provides certainty of the measurements recorded (Lemmon and Gerdan, 1999) (Figure 2.1).

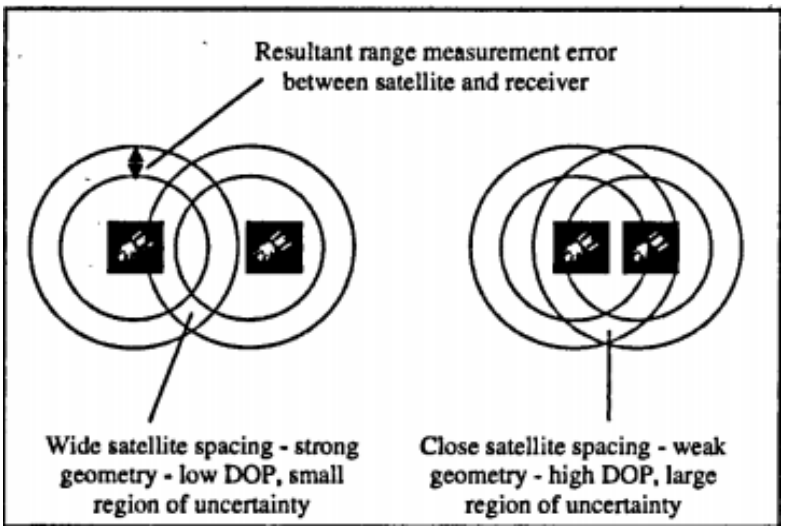

Figure 2.1: PDOP geometry, as explained by (Lemmon and Gerdan, 1999).

When there are more satellites, with an even spread across the sky, the PDOP value is small, and the position estimates are more reliable (Lemmon and Gerdan, 1999). According to Langley (1998), a PDOP value of 2 or less and more than eight satellites is optimal. The receivers must have a direct view of the satellites, without obstruction of the GPS signal (Teng and Wang, 2016).

2.2.3 Laser Scanning

Laser scanners are one of the most efficient methods for collecting point data over large areas (Bangen *et al.*, 2014). Laser scanning is frequently referred to as LiDAR (light detection and ranging) (Gallay *et al.*, 2013). Laser sensors can be mounted onto different platforms and may be either terrestrial or aerial (El-Ashmawy, 2015). The instrument emits a laser pulse, and uses the time it takes for the pulse to reach the surface feature and return to the scanner to calculate x, y, and z point data (Feagin *et al.*, 2014). The angle scanned in the vertical and horizontal plane varies between models. GCPs need to be established prior to the survey to geo-reference the laser scanned data (Bangen *et al.*, 2014).

The scan collects a high density of points, and can provide sub-metre to millimetre accuracy (Gallay *et al.*, 2013), suitable for producing DSMs. However, the high density of points slows the data processing (Gonçalves and Henriques, 2015). Unlike total stations and

RTK-GPS surveys, laser scanners tend to collect unwanted points (i.e. the scanner collects surface data from areas that are not intended to be surveyed, for example, the ocean) (El-Ashmawy, 2015). Unwanted/incorrect points can slow post-processing (Gallay *et al.*, 2013), as the points have to be removed from the dataset (El-Ashmawy, 2015) and the interpolation repeated. Another limitation is that the scans require line-of-sight; if the ground is not visible from the scanner, the top surface will be recorded (Liu, 2011). Therefore, scans in densely vegetated areas will not retrieve the ground elevation (Liu, 2011). However, ground filtering algorithms can be employed to convert the DSM to a DTM (Shaad *et al.*, 2016). Ground filtering algorithms differentiate between 'ground' and 'non-ground' areas, using only the areas identified as 'ground' for the interpolation. However, this type of algorithm can only be employed where bare ground is visible, and therefore, is not appropriate in densely vegetated areas.

Terrestrial laser scanners (TLS) are ground-based. TLS can be used statically, or can be mounted onto a vehicle and data can be collected in motion (Park *et al.*, 2011; Feagin *et al.*, 2014). One of the main limitations of laser scanning is that the scan is limited by line of sight (Hugenholtz *et al.*, 2013) (Figure 2.2). Steep and inconsistent topography can prevent the laser from reaching some areas (Gallay *et al.*, 2013), and as a result the TLS has to be moved and set-up multiple times to ensure all required surfaces are recorded (Nagihara *et al.*, 2004).

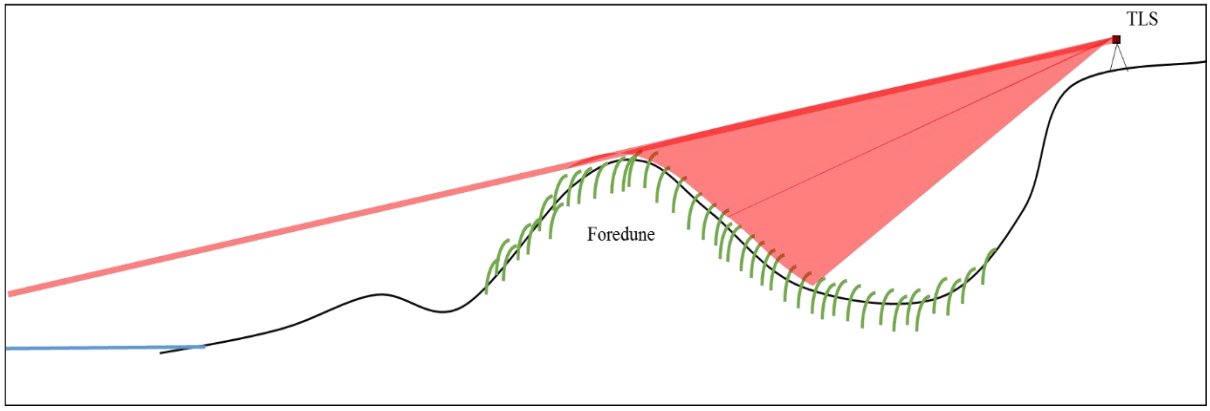

Figure 2.2: Schematic of TLS line-of-sight.

Aerial laser scanners (ALS) are suited to large-scale surveys (Hilary *et al.*, 2002; Liu, 2011). ALS is an efficient method that can survey large areas with sub-metre accuracy (Liu, 2011). A pilot is required to conduct the survey, which has advantages and disadvantages. The main advantage is that virtually no fieldwork is required by the researcher; the disadvantage is

that ALS surveys via piloted aircrafts are expensive – depending on the size of the survey, the topography and post-processing required, a single survey can cost tens of thousands of dollars (Bangen *et al.*, 2014). If a small survey is required, or if the survey needs to be repeated frequently, ALS can be economically unviable. Recent developments in RPAS platforms incorporate laser scanning attachments, which are less expensive than conventional ALS surveys (Wallace *et al.*, 2012).

2.2.4 Aerial photography and photogrammetry

Introduction

Aerial photography was established in the 19th Century, and has been continually developed since (Aber *et al.*, 2010a). This method is widely used for coastal research (for example, Kidson *et al.*, 1989; Hugenholtz *et al.*, 2008; Noernberg *et al.*, 2010; Yang *et al.*, 2010). Historic aerial photographs can be used to observe long-term temporal changes in coastal morphology, for example, Mathew *et al.* (2010) quantified morphological changes of the Greenwich Dunes from aerial photography between 1936 and 2005.

The establishment of Google Earth™ has provided a wider range of people access to free aerial imagery (Lisle, 2006). Aerial photography can be geo-referenced in GIS software using GCPs (Linder, 2009). In terms of coastal research, GIS software can be used to derive geographic information, for example, estimating shoreline position (Li *et al.*, 2003), mapping vegetation cover (Konlechner *et al.*, 2015; Li *et al.*, 2016), and identifying particular features from aerial photography (Hugenholtz *et al.*, 2013). Images of the same area at different periods in time can be used to observe temporal changes in beach and dune form (Mathew *et al.*, 2010). Aerial photographs (both vertical and oblique) can also be used to obtain elevation data using the process of photogrammetry (Linder, 2009).

Photogrammetry is the process of obtaining measurements of features and objects using photographs (Mikhail *et al.*, 2001). More specifically, this can be achieved by analysing multiple overlapping photographs of the same feature or area, known as stereo-paired images (Mikhail *et al.*, 2001). This works by creating depth based on the separate views of the left and right eyes (Egels and Kasser, 2003). Photographs of the same scene must, therefore, be taken from slightly different positions to recreate the separate images the human eye would see (Figure 2.3).

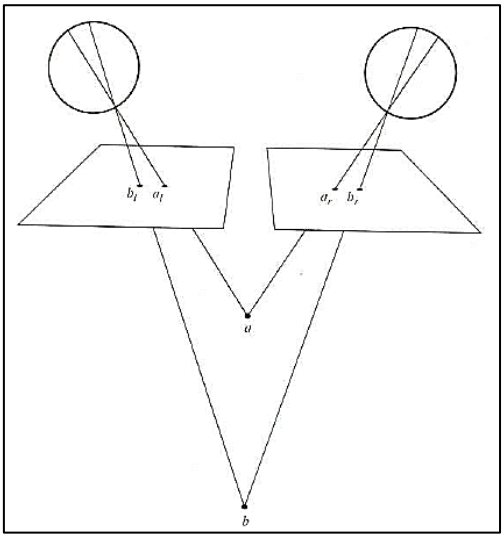

Figure 2.3*:* Height perception of each eye from stereo viewing of overlapping photos (Mikhail *et al.*, 2001).

Image overlap is important, as common points between subsequent photographs are used to link the images together. The sequence of overlapping images is required to create a photogrammetric model, whereby the relative position of the images to each other, and the surface is determined through triangulation. Traditional aerial photography required photographs to be taken at close intervals, to ensure a minimum 60% forward overlap and 30% side overlap of subsequent images and hence, full coverage of the survey area (Figure 2.4) (Linder, 2009).

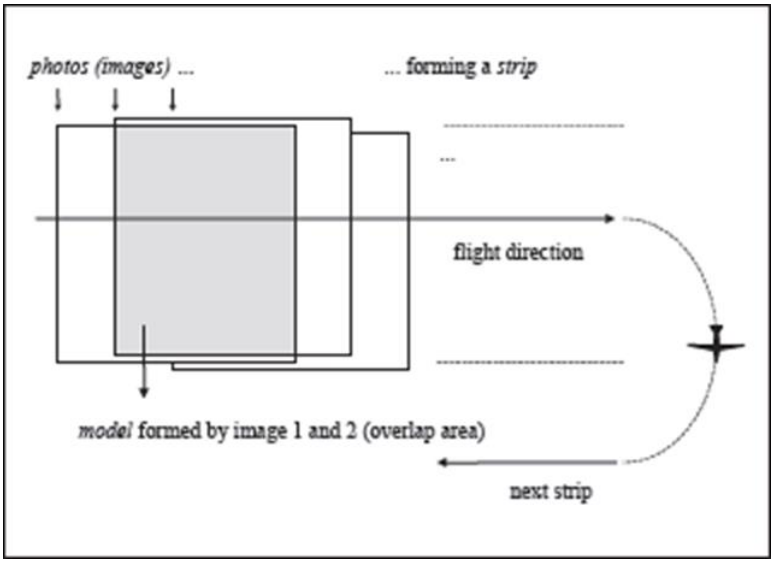

Figure 2.4: Image acquisition via a series of overlapping aerial photographs (Linder, 2009).

Modern photogrammetry automates the image matching process, and less images are required to produce a photogrammetric model. The remainder of this subsection will explain the theory behind photogrammetric modelling using vertical (nadir) aerial photography.

Interior orientation parameters

The process of positioning and orientating images into object space involves solving two sets of unknown parameters, referred to as the interior orientation parameters (IOPs) and the exterior orientation parameters (EOPs). The IOPs characterize the sensor and are described as the focal length of the lens, the principal point of autocollimation (PPA), and the image distortion caused by the lens. The PPA is a point on the image plane that is intersected by a perpendicular line from the perspective centre based on the optical axis of the camera (Mikhail *et al.*, 2001). The distance between the PPA and the perspective centre is called the principal distance (PD). The PD is equal to the focal length when the lens is focussed at infinity. The infinity focus prevents the "zoom" from being used, hence, the focal length and PD remain constant between the photographs, and a consistent image geometry is maintained. This is important for reducing the distortion in the resulting photogrammetric model (Sanz-Ablanedo *et al.*, 2012).

Lens distortion refers to the discrepancy of the projection of an object onto an image caused by the lens (Chari and Veeraraghavan, 2014). Two of the main distortion types are radial and tangential distortion. Radial distortion is the distortion caused by imperfections in the camera lens, causing the image projection to deviate from the rectilinear projection (Chari and Veeraraghavan, 2014). This deviation is radial, and distorts the object symmetrically from the centre of the lens (Weng *et al.*, 1992). Radial distortion can be further described as either barrel, pincushion or unbalanced distortion (Mikhail *et al.*, 2001). Barrel distortion (Figure 2.5) is characterised by magnification in the centre of the image, which decreases the further from the image centre (Chari and Veeraraghavan, 2014). Pincushion distortion (Figure 2.5) is when the image centre is compressed, and the outside of the image is enlarged (Chari and Veeraraghavan, 2014). Unbalanced distortion has attributes of both pincushion and barrel distortion, and has a distortion curve with both negative and positive values (Mikhail *et al.*, 2001).

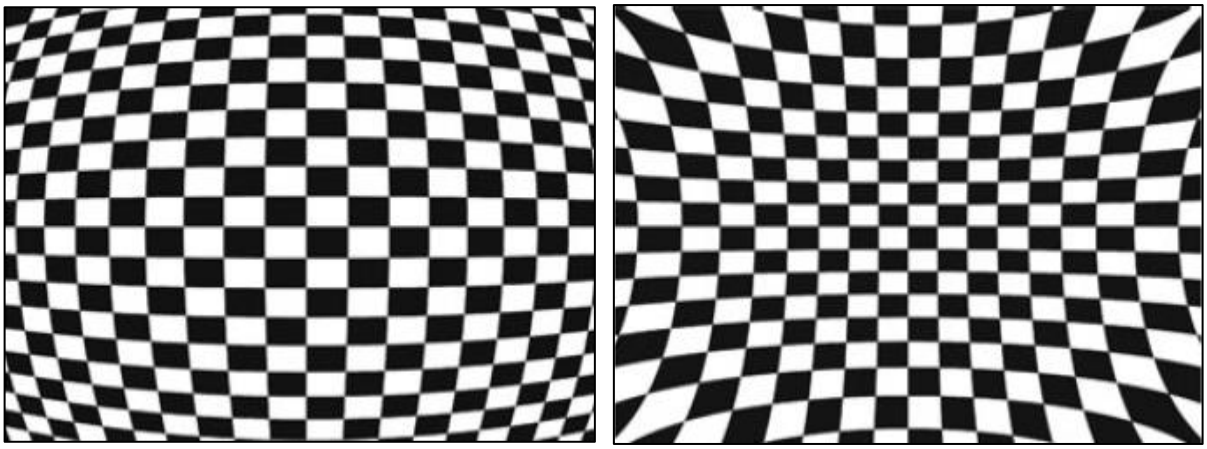

Figure 2.5: a) A visualisation of barrel (negative) distortion; b) A visualisation of pincushion (positive) distortion (Chari and Veeraraghavan, 2014).

Radial distortion from the image centre can be quantified using the Brown (1966) distortion model:

$$\Delta r = K1r^3 + K2r^5 + K3r^7, \quad (2.1)$$

where Δr is the amount of distortion, *K1*, *K2*, and *K3* are the radial distortion coefficients, and r is the radial distance. The radial distortion can be graphed against the radial distance to produce a distortion curve (Schenk, 1999). The distortion curve describes the type of distortion (Figure 2.6).

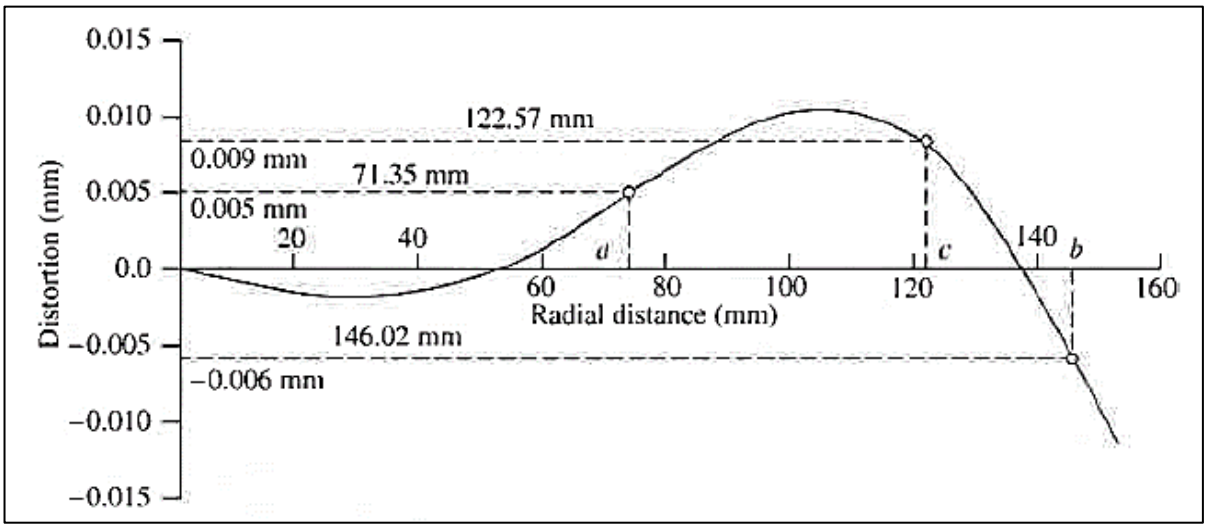

Figure 2.6: An example of a lens distortion curve (Mikhail *et al.*, 2001). The line represents the distortion along different radial distances from the image centre.

Tangential distortion is caused by imperfect centring of the elements forming the camera lens (Mikhail *et al.*, 2001). In particular, tangential distortion is common in cameras

with an adjustable focus/zoom (Mikhail *et al.*, 2001). This distortion can be reduced by using a lens that is focussed at infinity (the lens is at a fixed focus and the zoom cannot be used).

Exterior orientation parameters

The EOPs determine the position and orientation of the bundle of rays (the combination of image rays corresponding to the same perspective centre) relative to the object space coordinate system (Figure 2.7).

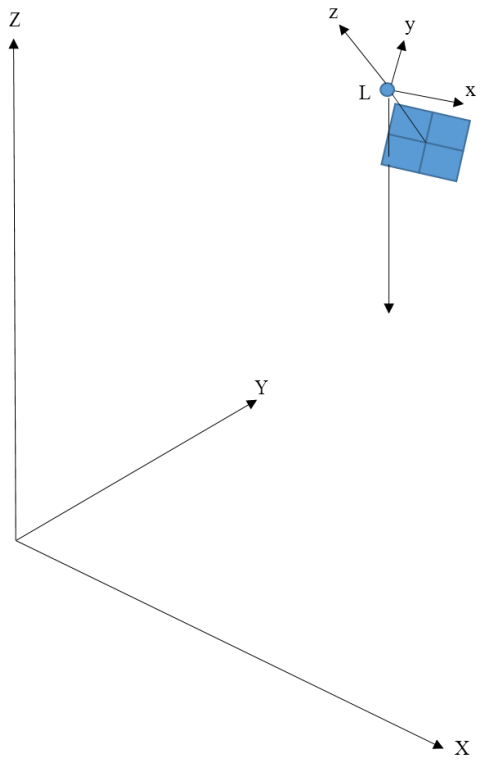

Figure 2.7: Object (X, Y, Z) and image (x, y, z) space coordinate systems, where L is the perspective centre (Mikhail *et al.*, 2001).

The coordinates of the perspective centre (L) are described by equation 2.2:

$$L = \begin{bmatrix} X_L \\ Y_L \\ Z_L \end{bmatrix} \tag{2.2}$$

The relationship between the object and image space coordinate systems is described as:

$$\begin{bmatrix} x \\ y \\ -f \end{bmatrix} = km \begin{bmatrix} X & - & X_L \\ Y & - & Y_L \\ Z & - & Z_L \end{bmatrix}, \tag{2.3}$$

where x, y and $-f$ are the image space coordinates, k is the scale factor, m ($M\omega M\phi M\kappa$) (2.4) is the rotation matrix transforming the object-space coordinate system to the image space (2.5), X, Y, and Z are the object space coordinates, and L is the perspective centre. Each bundle is positioned and oriented based on six parameters; x, y, z (the position of the optical centre), ω (x-axis rotation), ϕ (y-axis rotation), and κ (z-axis rotation).

$$M_\omega = \begin{bmatrix} 1 & 0 & 0 \\ 0 & \cos\omega & \sin\omega \\ 0 & -\sin\omega & \cos\omega \end{bmatrix}$$

$$M_\phi = \begin{bmatrix} \cos\phi & 0 & -\sin\phi \\ 0 & 1 & 0 \\ \sin\phi & 0 & \cos\phi \end{bmatrix} \qquad (2.4)$$

$$M\kappa = \begin{bmatrix} \cos\kappa & \sin\kappa & 0 \\ -\sin\kappa & \cos\kappa & 0 \\ 0 & 0 & 1 \end{bmatrix}$$

$$m = \begin{bmatrix} \cos\phi\cos\kappa & \cos\omega\sin\kappa + \sin\omega\sin\phi\cos\kappa & \sin\omega\sin\kappa - \cos\omega\sin\phi\cos\kappa \\ -\cos\phi\sin\kappa & \cos\omega\cos\kappa - \sin\omega\sin\phi\sin\kappa & \sin\omega\cos\kappa + \cos\omega\sin\phi\sin\kappa \\ \sin\phi & -\sin\omega\cos\phi & \cos\omega\cos\phi \end{bmatrix} \qquad (2.5)$$

The exterior orientation employs GCPs to orientate the images (Gonçalves and Henriques, 2015). GCPs are features within the study site that have known coordinates and elevations (Schiefer and Gilbert, 2007; Diefenbach *et al.*, 2012). Often GCPs are man-made features such as buildings or road markings, however, these features are not always present. Alternatively, new GCPs can be established prior to the collection of aerial photographs (Gonçalves and Henriques, 2015). For single surveys, temporary GCPs can be put in place, such as ground targets with a recognizable photographic pattern. The number and configuration of GCPs is important for accurate geo-referencing (Linder, 2009). The number of GCPs used depends on the sensor, the sensor resolution, (the ground sampling distance (GSD)), the area surveyed, the desired accuracy, and the method of collection (Toutin and Chénier, 2004). GCPs should be evenly distributed throughout the study area, which can be achieved by placing them in a triangular formation (Linder, 2009). The precision of GCPs largely depends on the GSD. When the GSD is smaller (i.e. the image has a higher resolution), it is important that the GCPs are surveyed with high precision (Toutin and Chénier, 2004). High precision GCPs are often surveyed using a total station or RTK-GPS unit (for example, Danzi *et al.*, 2012; Hugenholtz

et al., 2013; Casella *et al.*, 2014; Darwin *et al.*, 2014; Gonçalves and Henriques, 2015). A larger GSD does not require high precision GCPs because the target cannot be resolved in images with a low resolution.

Bundle block adjustment

Each image is the record of a bundle of image rays which connect points in object space with the corresponding point in image space, based on the perspective centre (Mikhail *et al.*, 2001). A bundle block adjustment (BBA) is a triangulation method used to position and orientate all bundles concurrently in a BBA. The BBA solves a system of collinearity equations relating the object space coordinates to image coordinates that involve interior and exterior parameters:

$$x = -f \frac{m_1(X-X_L) + m_2(Y-Y_L) + m_3(Z-Z_L)}{m_7(X-X_L) + m_8(Y-Y_L) + m_9(Z-Z_L)} \tag{2.6}$$

$$y = -f \frac{m_4(X-X_L) + m_5(Y-Y_L) + m_6(Z-Z_L)}{m_7(X-X_L) + m_8(Y-Y_L) + m_9(Z-Z_L)}, \tag{2.7}$$

Traditional photogrammetry only requires the BBA to solve the EOPs, as the IOPs are usually calibrated separately (Sirguey *et al.*, 2016). Hence, the triangulation is more suited to find the optimal solution. Conversely, modern photogrammetry consists of easily accessible, low-cost sensors that require self-calibration of the sensor. The self-calibration includes the IOPs in the BBA, along with the EOPs. As a result, the BBA has to solve for a greater number of unknown parameters. This makes it difficult for the triangulation to find the optimal solution, and hence creates errors in the photogrammetric model.

A study conducted by Sirguey *et al.* (2016) investigated this issue by comparing the BBA in two different photogrammetry software, and the influence of different GCP configurations. The study found discrepancies in the EOPs produced from the BBA, indicative of a suboptimal solution. The results suggest systematic distortion in the photogrammetric model outside of the confines of the GCP network. Hence, the suggested root mean square error of the model reported by the software should not be considered as normally distributed, in particular outside of the ground control network.

There has been a range of coastal research that has used RPAS sensors for photogrammetric modelling without investigating the potentially suboptimal solution of the IOPs and EOPs determined by the BBA (Delacourt *et al.*, 2009; Casella *et al.*, 2014; Gonçalves and Henriques, 2015). Therefore, the amount of un-modelled error in the photogrammetric

model needs to be investigated prior to drawing conclusions on the morphology presented by the model.

Aerial photography platforms

Aerial photography can be captured via a range of platforms (Figure 2.8). Satellite imagery is one of the most common forms of aerial photography (Andrews *et al.*, 2002). Photographs from multiple time periods are readily available on Google Earth™, and can easily be transferred into GIS software (Andrews *et al.*, 2002). However, the user lacks control over the timing and resolution of imagery from such sources.

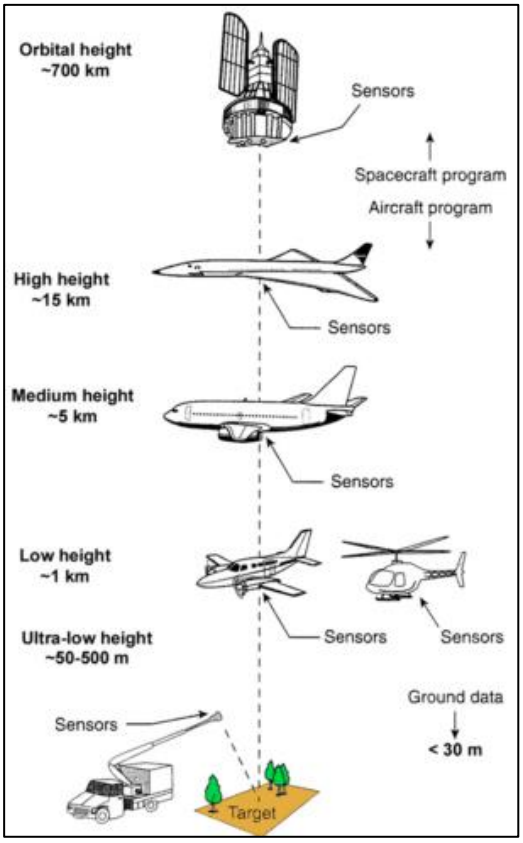

Figure 2.8: Schematic from Aber *et al.* (2010a) showing the different altitude classes for aerial photography platforms.

Aerial photography platforms within the Earth's atmosphere, can be categorised as either high-medium altitude, or low – ultra-low altitude. High-medium altitude aircrafts such as fixed-wing planes and helicopters are frequently used for large-scale surveys (Aber *et al.*, 2010c). This type of survey requires a pilot, which reduces the flexibility of surveys, and increases the cost (Aber *et al.*, 2010c). Cloud cover and shadows can cause issues for

photographs taken from satellite and high-altitude aircrafts (Aber *et al.*, 2010b). Such features can obscure the image, making analysis more difficult (Aber *et al.*, 2010b). Low-altitude platforms such as RPAS, are a cost-efficient alternative that can overcome these issues (Tahar *et al.*, 2012; Hugenholtz *et al.*, 2013).

RPAS are smaller than conventional platforms and are controlled from the ground (Hugenholtz *et al.*, 2013). Recreational RPAS flights are generally restricted to low altitudes, to avoid piloted traffic. In New Zealand, Australia, the USA, and the UK, the maximum flying height is 400 ft. above ground level (CASA, 2002; CAA, 2015; CAA, 2016; FAA, 2016). Flight regulations vary between countries, but the main restrictions are similar. A summary of some of the main regulations in New Zealand, Australia, the USA and the UK are outlined in Table 2.1.

Table 2.1: *Comparison of the main RPAS flight regulations in New Zealand, Australia, the USA, and the UK.*

	NZ Civil Aviation Authority	Australia Civil Aviation Safety Authority	USA Federal Aviation Administration	UK Civil Aviation Authority
Maximum flying altitude	400ft	400ft	400ft	400ft
Minimum distance from aerodromes	4 km	5.5 km	8 km	Not in areas with air traffic during the aerodrome's specified hours
Distance from operator	Direct line-of-sight	Direct line-of-sight	Direct line-of-sight	Direct line-of-sight
Flying over people	Only with permission	Only with permission	Only with permission	Unspecified
Flying at night	Not permitted	Not permitted	Not permitted	Unspecified

Low-altitude platforms can capture imagery with high spatial detail, suitable for small-scale feature mapping (Gonçalves and Henriques, 2015). RPAS platforms range from kites, to balloons, helicopters (including multirotor aircrafts), and fixed-wing planes (Aber *et al.*, 2010c). The price of an RPAS varies from $100 to over $100,000. The maximum flying time

ranges from 10–90 minutes for multi-rotor copters, to between 15–120 minutes for larger fixed-wing RPAS (Colomina and Molina, 2014). RPAS are typically equipped with a digital camera, with at least a ~12 mega pixel resolution, and video capabilities. However, the camera can be changed if a higher pixel resolution is required. Table 2.2 compares a range of RPAS available at the time of this study.

Table 2.2: *A comparison of RPAS available at the time of this study. The price corresponds to the cost of the aircraft with a RGB camera.*

RPAS	Type	Approx. Price (NZD)	Max. Flight Time (mins)	Take-off Weight (kg)	Available Sensors
DJI Phantom-3 Advanced	Quadcopter	$1,400	23	1.28	RGB 12.4 MP
DJI Phantom-4	Quadcopter	$2,200	28	1.38	RGB 12.4 MP
DJI Inspire 1 Pro	Quadcopter	$12,200	18	2.94	RGB 12.4 MP
Yuneec Typhoon H	Hexacopter	$1,299	25	1.95	RGB 12.4 MP
Quest UAV Q-Pod	Fixed-wing	$38,000	30-90	3.8-5	RGB 24.3 MP, NDVI, thermal, multispectral
Trimble UX5	Fixed-wing	$65,000	50	2.5	RGB 36 MP, NIR, multispectral
Sensefly eBee	Fixed-wing	$34,000	45	0.7	RGB 16 MP, NIR, multispectral, thermal
MAVinci Sirius Pro	Fixed-wing	$70,000	50	2.7	RGB 16 MP NIR
Vapor 55	Helicopter	$100,000	60	16	RGB, infrared, multispectral, LiDAR
Scout B1-100	Helicopter	Unspecified	90	18	RGB, LiDAR, hyperspectral

The type of RPAS employed depends on the characteristics of the survey (the type of sensor required and the size of the survey area) (Everaerts, 2008). RPAS vary in size; larger RPAS are generally >25 kg and are used commercially, smaller RPAS are more commonly used for research and recreational purposes (Klemas, 2015). Small RPAS are typically favoured due to the low cost (Klemas, 2015) and because larger, fixed wing RPAS generally

require more flying expertise (Aber *et al.*, 2010c). Fewer, small, off-the-shelf RPAS have been used for coastal research, such as Vousdoukas *et al.* (2011); Darwin *et al.* (2014); and Gonçalves and Henriques (2015). Off-the-shelf models can cost less than $10,000, and do not require a professional pilot. Small RPAS are limited by their instability in strong winds (depending on the model; smaller RPAS may only withstand up to 10 km/hr, larger models up to 25 km/hr) (Gonçalves and Henriques, 2015). Small RPAS also require minimum flight planning, and can be flown at short-notice (for example, directly after a storm), allowing for efficient survey repeatability. Certain RPAS can be equipped with LiDAR sensors, multispectral and hyperspectral cameras (Table 2.2), however, this substantially increases the price (Klemas, 2015). If low-cost RGB RPAS can provide data with comparable precision and accuracy to conventional surveying methods, then there is potential for them to be used more widely for coastal geomorphology (Gonçalves and Henriques, 2015).

2.2.5 Summary

A range of surveying methods and platforms exist for coastal surveying. Each method has advantages and disadvantages, which generally depend on the constraints of the survey. There is often a trade-off between the efficiency, accuracy, and cost of the survey. RPAS challenges this trade-off. RPAS platforms are becoming cheaper and more accessible for coastal research. RPAS have the potential to produce high-accuracy surface models for coastal research, however, the un-modelled errors caused by the self-calibration of the sensor need to be explored further.

2.3 Digital elevation models

Digital elevation models (DEMs) are representations of a surface, derived from elevation data (Bhattacharya *et al.*, 2013). DEMs can be described further as digital terrain models (DTMs) and digital surface models (DSMs). The former describes the elevation of the ground, and the latter describes the elevation of highest surface. Elevation models can be derived via spatial interpolation. An interpolation is conducted on a point cloud using GIS software, which uses the points to estimate the elevation of the unknown areas (Gallay *et al.*, 2013). The resulting product is a raster surface (i.e. a DTM or DSM) where all cells have an estimated elevation.

There are a range of point interpolations methods available (for example; nearest neighbour, kriging, spline, inverse distance weighting, and natural neighbour), and the method

used depends on the point distribution, and the purpose of the output surface. The suitability of a point interpolation method is determined by the sampling density, variations in the data, and the sampling method (Li and Heap, 2008). The interpolation method selected becomes more important when the sampling density is smaller (Li and Heap, 2008).

The density of the points influences the accuracy of the resulting DTM (Gallay *et al.*, 2013). The elevation assigned to any cell in the output surface is based on the elevation of the surrounding known points. Hence, to ensure variations in topography are captured by the interpolation, points need to be recorded where there is a change in elevation. For example, in Figure 2.9, to create a surface model that sufficiently describes the morphology of the dune, elevation points should be taken at the top and bottom of each slope, as well as at the high and low elevation points. The accuracy of the DTM/DSM is also influenced by the accuracy of the points in the imported dataset (Eamer and Walker, 2013; Gallay *et al.*, 2013).

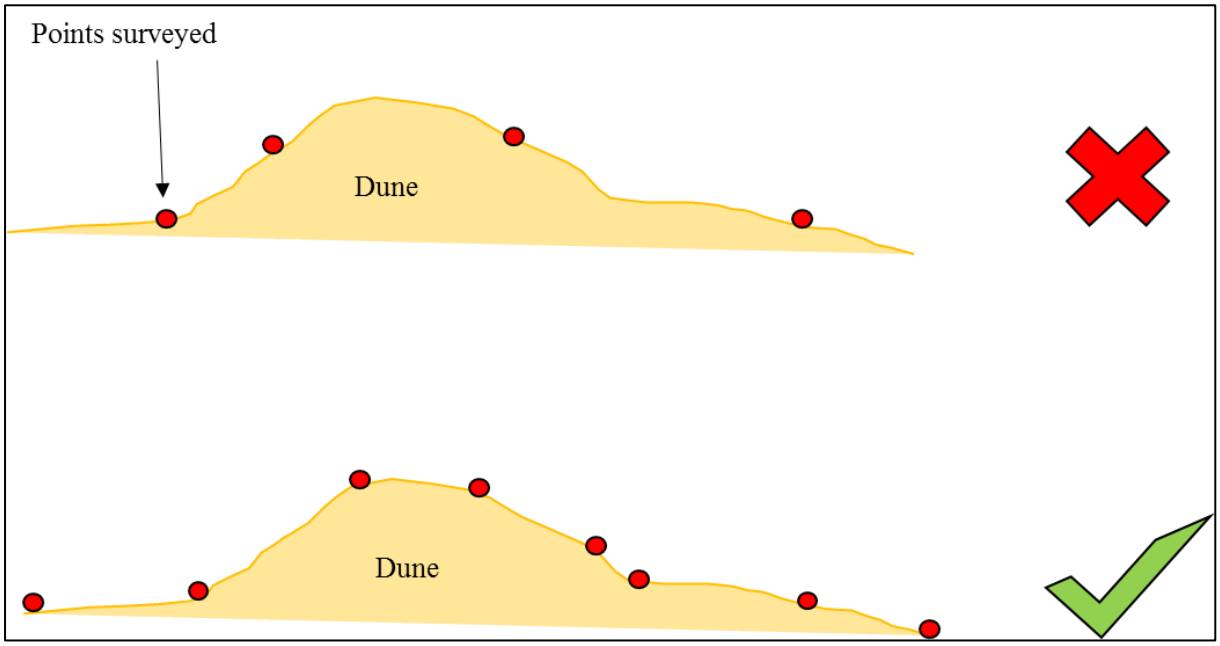

Figure 2.9: A graphical representation of surveying a dune to capture the topographic variations in the output surface.

DTMs/DSMs are widely used in the coastal geomorphology field to observe dune morphology (Levin *et al.*, 2004; Arbogast *et al.*, 2009; Yang *et al.*, 2010; Hugenholtz *et al.*, 2013). GIS software can be used to conduct a number of morphologic analyses from DTMs/DEMs, such as quantifying the volume of sand in the system (Arbogast *et al.*, 2009). DTMs/DSMs can help identify certain features, for example, the location of dunes or high/low points in the dune system. Transects can be extracted from a section of the DTM to show cross-

sectional elevation/volumetric differences (Andrews *et al.*, 2002). Temporal topographic and volumetric dune changes can be determined using DTMs (Mathew *et al.*, 2010). This can be achieved by subtracting subsequent DTMs/DSMs (given the cell size, reference system, and spatial extent are identical in both DTMs/DSMs) (Andrews *et al.*, 2002). This produces an elevation change surface that highlights different areas of change across the site (Andrews *et al.*, 2002) (Figure 2.10).

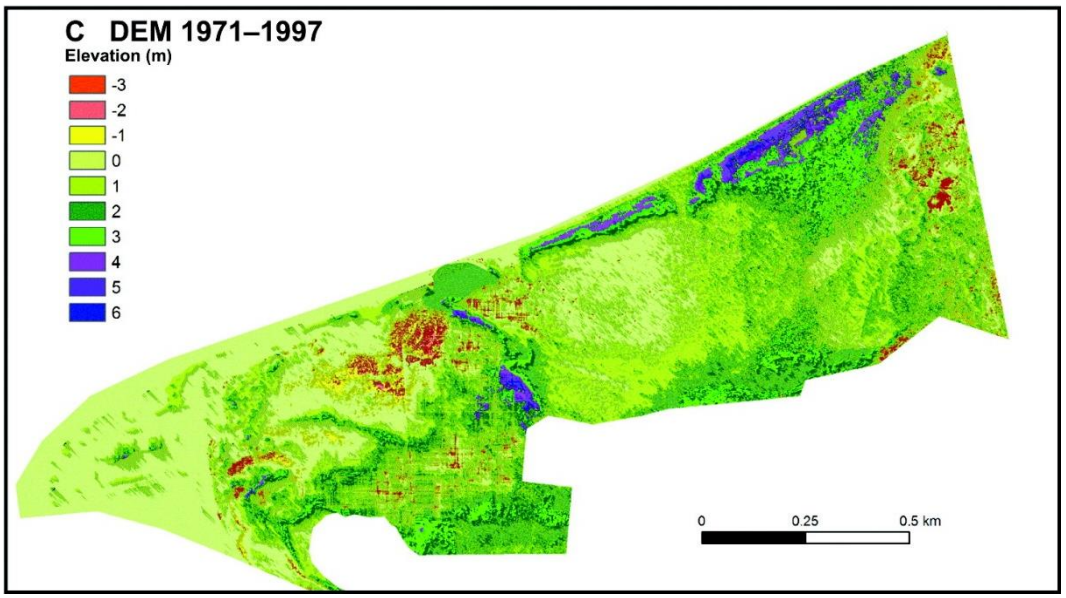

Figure 2.10: An elevation change DEM of the Greenwich dune system on Prince Edward Island, between 1971 and 1997 (Mathew *et al.*, 2010).

Elevation change surfaces present and quantify areas of accretion and erosion (Andrews *et al.*, 2002). In a study by Zhou and Xie (2009), the net volume change, sediment deposition, and erosion were calculated from DTMs. This information, used in conjunction with other data (for example, wind and wave data), can infer the processes or events causing the change in volume (Andrews *et al.*, 2002).

Certain dune morphologies can be attributed to geomorphic processes (Zhou and Xie, 2009). DTMs/DSMs can, therefore, aid in the inference of the geomorphic processes shaping the dune system (Zhou and Xie, 2009). Geomorphic processes have the potential to change the coast's morphology such as; storm events/wave run-up, human actions, climatic variables, sea-level rise, and tectonic movement (Zhou and Xie, 2009). For example, changes in beach profiles over an extended period in time can indicate a change in sea-level (Zhou and Xie, 2009) or variations in sea-level related to decadal processes such as El Niño (Sallenger *et al.*,

1999). Event-scale foredune erosion can result storm waves induced by low-pressure weather systems and spring high tide (You and Nielsen, 2013). Frequent erosion of an area may suggest a long dune recovery period (the rate at which a dune recovers following erosion) - a factor relating to dune morphology (Dissanayake *et al.*, 2015).

2.3.1 Accuracy and precision

Root mean square error and mean error

The accuracy and precision of DTMs/DSMs are important for deriving reliable morphologic measurements. Precision refers to the capacity of a survey to be repeated and obtain the same results. Accuracy is the combination of precision and the bias of the dataset. The accuracy and precision of a DTM/DSM can be calculated by comparing the values with a reliable dataset (i.e. a dataset that is considered accurate and precise). Vertical DTM/DSM precision and accuracy can be described in terms of the root mean square error (RMSE) (Bangen *et al.*, 2014). RMSE is calculated using the following equation;

$$\text{RMSE} = \sqrt{\frac{\Sigma\,(z_{DTM} - z_{Ref})^2}{n}} \tag{2.8}$$

The RMSE equation calculates the difference between a pixel value from the DTM (z_{DTM}) and the value of the corresponding point in the reference dataset (z_{Ref}) in relation to the number of sample points *n* (Fisher and Tate, 2006). The RMSE accounts for both random error and systematic error (Bangen *et al.*, 2014). Random errors are generally unpredictable and occur during both data collection and processing (Fisher and Tate, 2006). Systematic errors (bias) are consistent throughout a survey and hypothetically should be able to be explained (Fisher and Tate, 2006).

The mean error (ME) describes the overall bias of the dataset (i.e. over and under estimations) (Bangen *et al.*, 2014). The residuals are calculated by subtracting the reference dataset from the newly produced DTM (Bangen *et al.*, 2014). This difference describes how much the DTM deviates from the "truth" (i.e. the reference dataset) (Bangen *et al.*, 2014).

The RMSE and ME can be calculated using cross validation methods. Cross validation methods are employed to assess the quality of a spatial interpolation (Tomczak, 1998). The difference between the interpolated value and the data point value at the same location is compared. The *leave one out cross validation* (LOOCV) method is a type of cross validation, used to assess the accuracy of the triangulation employed to produce a 3D model (Brovelli *et*

al., 2006). LOOCV is a robust method for testing the quality of DSMs extracted from photogrammetry, however, it is only practical when the triangulation can be rapidly repeated (Sirguey and Cullen, 2014). To conduct a LOOCV, a set of known points is required. LOOCV uses an iterative process whereby all of the points except for one are marked as ground control (the remainder are marked as "check points") and the triangulation is conducted (Sirguey and Cullen, 2014). The process is repeated, with a different point marked as a check point, iteratively. This method assesses the robustness of the model generated by the triangulation. It does this by testing the model's reliance on each GCP (Brovelli *et al.*, 2006). The model calculates the x, y, z error for every GCP and the check point. The residuals are calculated using the difference between the value of the point produced in the model and the actual (measured) value of the point (Brovelli *et al.*, 2006). If the check point residuals are similar and small (relative to the desired accuracy), then it can be assumed that the resulting model has sufficient accuracy. The results can also provide confirmation that the GCP configuration is reliable.

2.4 Remotely piloted aerial systems and coastal vegetation

2.4.1 Vegetation and morphology

Quantifying coastal morphology using low-cost RPAS technology when vegetation is present can be challenging. Low-cost RPAS are typically equipped with RGB cameras, which do not penetrate vegetation. Consequently, the elevation of the top surface is recorded, not the terrain (Whitehead and Hugenholtz, 2014). The output is a digital surface model (DSM) as opposed to a digital terrain model (DTM) (Whitehead and Hugenholtz, 2014). The ground elevation is exacerbated where vegetation is present, hence, accurate dune morphology cannot be quantified (Whitehead and Hugenholtz, 2014). In coastal environments, the distribution and density of vegetation varies across the landscape. The variations result in a complex surface in the DSM.

Studies conducted by Gonçalves and Henriques (2015) and Turner *et al.* (2016) do not address the potential elevation discrepancy caused by vegetation. In other studies (Hugenholtz *et al.*, 2013; Scarelli *et al.*, 2016), the potential offset has been recognised, but not quantified. Mancini *et al.* (2013) compared DSMs of coastal dunes produced from an RPAS and a TLS. To address the elevation offset, densely vegetated areas, and areas that exceeded an elevation of 7.5 m, were not included in subsequent analysis. However, this method is not useful in

environments with large areas of dense vegetation, and it does not address the potential influence of vegetation that is < 7.5 m high in the DSM.

The detection of vegetation can be obvious within a DSM; vegetated areas appear more textured than areas without vegetation (Whitehead and Hugenholtz, 2014). Vegetation is also easily identified in RPAS imagery. The corresponding RPAS imagery can be useful for identifying areas in the DSM with a potential elevation offset.

2.4.2 RGB image classification

RPAS platforms equipped with RGB sensors are useful tools for mapping vegetation (Kaneko and Nohara, 2014). The low-altitude platforms provide high resolution imagery suitable for identifying vegetation type and distribution (Kaneko and Nohara, 2014). Remote sensing employed for vegetation mapping is typically conducted using multispectral, hyperspectral or infrared sensors (for example, Berni *et al.*, 2009), due to the low spatial and spectral resolution of conventional high-altitude RGB aerial photography (Turner *et al.*, 2011). However, the evolution of RPAS has provided a means to collect high resolution, low-altitude aerial photography using RGB sensors, suitable for vegetation mapping (Reid *et al.*, 2011; Turner *et al.*, 2011).

Vegetation can be mapped by 'reclassifying' RGB imagery in GIS software. Image reclassification changes the visible attribute of the pixel to map a certain aspect of the data (Gorte, 1999). For example, an image could be reclassified based on surface type, and the pixels in the output raster could represent the type of land cover (grass, water, soil) (Gallant, 2014). There are two main reclassification techniques; unsupervised classification, and supervised classification (Omran *et al.*, 2005).

Unsupervised classification uses the spectral bands of each pixel to form clusters based on a defined measure of similarity. Once the clusters are generated, the pixel categories are selected by the user (Omran *et al.*, 2005). In a supervised classification, firstly, the user defines the pixel categories. 'Training sites' are then selected and the software determines other pixels in the image with similar spectral properties. The training sites are saved as a signature file, which is then employed to reclassify the entire image (Omran *et al.*, 2005).

RPAS image reclassification can be used for a range of vegetation mapping applications. A common application is horticultural/agricultural mapping, whereby the life stage of crops is monitored (Torres-Sánchez *et al.*, 2014). Image reclassification can also be

used to map different types of cover, for example McConachie (2015) used it to identify the different types of vegetation cover present in the Mason Bay dune system.

Image reclassification is a useful tool for identifying 'vegetation' pixels, i.e. areas that may be offset by vegetation in the DSM. The orthomosaic (an image created via the collation of individual vertical photographs collected from an RPAS survey) can be reclassified into areas with and without vegetation (Konlechner *et al.*, 2015). This is useful for identifying the percent of vegetation cover/density in a dune system.

2.5 Summary

The purpose of this chapter was to outline the theory used to formulate the three research questions outlined in Chapter 1. Low-cost RPAS have the potential to overcome some of the issues associated with conventional surveying methods, for example, the trade-off between cost, efficiency, and accuracy.

Low-cost RPAS have the potential to yield sufficiently accurate and precise surface models, however, the errors unaccounted for in the BBA need to be investigated further. If RPAS can produce accurate and precise DSMs, RPAS could be employed for monitoring and managing coastal dune morphology.

Foredunes act as barriers protecting the hinterland from direct wind and wave action. DTMs and DSMs can be used to analyse morphological changes in coastal foredunes. Two of the key aspects that can be monitored using DTMs/DSMs are elevational and volumetric changes. Monitoring such changes is important for identifying both long- and short-medium term trends in the dune system. Morphological changes can highlight areas in the dune system that are vulnerable to erosion.

The impact of vegetation on DSMs derived from low-cost RPAS surveying needs to be investigated further for this method to be implemented more widely in coastal research. Off-the-self RGB RPAS sensors are sensitive to vegetation presence. RGB sensors only detect the top-most surface, hence, when vegetation is present, the canopy is recorded as opposed to the ground terrain. This is problematic when morphological changes need to be quantified, because the vegetation presence creates an elevational offset. Image classification can help identify areas where vegetation is present, and therefore aid in understanding which areas may have an elevational offset caused by vegetation.

Chapter 3

Coastal surveying methods

3.1 Introduction

Surveying foredune morphology and quantifying morphological change is important for understanding coastal processes (Saye *et al*., 2005). Digital terrain and digital surface models are tools commonly used to describe coastal morphology (Mathew *et al*., 2010; Papakonstantinou *et al*., 2016). Digital surface and elevation models are derived from elevation data collected via surveying. Accurate surveys are important for generating DSMs/DTMs, especially when the data is used to quantify change.

Coastal dune systems can be surveyed using a range of methods. The method selected depends on the technology available and the environmental constraints of the survey. In some situations there may be a variety of suitable surveying methods. Coastal surveys often have a trade-off between cost, efficiency, and accuracy. For example, LiDAR surveying can provide a vertical accuracy of 10-15 cm (in optimal conditions) efficiently over large areas (Liu, 2011). However, a single LiDAR survey can cost tens of thousands of dollars. Conversely, total station surveys can collect high accuracy data (within millimetres), at a fraction of the price of a LiDAR survey, but are inefficient for surveying large areas (Baily *et al.*, 2003). Small RPAS have the potential to overcome the trade-off between cost and efficiency. RPAS are becoming less expensive, and range between $100 and $10,000 (NZD). RPAS surveying is also efficient, and can cover large areas in a small timeframe. Survey methods that are inexpensive, efficient and accurate are appealing to coastal geomorphologists.

The ability to conduct surveys at short-notice provides an opportunity to quantify event-scale change, and undertake long-term monitoring. Hence, if low-cost RPAS can provide

DSMs with comparable accuracies to other methods (< 10 cm), this method could be employed more widely for coastal geomorphology research.

The aim of this chapter is to address the first research question (Chapter 1, Section 1.5); *how does the accuracy and cost of data collected by low-cost RPAS compare to other coastal surveying methods?* This aim will be achieved by testing a low-cost RPAS against conventional coastal surveying methods. Firstly, the surveying methods and the analyses taken to compare these methods will be explained. The results assessing the surveying efficiency, cost, atmospheric limitations, environmental limitations, accuracy and precision of each surveying method will then be described. Lastly, the findings from this study will be discussed, and conclusions drawn on the efficacy of low-cost RPAS surveying.

3.2 Study site

The study site is an 85 m × 65 m section of the St. Kilda Beach foredune, referred to as Area B (Figure 3.1). This particular study site was chosen for a number of reasons. Firstly, the study site is accessible, which allows the repetition of surveys if required. Secondly, the site contains areas of dense vegetation and bare sand (features which can vary between different dune systems). Vegetation can impact surveying methods in different ways; the site, therefore, provided an opportunity to investigate the influence of vegetation on each surveying method. Lastly, the study area has a steep foredune, which provided an opportunity to test the ability of each method for surveying undulating terrain. The RPAS survey was conducted over Area A, however, for the analysis, Area A was clipped to the extent of Area B. The Area A dataset was used for the analyses in Chapter 4.

Figure 3.1: A map of the flight area (Area A), and the study area (Area B).

3.3 Methods

This study compares three conventional coastal surveying methods (total station, RTK-GPS, and terrestrial laser scanning) against a small, low-cost RPAS. Comparisons are based on;

- the accuracy/precision of the DTMs/DSMs produced by each method;
- the efficiency of each survey;
- the surveying cost (purchasing equipment versus hiring personnel/equipment) and;
- the field limitations of each surveying method.

Area B was surveyed using all four methods. This involved recording the start and end time of each survey, the number of people required to conduct the survey, the number of points collected during the survey, the atmospheric and environmental limitations, and the equipment

used. The data collected from each survey were used to create either a DTM (total station and RTK-GPS), or a DSM (RPAS and terrestrial laser scanner). The accuracy and precision of each DTM/DSM was calculated using the mean error (ME) and root mean square error (RMSE) from the point interpolation. This section will describe and explain the methods used to address the first research question.

3.3.1 Total station survey

The total station survey was completed using a Leica 307 total station. The total station was set up on a known point (Site B Peg; 4913271.5 N, 1408257.7 E) located within the study area, and points were surveyed using New Zealand Transverse Mercator 2000, relative to the GRS80 ellipsoid. A topographic, systematic, stratified sampling technique was used; points were taken approximately every one metre over continuous topography, and where there were changes in topography, more points were taken (Figure 3.2).

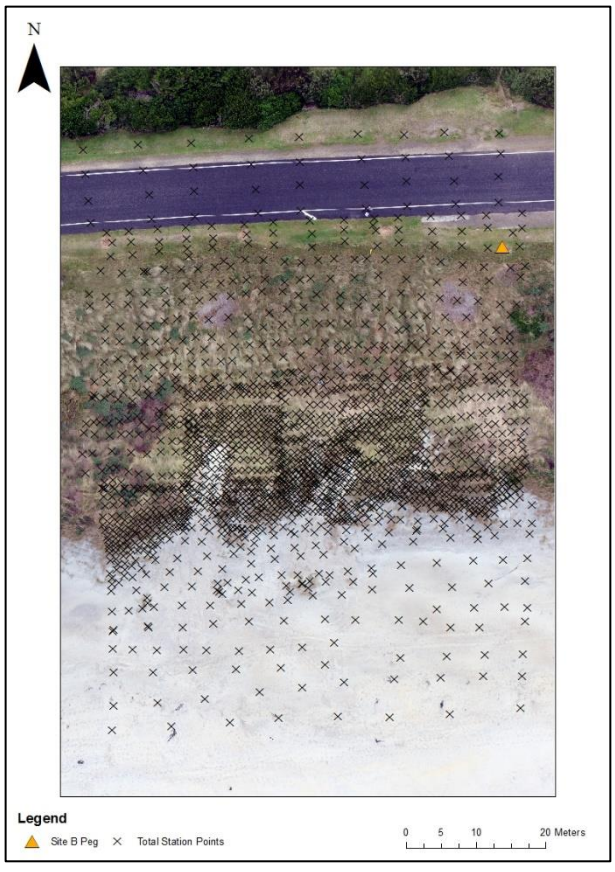

Figure 3.2: The location of each point taken in the total station survey. The location of the total station is denoted as 'Site B Peg'.

The survey took two and a half days to complete. The prism pole was extended from 2 m to 5 m on the beach and the face of the foredune, where the 2 m pole could not be seen from

the total station. The points were uploaded to Microsoft Excel via Leica GEO Office and then uploaded into ArcGIS for processing. A DTM was created using a thin plate spline interpolation from the *Geostatistical Analyst* toolbox. The *Geostatistical Analyst* conducted a cross validation to generate the ME and RMSE of the DTM (refer to Section 3.3.5).

3.3.2 Real-time kinematic global positioning survey

A Trimble R8 unit was used for the RTK-GPS survey. The base station was set up over Site B Peg (Figure 3.3), and radio communication between the base station and rover was achieved using an external antenna. The points were recorded using the default occupation time for "topo" points, which is five seconds. This occupation time was selected as an appropriate compromise to maintain surveying efficiency. A topographic systematic sampling strategy was used; a point was taken every metre where the terrain was continuous, and where the terrain was variable, more points were taken. This was employed to ensure any complexities in the topography were recorded (Figure 3.3).

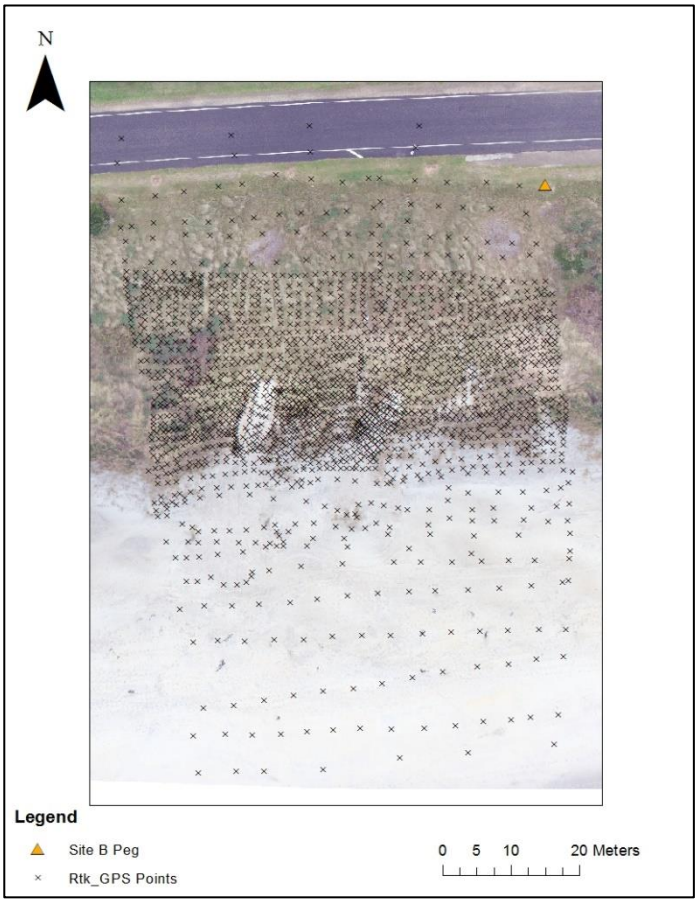

Figure 3.3: The location of each point taken in the RTK-GPS survey. The location of the base station is denoted as 'Site B Peg'.

The survey was conducted over two days. The RTK-GPS unit recorded points relative to the New Zealand Transverse Mercator 2000 coordinate system, and the elevations recorded relative to the GRS80 ellipsoid. The points were uploaded into Trimble Business Centre (TBC), and exported into a Microsoft Excel file. Using ArcGIS, a DTM was generated from the 3D points, using a thin plate spline interpolation from the *Geostatistical Analyst* toolbox. The ME and RMSE were calculated from a cross validation conducted by the *Geostatistical Analyst* (refer to Section 3.3.5).

3.3.3 Terrestrial laser scanner survey

A Trimble TX5 laser scanner was used to conduct the laser scan survey. The terrestrial laser scanner (TLS) survey was conducted for the author by the University of Otago School of Surveying. The TLS was set up at three locations on John Wilson Drive, three locations on the crest of the foredune, and three locations on the beach within Area B. The scans were stitched together using the Trimble Real Works Software, producing a 3D point cloud of the area. The point cloud was "cleaned", which removes unwanted points (for example, the ocean) and vegetation to generate a DTM. The point cloud was imported into ArcGIS, and a thin plate spline interpolation was used to derive a DSM. A cross validation was conducted by the *Geostatistical Analyst* to calculate the ME and RMSE (refer to Section 3.3.5).

3.3.4 Remotely piloted aerial system survey

A DJI Phantom-3 Advanced quadcopter was used for the RPAS survey. A Sony EXMOR 1/2.3" (sensor size 6.17 × 4.55 mm) 12.4 megapixel camera was used, with a field of view of 94° and a 20 mm lens (in 35 mm equivalent) focussed at infinity. The infinity focus prevents the "zoom" from being used, and therefore keeps the sensor's internal geometry consistent by maintaining the focal length between images. A change in focal length causes distortion in the output, and hence, can cause inaccurate results (Sanz-Ablanedo *et al.*, 2012). Each image is comprised of 4000 × 3000 pixels.

Flight planning software was not employed, and photographs were captured manually during the flight by the operator. The sensor information was used to calculate the 'real' focal length, using the following equation;

$$f_R = \frac{f_{35}\, S_w}{34.6} \ , \tag{3.1}$$

where f_R is the real focal length measured in millimetres, f_{35} is the focal length in the 35 mm equivalent, and S_w is the sensor width. To achieve a ground sampling distance (GSD) of 2.5 cm^2, the flying height was calculated:

$$H = \frac{f_R \, n_w \, GSD}{S_w} \tag{3.2}$$

where n_w is the number of pixels forming the width of the sensor. To achieve a GSD of 2.5 cm^2, the height of the aircraft should be at a maximum of 57.8 m. For each flight, the RPAS flew at 50 m (+/- 0.5 m) above the launch site which was located approximately 19 m above mean sea level. The same launch site was used to deploy the aircraft for each flight. This particular location was chosen because it gives a clear view of the entire study site (Figure 3.4).

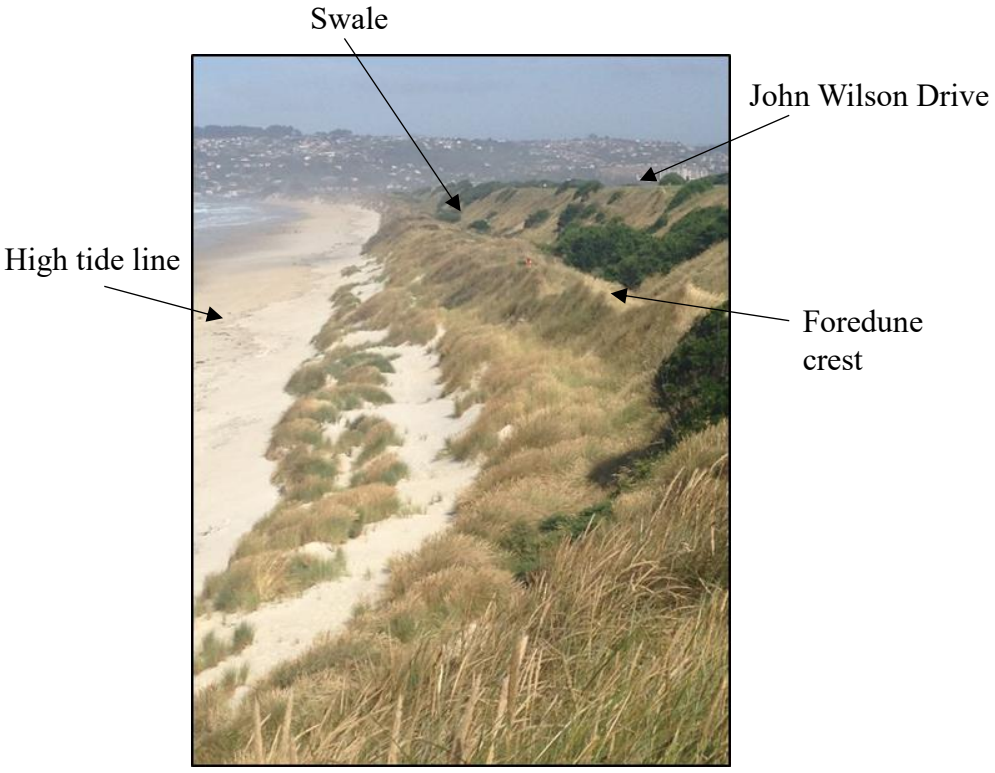

Figure 3.4: A view of the study area from the launch site.

The image footprint was calculated to determine the distance the RPAS needed to travel between subsequent photographs to obtain a forward image overlap of 85% and side-lap of 70%, believed to be an appropriate compromise to ensure satisfying photogrammetric modelling while being within the RPAS endurance. The approximate dimensions of the rectangular footprint of each image were calculated by multiplying the number of pixels in the width and length of each image by the desired GSD. The minimum distance between pictures

to achieve the desired 85% forward overlap was computed as 11.25 m. During image acquisition in the field, photographs were taken approximately every 10 m.

The image footprint was also used to determine the flight path. The width of the study area was approximately 85 m, therefore 70% side-lap was easily achieved with two parallel flight lines. The entire study area could have been covered by one flight line, however, at least two flight lines are required to strengthen the photogrammetric model using image side-lap as well as forward overlap.

Ground control points (a total of 23) were established along John Wilson Drive, in the swale of the foredune (the area in the lee of the foredune), on the foredune crest, and along the beach (Figure 3.5). This particular GCP layout was chosen to 1) ensure the points were evenly distributed throughout the study area, and 2) to ensure GCPs were present in the four areas with differing elevations (John Wilson Drive, swale, crest and the beach) (Figure 4.5), hence, providing confidence in the accuracy of the output DSM.

Figure 3.5: The location of the ground control point configuration for the RPAS flight. The permanent points are road markings and fence posts on the dune crest, the temporary points are foam targets placed on the beach.

The permanent and temporary GCPs were surveyed using a Trimble R8 RTK-GPS unit. The permanent points were surveyed using an occupation time of 1 minute, and the temporary

points 2 minutes. All points were intended to be surveyed for 2 minutes, however, the permanent points were inadvertently surveyed for just 1 minute. The PDOP value describes the strength of the configuration of satellites (Lemmon and Gerdan, 1999). When the PDOP is low (below 2), there is confidence that the position of the point recorded is precise, because the number of satellites and configuration of satellites is optimal (Lemmon and Gerdan, 1999). The average PDOP value of the permanent GCPs was 1.3. All points were recorded using the New Zealand Transverse Mercator coordinate system, and elevations were relative to the GRS80 ellipsoid. The average horizontal precision for the 13 permanent points was 0.011 m, and the average vertical precision was 0.016 m. The RMSE was 0.003. The temporary points had an average horizontal and vertical precision of 0.009 m and 0.012 m, respectively.

Pix4D Mapper was used to process the RPAS imagery. The imagery and GCP coordinates were uploaded into the software. The GCPs were marked in the imagery by the user. The software conducted a bundle block adjustment (BBA) to solve for the interior and exterior orientation parameters. The software then produced a DSM and orthomosaic, and reported the associated error via the Quality Report. Further explanation on the Pix4D Mapper process is presented in Chapter 4, Section 4.3.5.

3.3.5 Survey comparison

The surveying methods were compared based on the accuracy and precision of the DSM/DTM, the efficiency of the survey, the equipment cost, and the limitations of each method. The cross validation method was used to assess accuracy and precision, by calculating the ME and RMSE of each DSM/DTM. The cross validation takes each point sequentially and measures the elevation difference between them and the corresponding pixel in the DTM/DSM. The differences are averaged to calculate the ME, and the ME is then used to calculate the RMSE. The results describe the vertical accuracy and precision of the surface.

The cross validation for the total station, RTK-GPS and TLS surveys was conducted via the ArcGIS *Geostatistical Analyst*. The cross validation for the RPAS survey was completed using the *leave one out cross validation* method, whereby the elevation of the ground control points was compared with the elevation at the corresponding pixel location (as opposed to using each 3D data point recorded in the survey).

The efficiency of each survey was determined by its duration, recording the number of people required to conduct the survey, and noting the equipment required. The ideal survey would take the least time, the least number of people and would require minimal equipment.

The start and end time of each survey was recorded in the field. The "effort" required for each method was described as the number of points collected per hour. The set-up and processing durations were estimated, because the duration of both tasks varies depending on the surveyor.

A cost analysis was conducted to compare the expense of each method. The analysis looked at three scenarios, 1) purchasing the equipment; 2) hiring the equipment; and 3) hiring a surveyor to conduct the survey. It was expected that purchasing the equipment is less expensive than hiring either a surveyor or the equipment, when surveys need to be repeated. However, for one-off surveys hiring the equipment or a surveyor is likely to be more cost efficient.

The surveying 'limitations' were separated into two categories; atmospheric and environmental. Atmospheric limitations refer to the implications of wind, rain, illumination and cloud cover on the survey. Environmental limitations refer to any physical factors of the site that impact each survey, for example, variations in topography. The limitations for each method were recorded in the field.

3.3.6 Summary

DTMs/DSMs derived from total station, RTK-GPS, and TLS surveys were compared with a DSM generated from low-cost RPAS photography. The surveys were conducted over Area B, located at St. Kilda beach, Dunedin. The methods were compared based on the accuracy/precision of the DTMs/DSMs produced by each method; the efficiency of each survey; the surveying cost; and the environmental and atmospheric limitations of each surveying method.

3.4 Results

3.4.1 Efficiency

The results from the efficiency assessment show that the RPAS survey was the most efficient method (Table 3.1), and could obtain 48 million points/hour. The total station and RTK-GPS surveys had a similar duration (10 hours and 58 minutes, and 13 hours and 14 minutes, respectively) and number of 3D points. Both surveys were completed over multiple days. The TLS and RPAS surveys were completed within one day. The RPAS survey had the shortest surveying duration of 10 minutes. The duration does not include the time taken to set-up equipment or process the data, however, these were estimated following the survey.

Table 3.1: *A summary of the efficiency of each surveying method.*

	Set-up Time (Hours)	Survey Duration (Hours)	Processing Time (Hours)	Total Duration	No. of People Required	No. of Points	Effort (Points/ Hour)
TS	0.25	10.9	0.5	11.65	2-3	1936	178
RTK-GPS	0.25	13.2	0.5	13.95	1	2250	171
TLS	0.5	3.16	5-8	11.66	2-3	5,893,427	1,865,009
RPAS	1	0.16	4	5.16	2-3	981,909 (7,702,621 Site A)	48,141,381

The GCP establishment for the RPAS survey took approximately 1 hour, whereas the total station and RTK-GPS units took less than 15 minutes. The set-up time for the TLS survey was approximately 30 minutes. The total station and RTK-GPS surveys took the least time to process (approximately 30 minutes). The RPAS data processing was approximately 4 hours, which includes downloading the imagery and GCP coordinates, and generating a DSM in Pix4D Mapper. The TLS data processing was the longest, approximately 5-8 hours from the download to the final DSM.

The total station collected a total of 1,936 data points, the RTK-GPS 2,250 points, the TLS 5,893,427 points and the RPAS 7,702,621 points. The RPAS survey was conducted over the larger study area (Figure 3.1), and the Area B points were extracted from the larger dataset. The total RPAS 3D points collected within Area B was 981,909. The RPAS survey required the least effort, and is capable of obtaining approximately 48 million points per hour. The total station and RTK-GPS units retrieved 178 and 171 points/hour, respectively.

All surveys required 2-3 people to conduct, except for the RTK-GPS survey which required one person. The TLS survey required the most equipment; a total station, a prism and its pole, 5 tripods, 2 geo-referencing spheres and a laser scanner. The total station required the least equipment, only needing the total station itself, a tripod, prism and prism pole. The RTK-GPS unit needed two GPS receivers, a tripod, a bipod, two range poles, an external battery pack, and an external antenna. The RPAS only required the RPAS itself, and a controller, but because the GCPs needed to be surveyed with high accuracy, the entire RTK-GPS kit was also required.

3.4.2 Cost analysis

The first analysis assessed the cost of purchasing the surveying equipment brand new. The cost of all of the equipment required and the cost of the software used to process the data was included in the cost analysis. The total station model employed in this study is an outdated model, therefore, the price listed is the typical price of a total station at the time of this study. Additional equipment such as tripods are based on the current retail price. The prices listed in Table 3.2 are estimates; the software and equipment price varies depending on the supplier and the type of software. The software prices listed in Table 3.2 correspond to unlimited licenses.

Table 3.2*: A summary of the equipment cost for each survey. The equipment is the estimated cost of purchasing all of the equipment required to conduct the survey, based on current retail price.*

Surveying Method	Instrument Cost (NZD)	Equipment Cost (NZD)		Software Cost (NZD)	Total Survey Cost (NZD)
		Item	Cost		
Total Station	$8,000-$10,000	Tripod	$279	Leica Geo Office $1,370	~ $12,324
		Prism Pole	$245		
		Prism	$430		
Trimble R8 RTK-GPS	$25,000-$30,000	Tripod	$279	Trimble Business Centre $1,650	~ $33,064
		Range Poles	$654		
		Antenna	$133		
		Bipod	$348		
Trimble TX5 Laser Scanner	$50,000	Tripod x5	$1,395	Trimble Real Works $19,326	~ $83,661
		Total Station Kit	$12,324		
		Sphere Set	$616		
DJI Phantom 3	$2,000	RTK-GPS Kit	$33,064	Pix4D Mapper $12,000	~ $47,064

The laser scanned survey is the most expensive with a total cost of approximately $83,661 NZD (Table 3.2). The total station survey was the least expensive with a total cost of

$12,324. The total RPAS survey cost included the RTK-GPS unit, because a high-precision surveying method is required to establish GCPs. The laser scanned survey and the RPAS survey require the most expensive software, which cost $19,326 and $12,000, respectively.

It is unrealistic that surveying equipment and software would be purchased to conduct one survey, therefore, the estimated cost of hiring a surveyor, and the cost of hiring the equipment were also assessed (Table 3.3). The equipment and surveyor hire costs for the total station, RTK-GPS, and the surveyor hire for the RPAS, are based on quotes from *Overview Surveying* in Dunedin. The RPAS equipment hire is based on the current price from the *Drone Hire* website.

Table 3.3: *Cost analysis of each surveying method for a) hiring the equipment; b) hiring a surveyor; and c) purchasing the equipment. * The RPAS hire is for a DJI Phantom-3 Professional, typically photogrammetry RPAS are not available for hire due to the risks associated with the method.*

	Equipment Hire	Surveyor Hire	Purchase brand new
Total Station	$150-$300/day	$1,500/day	$12,000
RTK-GPS	$450/day	$1,500/day	$33,000
Terrestrial Laser Scanner	$1,000-$1,250/day	$1,700/day	$84,000
RPAS	$135/day *	$3,000/flight	$47,000

Purchasing equipment is more expensive than hiring it, or a surveyor. However, if frequent surveys are required, purchasing the equipment is likely to be more cost-efficient in the long-term. Hiring the equipment is the least expensive of the options. The total station is the least expensive for all scenarios. The RPAS requires the most expensive surveyor hire. However, the RPAS can cover large areas rapidly, and hence, is more cost-efficient for large scale surveys. Hiring a surveyor to conduct a total station or RTK-GPS survey is the least expensive. However, these methods are the most time consuming. Therefore, the methods become less cost-efficient as the surveying area increases.

3.4.3 Atmospheric limitations

Each surveying method was impacted by at least one atmospheric limitation. Precipitation is a limiting factor for all survey methods. Precipitation makes it difficult to see through the total station lens, and makes the ground slippery to traverse with the prism pole. However, surveying with a total station is possible in light showers and rain, but unfavourable. In contrast, the TLS cannot be used at all during precipitation. The RPAS is not waterproof and cannot be operated in the rain. The RTK-GPS unit is water proof (Trimble R8 Data Sheet, 2004), but rain makes the terrain slippery and difficult to traverse with the roving receiver.

Table 3.4*: Summary table of the atmospheric limitations for each surveying method.*

	Precipitation	Wind	Sunlight
RTK-GPS			
Total Station			
RPAS			
TLS			

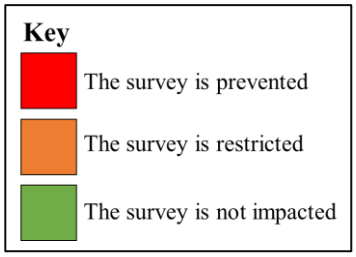

The total station, RPAS and RTK-GPS are affected by wind. The prism and range poles need to be held level when conducting surveys with a total station or RTK-GPS. Wind generally did not impact the operator's ability to hold the 2 m pole level. However, a 5 m extension pole was required for some sections of the survey. The 5 m pole was difficult to level, and the difficulty was exacerbated as wind speed increased. The RTK-GPS reports an 'excessive movement' error during point measurement if the roving pole is tilted or is moving, preventing measurement (Trimble, 2013). This message appears when the receiver is shaking due to wind, and when the pole is not held steady, which can occur when holding the pole on steep terrain. The DJI (2015) User Manual states that the RPAS can be flown in wind speeds up to 10 ms^{-1}. However, for surveying purposes, winds greater than 5 ms^{-1} are unfavourable, and near calm conditions are more suitable. All surveys conducted in this study by the RPAS were undertaken in wind speeds below 4 ms^{-1}. The RPAS endurance is approximately 20 minutes, however, operating in greater wind speeds reduces this endurance.

Sunlight was limiting for the total station and the RPAS surveys. Due to the orientation of the dune, and the relative location of the total station, the sun was facing the prism at all

times. At certain angles, the sun reflects on the prism directly into the lens of the total station, preventing the machine from recording a point and forcing sunlight into the operator's eyes. Sunlight was also a minor limitation for the drone survey, mainly due to the steep terrain. The sun cast a shadow of John Wilson Drive, placing the swale and seaward slope of John Wilson Drive in shade. The stark contrast in illumination over different areas makes it more difficult to differentiate features. Changes in sunlight throughout the flight caused colour distortions in the orthomosaic, and saturation of sand in the image.

3.4.4 Environmental limitations

The surveying methods were either restricted or unaffected by environmental limitations and none were completely prevented (Table 3.5). The topography of the site was a limiting factor for the total station, RTK-GPS and terrestrial laser scanning surveys. The crest of the foredune is approximately 12 m high (above MSL), and has a gradient between 10 and 35 degrees between the crest and the base of the seaward slope. It was difficult to survey with the total station due to the foredune gradient. Two options were available; 1) set-up the total station at two different locations, or 2) use the 5 m pole for the sections that could not be surveyed with the 2 m pole. The second option was employed to avoid moving the total station, and hence, having to merge datasets. However, the 5 m pole was difficult to carry due to its size, meaning that handheld radios had to be used by the total station operator and the person holding the prism pole, in order to communicate. Line-of-sight was also an issue for the TLS. The topography meant that the TLS needed to be set up at 9 different locations to survey the entire study area.

Table 3.5: *Summary table of the environmental limitations of each surveying method.*

	Topography	Vegetation
RTK-GPS		
Total Station		
RPAS		
TLS		

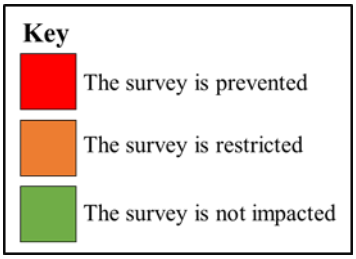

The total station and RTK-GPS surveys require walking over the terrain to collect points, this was difficult where the terrain was steep. This caused trampling of the study area,

as sand compacts when it is walked over. This was avoided by standing behind the instrument (i.e. only walking over areas that have already been surveyed).

The presence of dense vegetation was a limiting factor for all surveying methods. The St. Kilda foredune is densely vegetated by *Ammophila arenaria* (marram grass), and *Lupinus arboreus* (tree lupin) in some places. The dense vegetation was difficult to traverse with the total station and RTK-GPS. The TLS and the RPAS captured the elevation of the top-most surface. Therefore, in locations with dense vegetation, the top of the canopy was recorded by both methods. Conversely, the total station and RTK-GPS units recorded the elevation of the ground.

3.4.5 Accuracy and precision

The total station and RTK-GPS surveys produced DTMs, whereas the TLS and RPAS surveys produced DSMs. The total station and RTK-GPS DTMs show a similar range in elevation values. The DSMs (Figure 3.6c and d) have slightly higher elevations than the corresponding areas in the DTMs (Figure 3.6a and b). The RPAS and TLS DSMs have more 'noise' than the DTMs (Figure 3.6).

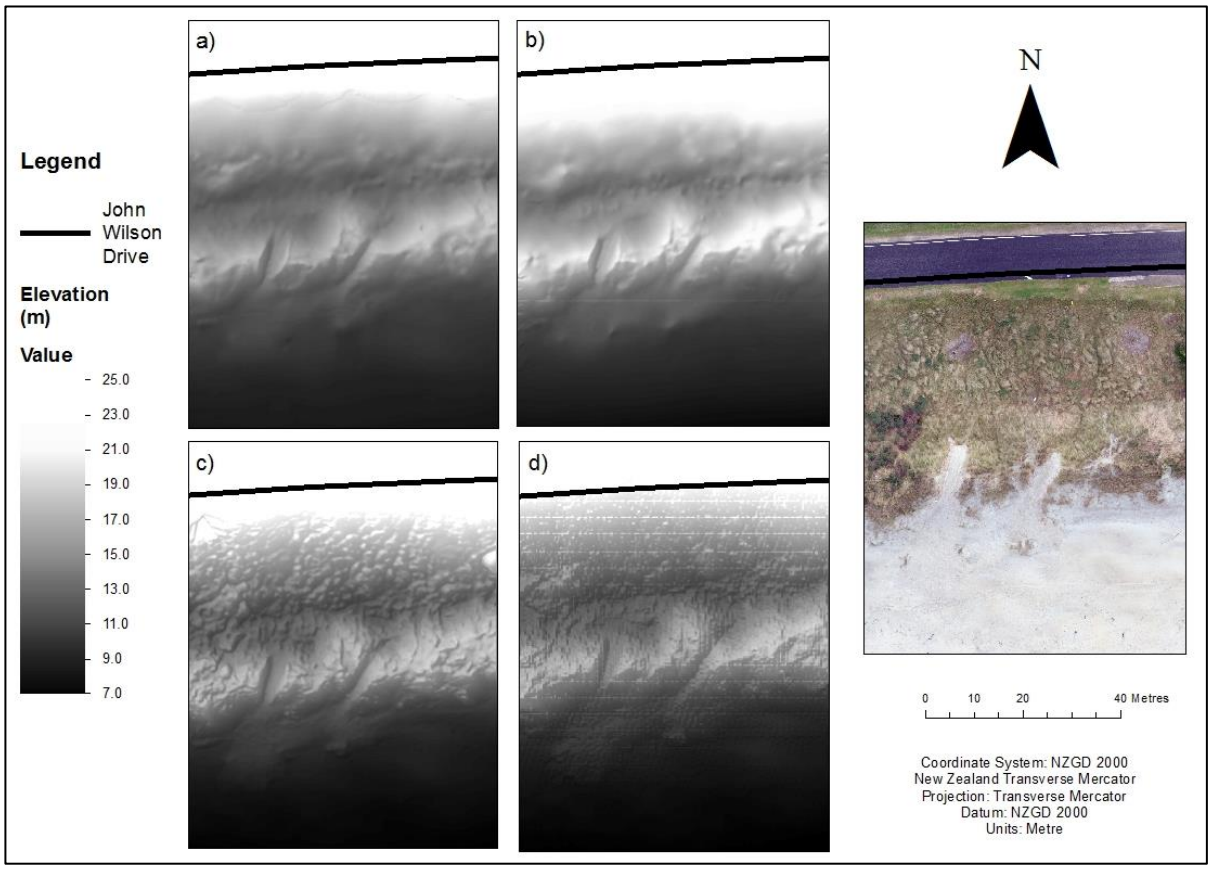

Figure 3.6: Output DTMs/DSMs from each method. a) RTK-GPS DTM; b) Total station DTM; c) RPAS DSM; d) TLS DSM. The photograph on the right is an orthomosaic of Site B from the RPAS survey.

The total station and RTK-GPS DTMs had the highest RMSE of 10 cm, and the TLS had the lowest RMSE of 2 cm (Table 3.6). The RMSE of the RPAS DSM was 8 cm. The RPAS DSM had the largest ME, - 3 cm. The lowest ME was attributed to the TLS DSM, 0.01 cm.

Table 3.6: *Vertical mean error (ME) and root mean square error (RMSE) for the DSMs/DTMs produced from each surveying method.*

	ME (m)	RMSE (m)
Total Station	0.002	0.103
RTK-GPS	0.001	0.100
TLS	0.0001	0.022
RPAS	-0.028	0.080

A profile was extracted from each DTM/DSM at the same location (Figure 3.7) to compare the differences in elevation between each model (Figure 3.8). All of the profiles follow the same general dune shape. The RTK-GPS and total station profiles are very similar in elevation, and are smoother compared to the RPAS profile. The RPAS profile is elevated slightly above the RTK-GPS and total station profiles. The TLS profile is between 0.5–1 m lower than the other profiles on the crest of dune, and is relatively consistent with the other profiles along the beach. Along the slope of John Wilson Drive (between 6 m and 28 m), the TLS deviates from the RTK-GPS and total station surveys. The largest deviation between the TLS survey and the RTK-GPS/total station surveys is 3.04 m, located at 11 m along the profile.

Figure 3.7: The profile line at Site B, extracted from each DTM and DSM.

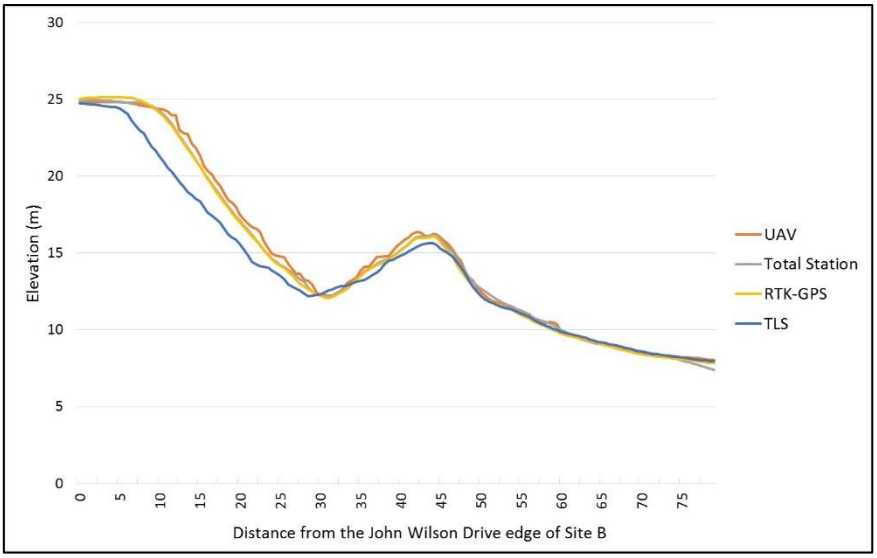

Figure 3.8: Profiles from each DTM/DSM along a profile line in Site B (Figure 3.7). The elevation is measured in metres above the GRS80 ellipsoid.

3.5 Discussion

This chapter compares coastal foredune surveying using a total station, RTK-GPS and terrestrial laser scanner with a low-cost RPAS. This section begins with the 'limitations' of each method. Each method is affected by environmental and atmospheric limitations. However, the extent of the impact of each limitation depends on the surveying method. This section will then explain the efficiency of each surveying method. The efficiency is focussed on the data collection itself, however, set-up and data processing will also be considered. The results of the cost analysis will be discussed, and lastly, the precision and accuracy of each DTM/DSMs will be analysed.

3.5.1 Atmospheric limitations

Precipitation

All of the surveying methods were impacted by precipitation. The total station can be operated in light rain, however, water on the telescope lens and prism impacts the ability to record points. The RTK-GPS is water proof (Trimble, 2004), and hence, is unaffected by precipitation. The TLS cannot be operated in the rain at all; rain causes unreliable TLS measurements, and the moisture can damage the instrument (Trimble, 2012). This is problematic due to the length of the survey (3 hours). Similarly, the RPAS cannot operate in the rain (DJI, 2015). However, the RPAS flight can be completed within 15 minutes, therefore, wet weather can easily be avoided.

Wind

Wind impacted all of the surveying methods except for the TLS. Total station and RTK-GPS require level range poles for precise surveying. However, this was difficult during windy conditions. Wind had a greater impact on the 5 m pole, which was difficult to hold level. An 'excess movement' error prevents the measurement of RTK-GPS points during high wind. The atmospheric limitations of the total station and RTK-GPS do not prevent the surveys from taking place.

The RPAS cannot operate at all in strong winds. According to the DJI Phantom-3 Advanced user manual, the aircraft can technically be flown in wind speeds up to 10 ms^{-1}. In the current study the RPAS was not flown in winds greater than 4 ms^{-1}. The RPAS can fly in winds up to 10 ms^{-1}, however, it is difficult to photograph in such conditions. The RPAS also requires more battery power when flying in higher wind speeds as it uses more power to

stabilise its position. This is problematic because the battery capacity in calm conditions is approximately 20 minutes, hence, higher wind speeds further reduce the endurance. All flights in the current study were completed between 10-12 minutes and at the end of the survey the low battery warning was signalled. The total survey area is approximately 40,000 m^2, completed in two flight lines. The Phantom 3 Advanced would, therefore, not be capable of covering an area much larger, unless multiple batteries are used per flight.

The limited flight time of the RPAS in this study are relatively consistent with other low-cost RPAS models. The total flight time for the DJI Phantom 3 Advanced is 23 minutes, in calm conditions (DJI, 2015). The other low-cost drones produced by DJI include the Mavic ($1,803 NZD) and the Phantom 4 ($2,227 NZD). The Mavic has a total flight time in ideal conditions of 27 minutes (DJI, 2016a), and the Phantom 4 has a total flight time of 28 minutes (DJI, 2016b). Yuneec's Q500 4K quadcopter ($2,086 NZD) has a flight time of 25 minutes (Yuneec, 2015).

Sunlight

The impact of sunlight on different surveying methods depends on the topography and orientation of the survey. In the current study, the total station prism was oriented toward the sun, due to the location of the total station. At certain angles the sunlight is reflected by the prism and into the lens of the total station, preventing the point from being recorded. This limitation is dependent on the direction the prism is facing and the cloud cover, hence, it is a limitation that could be avoided.

Sunlight does not affect the RPAS flight, however, it does impact the quality of the data collected. Variations in cloud cover over the duration of the flight can create "artefacts" (visible errors) in the resulting orthomosaic (Whitehead and Hugenholtz, 2014). John Wilson Drive cast a shadow over the swale of the foredune, creating a stark colour contrast between it and the foredune. The areas in the shadow are more difficult to interpret. Bright, direct sunlight is problematic, especially in sandy environments. Bright sunlight over sandy areas can cause adjacent pixels to appear homogenous (i.e. 'saturated'), and as a result features are more difficult to interpret. Differences in illumination alter the spectral properties of the pixels, and can create errors in the point cloud (Eltner *et al.*, 2016).

3.5.2 Environmental limitations

Terrain

Environmental limitations were identified as terrain or vegetation limitations. Terrain does not impact the application of the RPAS survey. This is due to the remote nature of the survey (once the GCP network is established). However, the type of terrain needs to be taken into consideration, as the surface reflectivity can affect the imagery (Aber *et al.*, 2010b). For lightly coloured terrain such as sand and snow, it is suggested that image overlap is increased to 80-85% (Pix4D, 2016). Image overlap in this study was 85%, even though the vegetation cover was primarily grass. Imagery for the flight in this chapter was taken on an overcast day, however, other flights in this study were flown during sunny conditions. The sun can cast a shadow over the swale of the foredune, causing colour contrast in the images. Colour contrast makes it more difficult to mark GCPs in the images. This is especially difficult for the GCPs surrounded by sand, in this case the GCPs were white paper plates. These were difficult to identify when the illumination was too bright. The contrast also impacts the creation of orthomosaic images. Bright illumination can result in incorrect colour balancing, which creates patches of bright colour variations in the orthomosaic (Whitehead and Hugenholtz, 2014). This can be avoided by flying on overcast days. However, in some situations it is necessary to survey as soon as possible, which can result in flying during bright conditions. It is also difficult to avoid the impacts of sunlight when it is a cloudy day, where clouds move in front of the sun. As a result, images taken from the same flight can appear different in colour (Whitehead and Hugenholtz, 2014). Variations in the spectral properties of the pixels can create errors in the output DSM (Whitehead and Hugenholtz, 2014).

The terrain at St. Kilda limited the total station, RTK-GPS and TLS surveys. The foredune at St. Kilda is approximately 12 m above mean sea level, and has a gradient between 10 and 35 degrees. The total station and TLS surveys require line-of-sight. For the total station survey, the person operating the total station (located on John Wilson Drive, refer to Figure 3.2) needs to have line-of-sight with the prism. Line-of-sight was not possible with the 2 m pole in some areas due to the steep foredune. Instead, a 5 m pole was employed in the areas where the 2 m pole was not visible (Figure 3.9).

Figure 3.9: A map of the area surveyed with the 5 m prism pole.

The 5 m prism pole was problematic for a number of reasons. Firstly, it was difficult to carry, and it slowed down the survey. Secondly, even a slight breeze made it difficult to hold the prism level. Lastly, even though the prism could be seen from the total station, the person holding the total station could not be seen. To alleviate this issue handheld UHF radios were used to communicate. Another option was to move the total station to the foredune crest. However, in this case the total station was not moved, to ensure all of the observations were related to the same point (Site B Peg), and to avoid merging datasets.

The TLS requires line-of-sight with the surface; the TLS had to be set-up at nine locations, because the topography of Area B limited the line-of-sight. Consequently, this

increased the survey duration. Each scan is 8 minutes long, and the scanner then has to be moved and set-up at each location.

It was difficult to traverse the foredune with the total station and RTK-GPS range poles, due to the steep gradient. This is especially problematic in sandy environments because sand compacts when traversed, or steep slopes collapse which alters the elevation of the area by approximately 1-2 cm, or more. Care was taken to only step on areas that had already been surveyed, however, this can be difficult and there is no guarantee that the study area was not trampled. Both the prism and rover poles have a sharp point on the end which can fall through the sand. This issue is specific to sandy and similarly unconsolidated surfaces, and is avoided when using remote surveys such as RPAS.

Vegetation

Vegetation is a limiting factor for all methods. Dense shrubs such as *Coprosma repens* (Taupata) and *Lupinus arboreus* (tree lupin) restricted the total station and RTK-GPS surveys. The total station and RTK-GPS range poles were not always capable of obtaining measurements inside dense *C. repens* and *L.arboreus*. In such cases, points were taken as far through the vegetation as possible, or where the shrub was too dense, points were recorded directly next to it. This was expected to compromise the interpolation, however, the output surfaces showed agreement to the other surveys, suggesting that this was not the case.

The laser scanner and RPAS are remote surveys – points are collected from a distance. For both methods, the sensors record the surface elevation as opposed to the ground elevation. The TLS records the elevation of the first surface the laser contacts. The RPAS records elevation based on its ground sampling distance (GSD) (the distance between neighbouring pixels); the GSD for this flight was 2.5 cm^2, hence, the elevation was recorded for every 2.5 cm^2 area on the ground. Where dense vegetation is present, both methods record the vegetation canopy. Conversely, the total station and RTK-GPS record the elevation of the terrain itself. Consequently, the TLS and RPAS produce digital surface models as opposed to digital terrain models. The RPAS and TLS are not able to accurately quantify the ground morphology in densely vegetated areas. In some cases, it is desirable to capture the vegetation cover (Fraser et al., 2016). However, if accurate volumetric or elevation changes need to be calculated, the elevation values will be off-set by the vegetation height.

3.5.3 Efficiency

The results show that the RPAS is the most efficient surveying method, and requires minimal 'effort' to acquire the most point measurements. The RPAS had the shortest survey duration, with a total duration of 0.2 hours (10 minutes), this was over 60 times faster than the longest survey (the RTK-GPS, which had a total duration of 13.2 hours). The total station and RTK-GPS had similar survey durations, however, the RTK-GPS took 2.3 hours longer than the total station. This was unexpected, as other studies have shown that RTK-GPS surveys are typically faster than total station surveys (Bangen *et al.*, 2014). In this study, the difference was likely a result of the efficiency of the surveyor, and it should not be assumed that surveying with a total station is faster than surveying with an RTK-GPS unit. When the amount of "effort" was considered, the total station and RTK-GPS surveys were very similar; 178 and 171 points/hour, respectively. The RTK-GPS survey took longer to complete, however, more points were collected and as a result both the RTK-GPS and total station surveys collected a similar number of points per hour.

The RPAS recorded the highest number of points (~ 1 million), which is over 500 times more than the points recorded by the total station (1,936). The RPAS could, therefore, derive over 48 million points per hour. It should be noted that the RPAS survey duration (10 minutes) is of Area A, not Area B. Hence, surveying Area B would take less time. However, 'effort' does not account for the time taken to set-up each survey, nor the time it takes to process the data. The TLS and RPAS had the shortest surveying durations out of the four methods. However, both require the most time to set-up and process the data.

The total station set-up required the tripod to be levelled, and the surveying "job" set, which took approximately 10-15 minutes. The RTK-GPS set-up required the base station to be assembled and approximately 15 minutes for the base station and rover to gain communication with the surrounding satellites. There was minimal data processing required for both the total station and the RTK-GPS. This is because the data for each method is recorded via point measurements, hence, the data is already in the desired format for DTM generation. The processing required the data download (10-15 minutes) and the point interpolation (15 minutes).

The TLS set-up time was difficult to record because data was collected in sections, and the TLS was moved and set-up multiple times. Therefore, the total surveying time recorded in Table 3.1 includes the set-up of the TLS. GCPs were also required within the study area, which

needed to be surveyed to obtain the coordinates. The total data processing time took between 7 and 8 hours, from the data download, to the data "cleaning", point cloud extraction and then the interpolation to create a DSM.

The total set-up time for the RPAS is approximately 1 hour. The RPAS set-up includes the establishment of GCPs, and approximately 5 minutes to set-up the aircraft. Semi-permanent GCPs were established on John Wilson Drive, in the swale of the foredune, and on the foredune crest. Once the coordinates were obtained, the points were available as GCPs for subsequent flights. A line of temporary GCPs were established on the beach before each flight, and needed to be surveyed using the RTK-GPS. Permanent points could not be established on the beach due to the dynamic nature of this environment. The RPAS set-up time includes the time taken to set-up the RTK-GPS. Prior to each flight, white paper plates ('targets') were placed on the pegs in the swale of the foredune, and on the beach. The plates had to be retrieved following each flight.

The RPAS data took approximately 2-3 hours to process. The imagery download (between 50-85 images per flight) takes approximately 5-10 minutes. GCPs are marked in the images using photogrammetry software (40-60 minutes). The remaining processing was automated within the photogrammetry software and required 1-1.5 hours to generate the DSM and orthomosaic.

The RPAS is the most efficient method (3.2 hours), including the set-up and data processing duration. The total station, RTK-GPS and TLS, had relatively similar durations of 11.7 hours, 14.0 hours, and 11.2 hours. Therefore, not only does the RPAS collect the highest number of points in the smallest amount of time, it also requires the least time to conduct the survey. However, the results from this study largely reflect the topography of the study site. A site that is relatively flat could be surveyed by the total station and RTK-GPS in less time than what was found in this study.

Lastly, the equipment needed for one survey needs to be considered. This is important for transporting equipment, and for sites that are difficult to access and traverse. It can, therefore, be desirable to use light-weight equipment. The total station survey required the least equipment – the total station, a tripod, prism and prism pole (weighing a total of 16 kg). This equipment required minimal space, and can easily be transported by car. The RTK-GPS kit is larger and included two 'pelican' cases (protective cases) that hold the equipment for each receiver, and together weigh approximately 19 kg. A tripod, two 2 m range poles, a bipod, and

an external antenna were also required. The RPAS itself requires the least equipment (with a total weight of 11 kg), however, to geo-reference the survey, GCPs needed to be established which also required the RTK-GPS. The TLS had the most equipment, including; 5 tripods, 3 geo-referencing spheres, the total station kit, and the laser scanner itself. The study site in the current study was easily accessed, however, in a situation where the study site is difficult to access, and equipment has to be manually transported, in such cases the TLS might not be suitable.

3.5.4 Cost analysis

The results from the cost analysis show that the laser scanned survey was the most expensive with an approximate total cost of $83,661. This was approximately $36,000 more expensive than the RPAS survey (the second most expensive). The RPAS survey had a total cost of $47,064, however, this included the price of the RTK-GPS equipment. The use of RTK-GPS was necessary in this study to survey the GCPs, however, a total station could have been used instead. Another option is to purchase the RPAS, and hire a surveyor to survey the GCPs.

Hiring the TLS equipment is the most expensive ($1,000-$1,250/day), and hiring an RPAS is the least expensive ($135). However, the RPAS hire is for a DJI Phantom 3 Professional, from a drone hire website. More expensive, purpose-built surveying drones are generally not available for hire. However, a surveyor can be hired to conduct a RPAS survey. Compared to the other methods, hiring an RPAS surveyor is more expensive than hiring a total station or RTK-GPS surveyor. However, RPAS surveys have the capacity to survey large areas efficiently, hence, RPAS surveys are more cost-efficient for surveying large areas.

3.5.5 Model accuracy and precision

All of the surveying methods, except for the RPAS, produced DTMs/DSMs with millimetre vertical accuracy. The RPAS DSM had a ME of –3 cm. Interestingly, the total station and RTK-GPS DTMs both had RMSE of 10 cm, despite the methods themselves being capable of recording points with millimetre-centimetre vertical accuracies (Eamer and Walker, 2013; Lee *et al.*, 2013). This is attributed to the density of points collected by each method. The TLS and RPAS surveys both collected millions of 3D points, resulting in high density point clouds. The total station and the RTK-GPS surveys obtained approximately 2,000 3D points in each dataset. The interpolation estimates the elevation in the gaps between the data points to create a 3D surface. Therefore, the total station and RTK-GPS datasets have more areas with an unknown elevation. Hence, it is expected that the TLS and RPAS DSMs are more

precise, because the interpolation had more points to estimate the unknown areas. However, the accuracy and precision is calculated using the cross validation method. This only determines how close the surface is to the elevation of the points in each dataset. Therefore, precision and accuracy of the surface model depends on the precision and accuracy of the data points. The RPAS accuracy and precision was calculated using the LOOCV method, using the ground control points in the survey. The GCPs were surveyed using the RTK-GPS unit. Therefore, the vertical accuracy and precision values of the RPAS survey are reliant on the accuracy of the GCPs. The GCPs had a vertical precision of 2 cm.

The cross validation suggests the TLS DSM is the most accurate and precise, however, the comparison of the surfaces show that the TLS surface deviates from the other surfaces. In areas with vegetation the TLS surface is below the other surfaces. The TLS data was 'cleaned' before it was received for subsequent analysis, this involved noise removal from the dataset; noise can be caused by vegetated (Whitehead and Hugenholtz, 2014). The results suggest that the noise removal has caused the TLS surface to deviate, as the surface is lower than the surfaces produced by the other methods, only in the vegetated areas.

The RPAS DSM is more textured compared to the total station and RTK-GPS DTMs. In the vegetated areas, the DSM is higher than the DTMs. However, on the beach and John Wilson Drive, the RPAS surface overlays the DTMs.

3.6 Conclusions

The results from this chapter have shown that surveying a coastal foredune using a low-cost RPAS is comparable with other coastal surveying methods. There are a number of atmospheric and environmental limitations for this type of surveying method, however, the limitations are also often associated with other surveying methods. In many cases rain and sunlight can be avoided, however, strong winds can be restricting, especially when the area of interest is the coast.

RPAS surveying was the most efficient method examined. The RPAS is capable of collecting millions of data points over a short period of time, which is especially beneficial for surveying areas of variable topography. The RPAS survey is also cost efficient, however, there is a high cost associated with the purchasing the software. The Pix4D software used in this study is one of the most expensive RPAS photogrammetry software packages available, however, comparably inexpensive photogrammetry software is available.

The accuracy and precision of DSMs is important for reliable coastal morphology analysis, especially when volumetric and elevation changes are calculated. The RPAS produced a DSM with a ME of -3 cm, and a RMSE of 8 cm. The RPAS DSM was not the most accurate nor the most precise of the DTMs/DSMs in this study. However, the RPAS DSM did have a higher vertical precision than the total station and the RTK-GPS DTMs. Overall, small, low-cost RPAS have the potential to be used more widely for surveying coastal morphology.

Chapter 4

Quantifying morphologic changes of a coastal foredune

4.1 Introduction

This chapter is focussed on quantifying morphologic changes and foredune morphodynamics, using a small RPAS. The morphology of a foredune is indicative of factors such as sand supply, vegetation presence, vulnerability to erosion, and human interference (Hesp, 2002). Foredunes are one of the most seaward features of sandy coasts and are directly exposed to wind and wave action (Benavente *et al.*, 2013). Foredunes often act as coastal defence mechanisms by absorbing wind and wave energy (Bochev-van der Burgh *et al.*, 2011; Taylor *et al.*, 2015). Monitoring changes in foredune morphology can provide clues to the processes influencing the morphology, and predictions for future morphologic change (Saye *et al.*, 2005).

Sandy coasts are dynamic environments that are susceptible to short/medium-term change occurring on timescales ranging from days to month. Changes at such time scales are typically a result of erosion and scarping, often caused by waves during storm events (Dissanayake *et al.*, 2015). Quantifying changes in foredune morphology can indicate areas vulnerable to erosion. Short-term changes in morphology may be part of a long-term cycle. For example, a study conducted by Gares and Nordstrom (1995) found that dune blowouts (gaps in the dune initiated by the destabilization of sediment) in the short-term, experience a number of morphologic stages that lead to a larger overall long-term change. Long-term (years to decades) changes in foredune morphology can result from a number of factors. For example, the dune could be recovering from erosion, which can occur over years (Benavente *et al.*, 2013). The dune could be undergoing a constant long-term change, as a result of factors such

as a change in sediment supply or stabilisation of the dune by vegetation (Seeliger *et al.*, 2000; Psuty, 1993).

Monitoring morphologic changes is important for identifying trends in foredune movement, and the management of such systems (O'Shea and Murphy, 2013). For example, in the long-term, both the establishment of vegetation on a foredune (Rozé and Lemauviel, 2004), and the de-vegetation of a foredune (Konlechner *et al.*, 2016), can alter the foredune morphology. Long-term monitoring can quantify the change, and highlight the causes of the change over an extended period of time. In the short-term, monitoring can quantify morphologic change caused by isolated events, such as the effects of storms.

RPAS technology can be a useful tool for monitoring morphologic change (Gonçalves and Henriques, 2015). Monitoring short to medium-term changes in coastal foredunes requires prompt, efficient and short-notice surveys, all which can be achieved with a small, low-cost RPAS. If low-cost RPASs can derive accurate and precise morphologic information, this technology would be an effective tool for monitoring coastal dune systems.

The aim of this chapter is to investigate the second research question; *how can data recorded by a low-cost RPAS be used to quantify morphologic change in a coastal foredune?* To explore this research question a Phantom-3 Advanced RPAS was used to obtain aerial photographs of the study area, to create digital surface models (DSMs). Four flights were conducted over the study area to identify short and medium-term morphological change. An initial flight was undertaken to assess the robustness of the ground control/check point configuration using the *leave one out cross validation* method (LOOCV), and to assess the variability associated with the self-calibration of the sensor's interior orientation parameters (IOPs). The GCP network established for subsequent flights was decided based on the robustness of the GCP configuration in Flight One. The residuals and IOPs were assessed from each flight and compared to assess the robustness of the photogrammetric model. The insight gained from assessing the IOPs and the residuals allowed an informed assessment of the quality of the DSMs produced from each flight. The DSMs were corrected for the model bias, and were then used to spatially resolve morphologic change of the St. Kilda foredune. Elevation change surfaces (ECS) were produced, and the volumetric changes were computed to investigate the morphological change of the study site over the four month period.

This chapter starts with a description and justification of the study site. The method section explains the analysis of the first flight in detail, and the importance of this assessment.

The methods employed for the assessing subsequent flights are then explained. Lastly, the methods section explains the steps taken to derive ECSs, and the associated errors. The results section uses the same structure as the methods section, and presents the results of the residual and lens assessments. This chapter concludes with a discussion of the findings and a summary of the key findings in relation to the research question addressed in this chapter.

4.2 Study site

The RPAS surveys were conducted at St. Kilda beach, Dunedin. The site was divided into three sections; Area A, B and C. Area A is approximately 400 m long, and 85 m wide, encompassing the St. Kilda foredune and the beach. The autonomy of the battery limited the size of the site, and two flight lines along the 400 m stretch of coast required the entire battery capacity. Area A was chosen because it has undergone erosion in the past. Therefore, if the dune were to erode during this study, the morphologic change could be quantified from the RPAS imagery.

Areas B and C are subsections of Area A, and were selected to quantify short-term morphologic change. Areas B and C encompass three constructed notches, designed to investigate sedimentation and deposition in the lee of the foredune. The sites, therefore, provided an opportunity to test the RPAS for quantifying short/medium-term morphologic changes through the notches. The study site is outlined in Figure 4.1.

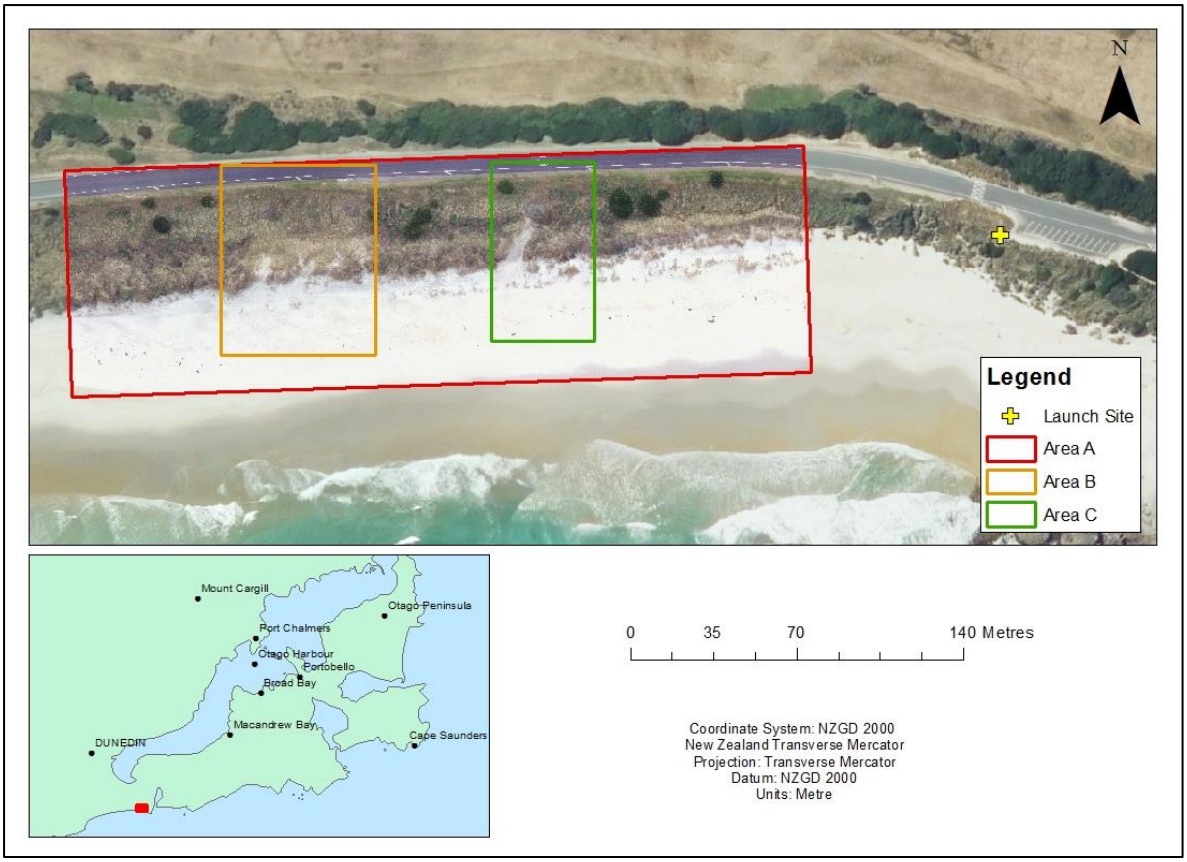

Figure 4.1: A location map of study Areas A, B and C, at St. Kilda beach, Dunedin.

4.3 Methods

This section explains the methods employed to investigate the validity of photogrammetric modelling using low-cost RPAS photography, and to quantify morphologic changes in the study areas. The RPAS was flown on four occasions to gather aerial photographs of the site. The first flight was used as a base survey for determining morphologic changes from subsequent flights, and to assess how the GCP configuration affected the quality of the DSM. The GCP layout for subsequent flights was determined based on the results from the initial flight. At least two processing scenarios were conducted per flight to assess the GCP and check point residuals. The GCP and check point residuals, and the IOPs from all of the scenarios for each flight were compared to understand the error resulting from this type of low-cost sensor. The associated bias was corrected in the DSMs from each flight, and hence, could be used for subsequent morphologic analysis with a mean error (ME) of 0.

ECS were derived from the DSMs from each flight, and were used to estimate volumetric changes. Three time periods were chosen to quantify the changes. The first epoch was between the 8th (Flight One) and the 24th of May (Flight Two), which encompassed a storm

event occurring between the 16th and the 23rd of May. The second epoch was between the 14th of June (Flight Three) and the 10th of September (Flight Four), and encompassed a storm event on the 7th of September. The final epoch was from the 8th of May to the 10th of September (the entire four month study period). Elevation and volume change analyses were conducted in ArcGIS.

4.3.1 Flight planning

A DJI Phantom-3 Advanced quadcopter employed used for the RPAS survey. A Sony EXMOR 1/2.3" (sensor size 6.17 × 4.55 mm) 12.4 megapixel camera was attached, with a field of view of 94° and a 20 mm lens (in 35 mm equivalent) that was focussed at infinity. The infinity focus prevents the "zoom" from being used, and therefore, keeps the sensor's internal geometry consistent by maintaining the focal length between images. A change in focal length causes more distortion in the output surface (Sanz-Ablanedo *et al.*, 2012). Each image contained 4000 × 3000 pixels.

Flight planning software was not employed; photographs were captured manually during the flight. The individual flight paths differ slightly, as a consequence of manually capturing the photographs. The sensor information was used to estimate the 'real' focal length, using the following equation:

$$f_R = \frac{f_{35}\, S_W}{34.6}\ , \tag{4.1}$$

where f_R is the real focal length measured in millimetres, f_{35} is the focal length in the 35 mm equivalent, and S_w is the sensor width. The flying height to obtain a ground sampling distance (GSD) of 2.5 cm^2 was determined using the following equation:

$$H = \frac{f_R\, n_W\, GSD}{S_W}\ , \tag{4.2}$$

where n_w is the number of pixels forming the width of the sensor. To achieve a GSD of 2.5 cm^2, the height of the aircraft should be at a maximum of 57.8 m above the ground. For each flight, the RPAS flew at 50 m (+/- 0.5 m) above the launch site which was approximately 19 m above mean sea level. The same launch site was used to deploy the aircraft for each flight (Figure 4.1). This particular location was chosen because it gives a clear view of the entire study site (Figure 3.4).

The image footprint was calculated to determine the distance the RPAS needed to travel between subsequent photographs to obtain a forward image overlap of 85% and side-lap of 70%, believed to be an appropriate compromise to ensure satisfying photogrammetric modelling while being within the RPAS endurance. The approximate dimensions of the rectangular footprint of each image were calculated by multiplying the number of pixels in the width and length of each image by the desired GSD. The minimum distance between pictures to achieve the desired 85% forward overlap was computed as 11.25 m. During image acquisition in the field, photographs were taken approximately every 10 m.

The image footprint was also used to determine the flight path. The width of the study area was approximately 85 m, therefore, 70% side-lap was easily achieved with two parallel flight lines. The entire study area could have been covered by one flight line, however, at least two flight lines are required to strengthen the photogrammetric model using image side-lap as well as forward overlap.

Flights were weather dependent and were only planned a few days in advance. Mornings with very light winds (<5 ms^{-1}) and overcast skies were preferred. In some cases there were clear skies, causing the sun to cast a dark shadow over the swale behind the foredune. This created a strong contrast between shadowed areas and illuminated areas, making it difficult to identify features. Due to the saturation of the images caused by the illumination, some of the photographs could not be processed in Pix4D, however, there were enough suitable images processed to create a DSM and orthomosaic. Figure 4.2 shows a section of the study area on a cloud-free day, and an overcast day.

Figure 4.2: Photographs taken by the RPAS on separate days, the photograph on the left was taken in clear-sky conditions, and the photograph on the right was taken during overcast conditions.

Additional ground control points were established on the day of each flight, and then removed after the flight. The layout of the points depended on the survey taking place. For the initial survey which covered the entire study area, ten temporary points were used in addition to the thirteen permanent points (Figure 4.3).

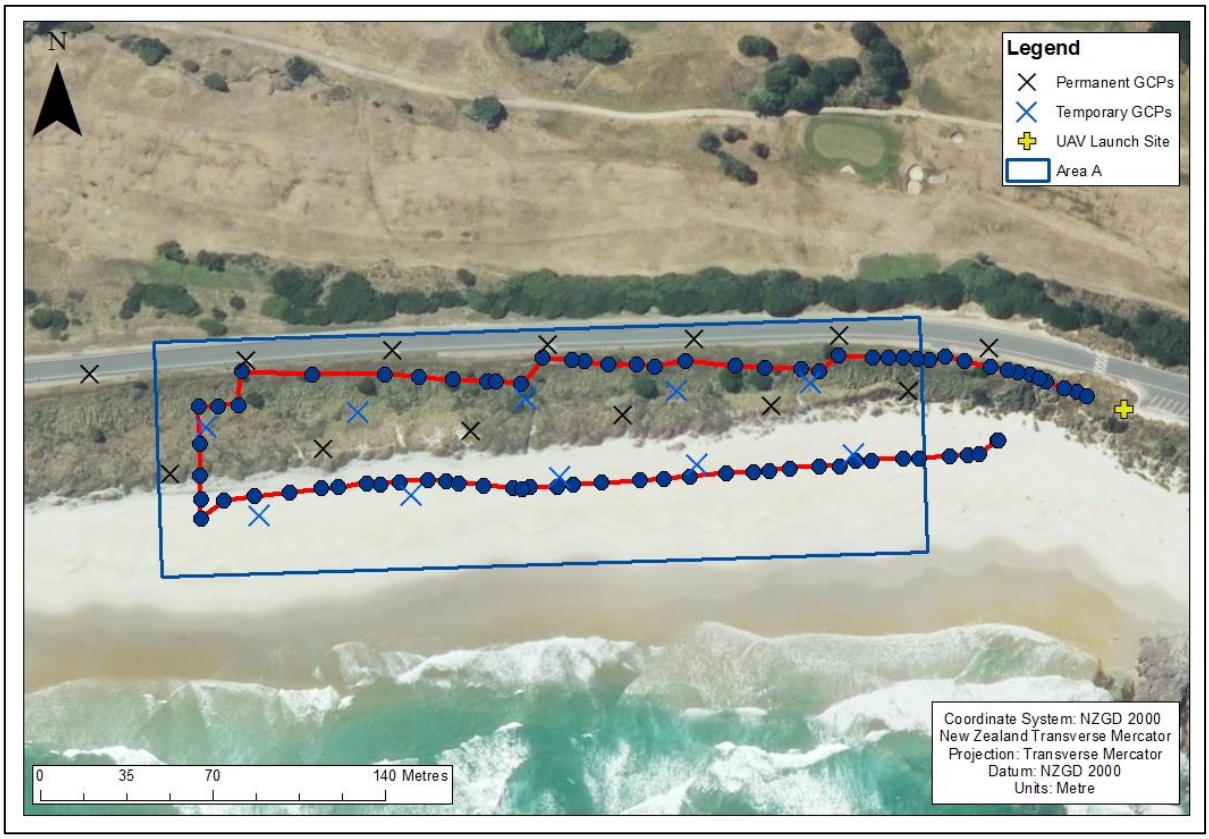

Figure 4.3: The ground control point configuration for Flight One.

The temporary points were established in two lines; one along the beach, and the other in the swale of the foredune. This particular layout was selected to account for the major elevation differences in the study area – the beach, foredune, swale, and John Wilson Drive (Figure 4.4).

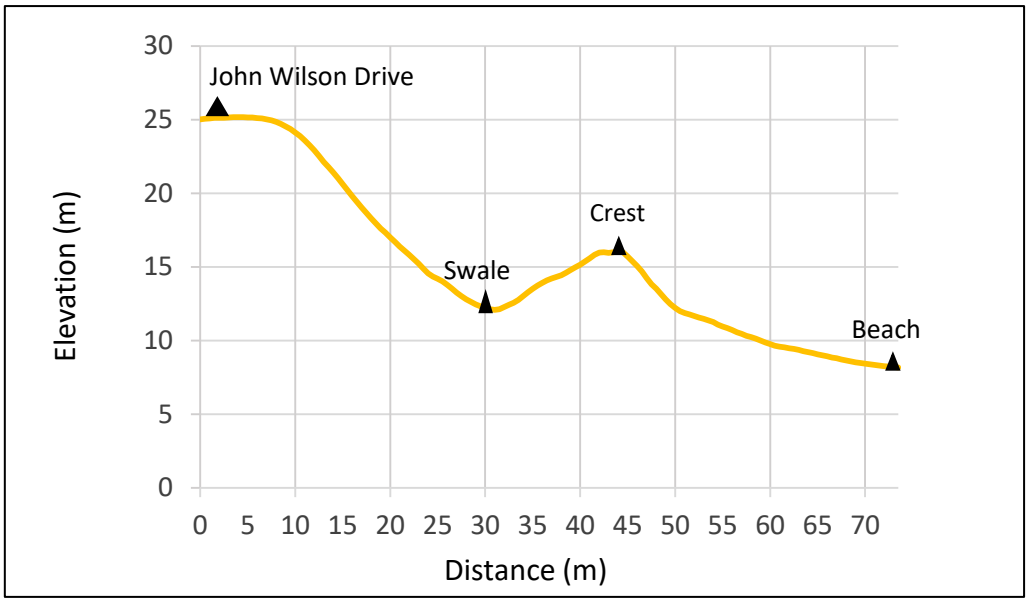

Figure 4.4: A cross section through the study site, depicting the location of the four lines of GCPs. The elevation is relative to the GRS80 ellipsoid.

The layout of the GCPs was also used to test the sensitivity of the DSM reconstruction to the GCP configuration, and to determine the number and configuration of GCPs required for subsequent surveys. Foam mats 60 cm × 60 cm in size, with targets painted on top were used for the initial survey (Figure 4.5a). White paper plates (26 cm in diameter) were used for subsequent flights (Figure 4.5b).

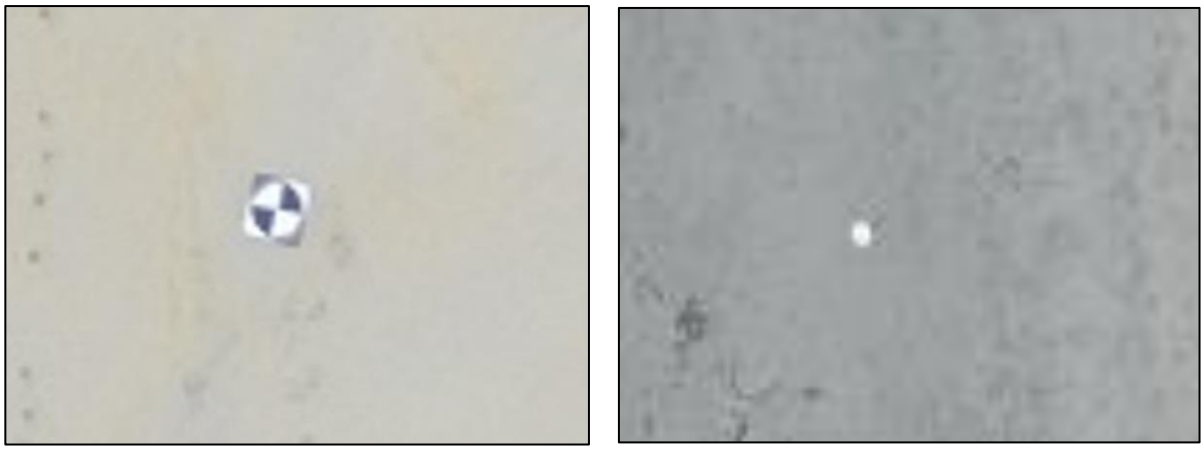

Figure 4.5: a) 60 cm x 60 cm foam mats used as temporary points for the initial flight; b) 26 cm diameter white paper plates used as the temporary points for Flights Two, Three and Four.

All of the points were surveyed using a Trimble R8 RTK-GPS unit. The permanent points were surveyed with an occupation time of 1 minute, and the temporary points were surveyed with an occupation time of 2 minutes. All of the points were intended to be surveyed for 2 minutes, however, a mistake in the field resulted in the permanent points only being

surveyed for 1 minute. The PDOP value describes the strength of the configuration of satellites (Lemmon and Gerdan, 1999). When the PDOP is low (below 2), there can be confidence that the position of the point recorded is precise, because the number of satellites and configuration of satellites is optimal (Lemmon and Gerdan, 1999). The average PDOP for the permanent points was 1.247. All of the points were recorded in the New Zealand Transverse Mercator coordinate system, and elevations were relative to the GRS1980 ellipsoid. The PDOP values, horizontal and vertical error for each point were recorded by the RTK-GPS unit. The permanent points had an average horizontal precision of 0.011 m, and an average vertical precision of 0.016 m. The PDOP, horizontal and vertical precision for the temporary points of each flight are presented in the corresponding subsections (Sections 4.3.3 and 4.3.4).

4.3.2 Civil Aviation Authority (CAA) regulations

The RPAS surveys were controlled under Part 101 of the CAA RPAS flight regulations. The RPAS operator, the author, was required to complete a Wings Badge flying test from the local MfNZ club (Model Flying New Zealand) because the study site was located within 4 km of the Kitchener Street helipad (Figure 4.6), and to meet the University of Otago Geography Department RPAS flying policy.

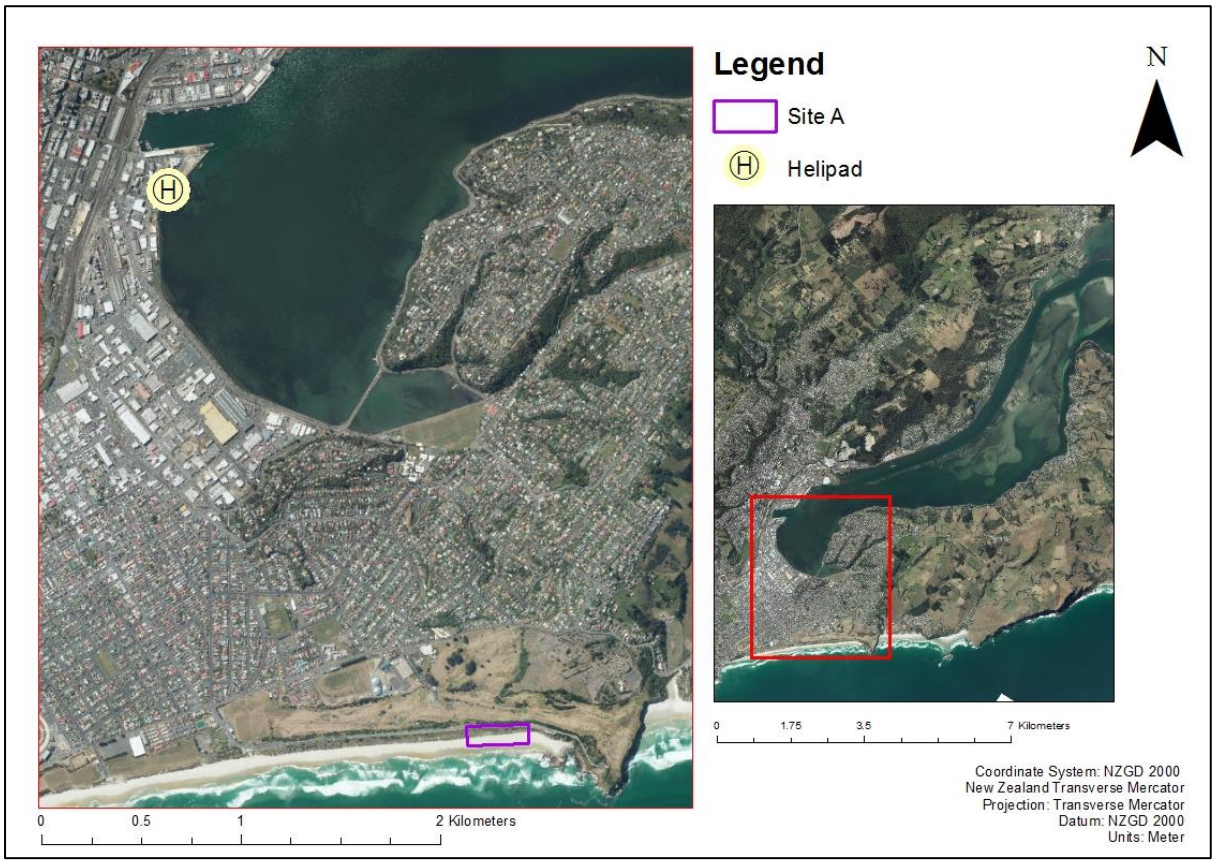

Figure 4.6: A map showing the location of the Kitchener Street helipad in relation to the study site.

Part 101 also states that the operator must obtain landowner permission prior to the flight. In this case, the St. Kilda foredune is council land, and permission to conduct multiple flights throughout the year was granted by the Dunedin City Council. In addition, permission from any person directly beneath the flight needs to be granted. John Wilson Drive is a popular location for dog-walkers, and is closed to motor vehicles between 11 am and 3 pm daily. To avoid flying over people in the area, flights occurred between 8 am and 9 am. This also meant that moving cars were not captured in the photographs, which would create blurs in the images and negatively impact image processing. Orange road cones were placed on John Wilson Drive at both ends of the study area, as well as on the beach. Each cone had an information sign explaining the flight, approximate flight time, and included the contact number of the operator. A colleague in a Hi-Viz vest stood at the edge of the study area where dog-walkers begin the walk along John Wilson Drive, explaining the flights to people entering the flight zone. A second person was stationed with the RPAS operator as a "spotter". The "spotter" is a second

set of eyes, who watches the RPAS for the entire duration of the flight, and warns the operator of any potential hazards.

All of the flights in this study were registered on the Air Share website. Due to the proximity of the study site to the Kitchener Street helipad, each flight needed to be confirmed by ringing the Dunedin Air Traffic Control Tower (ATC) at least one hour before the flight. Following this, ATC were called two minutes before take-off, to confirm the flight time, and contacted a third time once the flight was completed.

4.3.3 Flight One

The first flight was completed on the 8th of May 2016, over Area A. Flight One was also employed to test the effect of the GCP configuration on the photogrammetric reconstruction (Figure 4.4). The temporary points were laid out prior to the flight, and surveyed using RTK-GPS with an occupation time of 2 minutes. The temporary GCPs had an average PDOP of 1.350, a horizontal precision of 0.009 m, a vertical precision of 0.012 m, and a RMSE of 0.003 m.

The RPAS camera was positioned nadir (with the lens pointing to the ground), and the RPAS was stopped approximately every 10 m to capture the images. The RPAS was flown 50 metres (+/- 0.5 m) above the launch site, which is located approximately 19 m above MSL. A total of 83 photographs were captured. Altitude was recorded internally by the RPAS, and is measured using barometric pressure. Figure 4.4 shows the flight route, and the location of each photograph.

Images obtained from Flight One were uploaded into Pix4D Mapper software for processing. The images and GCP coordinates from the RTK-GPS surveys were uploaded to conduct the initial processing within the software. The images underwent four processing scenarios. Firstly, all of the points were marked as 3D GCPs, using the *Ray Cloud* to identify the images that contained each point. The point cloud was "re-optimized" once the points were marked in the images. For the second scenario, every second point was marked as a "check point", and the point cloud was "re-optimized". This scenario was an independent assessment of the quality of the model, using a conservative number of GCPs. The third scenario tested a GCP layout only surrounding Area B. This scenario used all of the permanent GCPs, and the temporary GCPs that were within Area B. For the LOOCV method, each point was marked iteratively as a check point, while the remainder were marked as 3D GCPs. The residuals were analysed to identify the points that caused the residual value to increase when marked as check,

and any outliers could, therefore, be identified. The residuals and internal camera parameters were recorded after each re-optimization. The residuals (x, y and z) of each point (at this stage all marked as 3D GCPs) were recorded, along with the interior orientation of the sensor (the focal length; principal point of autocollimation (PPA); radial distortion; and tangential distortion).

The LOOCV assessed the robustness of the photogrammetric model. Modern photogrammetry solves the interior orientation parameters (IOPs) and exterior orientation parameters (IOPs) concurrently in the bundle block adjustment (BBA), as opposed to traditional photogrammetry which only uses the BBA to solve for the EOPs. Modern photogrammetry, therefore, requires the BBA to solve a greater number of parameters with the potential correlation between EOPs and IOPs that can yield suboptimal solutions and compromise the robustness of the model. A study conducted by Sirguey *et al.* (2016) investigated the ability of BBAs for accurately determining IOPs and EOPs simultaneously. The study compared different photogrammetry software for solving the IOPs and EOPs of a photogrammetric model produced from RPAS imagery, it also investigated the impact of different GCP configurations on the model. The study found discrepancies in BBA results between the different software, and a reliance on a strong GCP network to produce an accurate photogrammetric model. Hence, indicating that the BBA may not sufficiently resolve both IOPs and EOPs, which can produce errors in the output surface. Therefore, the current study investigated the solution of the IOPs via the LOOCV.

Pix4D reports the radial distortion parameters as R1 pixel^{-2}, R2 pixel^{-4}, and R3 pixel^{-6}, which needed to be converted to K1 mm^{-2}, K2 mm^{-4} and K3 mm^{-6} to use in the Brown (1966) distortion model. The radial distortion parameters reported by Pix4D were converted using the following equations:

$$K1 = \frac{R1}{f^2}, \tag{4.3}$$

$$K2 = \frac{R2}{f^4}, \tag{4.4}$$

$$K3 = \frac{R3}{f^6}, \tag{4.5}$$

where f is the corresponding focal length in millimetres. To assess the robustness of the photogrammetric model, the radial distortion curve corresponding to each GCP scenario was

plotted. The radial distortion (Δr) was calculated with the distance from the image centre (r) using the following equation:

$$\Delta r = K1 \times r^3 + K2 \times r^5 + K3 \times r^7 . \quad (4.6)$$

4.3.4 Subsequent flights

Following the initial flight, three subsequent flights took place to capture changes in morphology over the four month period. The timing of each flight was determined by the occurrence of south-westerly storm events causing visible sediment deposition through the notches. The GCP configuration of the subsequent flights was decided based on the results of the first flight.

Flight Two occurred on the 24th of May, and aimed to capture the sand deposition facilitated by storm events between the 16th and the 23rd of May. Area A was flown, however, the area of interest was Area B. Hence, temporary GCPs were only established surrounding Area B. The temporary GCP layout was determined based on the findings from the Flight Two simulation conducted with the Flight One GCPs. Five temporary points were established in total, two in the swale of the dune, and three on the beach in front of the foredune (Figure 4.7).

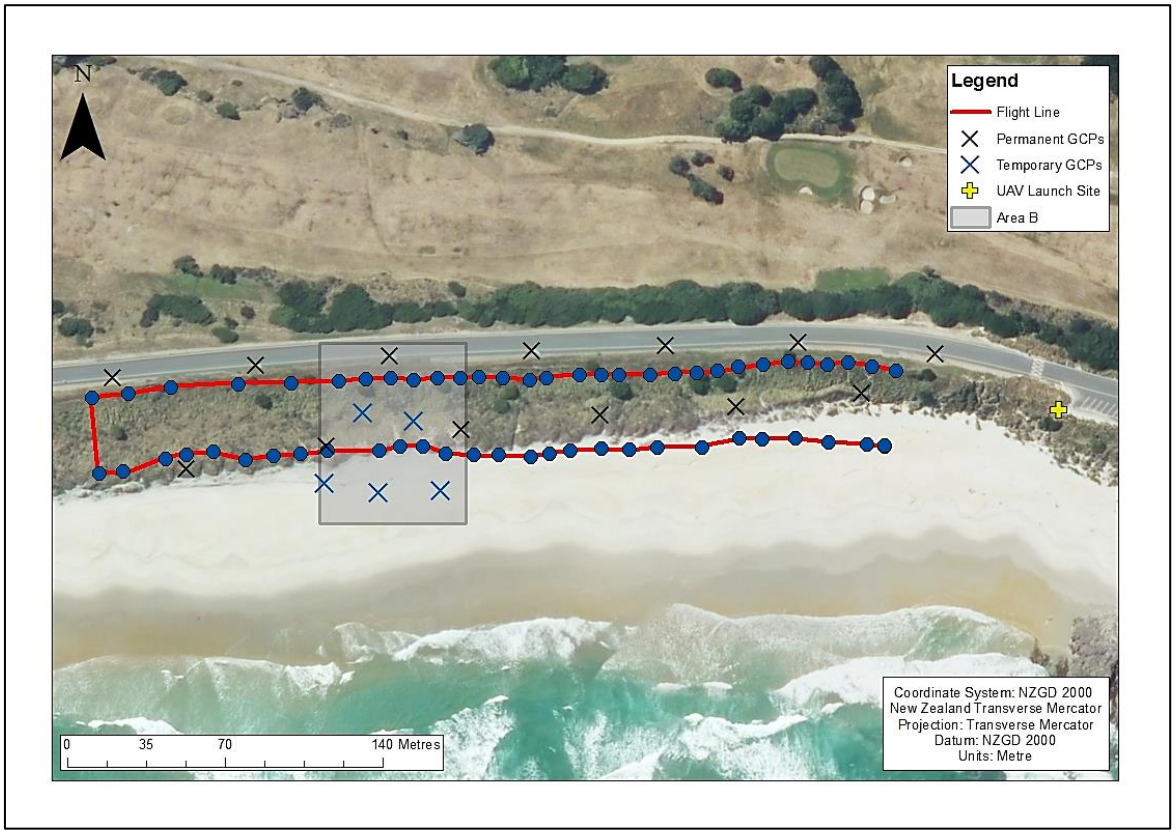

Figure 4.7: A map showing the Flight Two path, and the GCP layout. The blue dots represent the location each image was taken, the black crosses are the location of each permanent GCP, and the blue crosses are the temporary GCPs.

The GCPs were white paper plates nailed to the top of a wooden peg in the ground. The points were surveyed using RTK-GPS, with an occupation time of two minutes. The points had an average PDOP value of 1.377, a horizontal precision of 0.010 m, a vertical precision of 0.015 m, and RMSE of 0.003 m. A total of 58 photographs were taken.

Flights Three and Four were conducted on the 14th of June and the 10th of September, respectively. A total of 58 photographs were taken in Flight Three, and a total of 73 in Flight Four. Both flights covered Area A. Figure 4.8a and 4.8b show the flight paths for each flight.

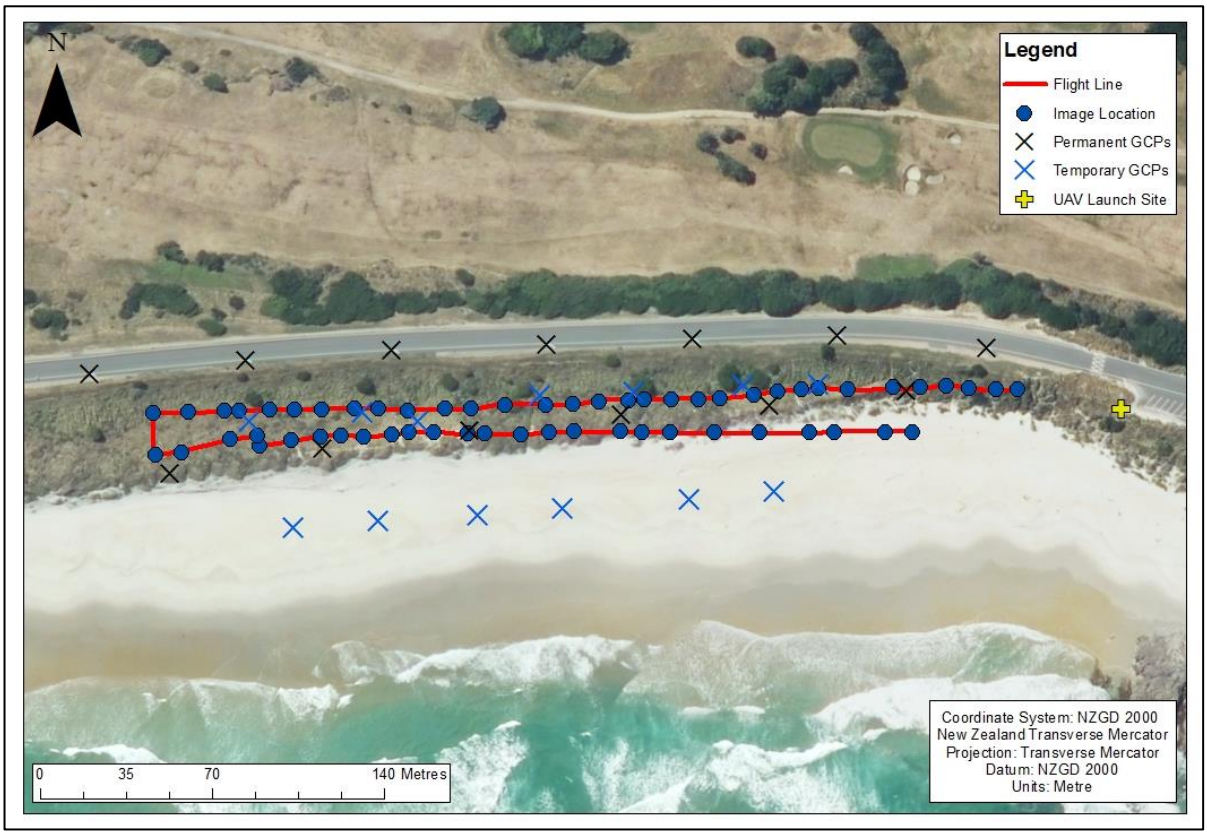

Figure 4.8a: A map showing the Flight 3 path, and the GCP layout. The blue dots represent the location each image was taken, the black crosses are the location of each permanent GCP, and the blue crosses are the temporary GCPs.

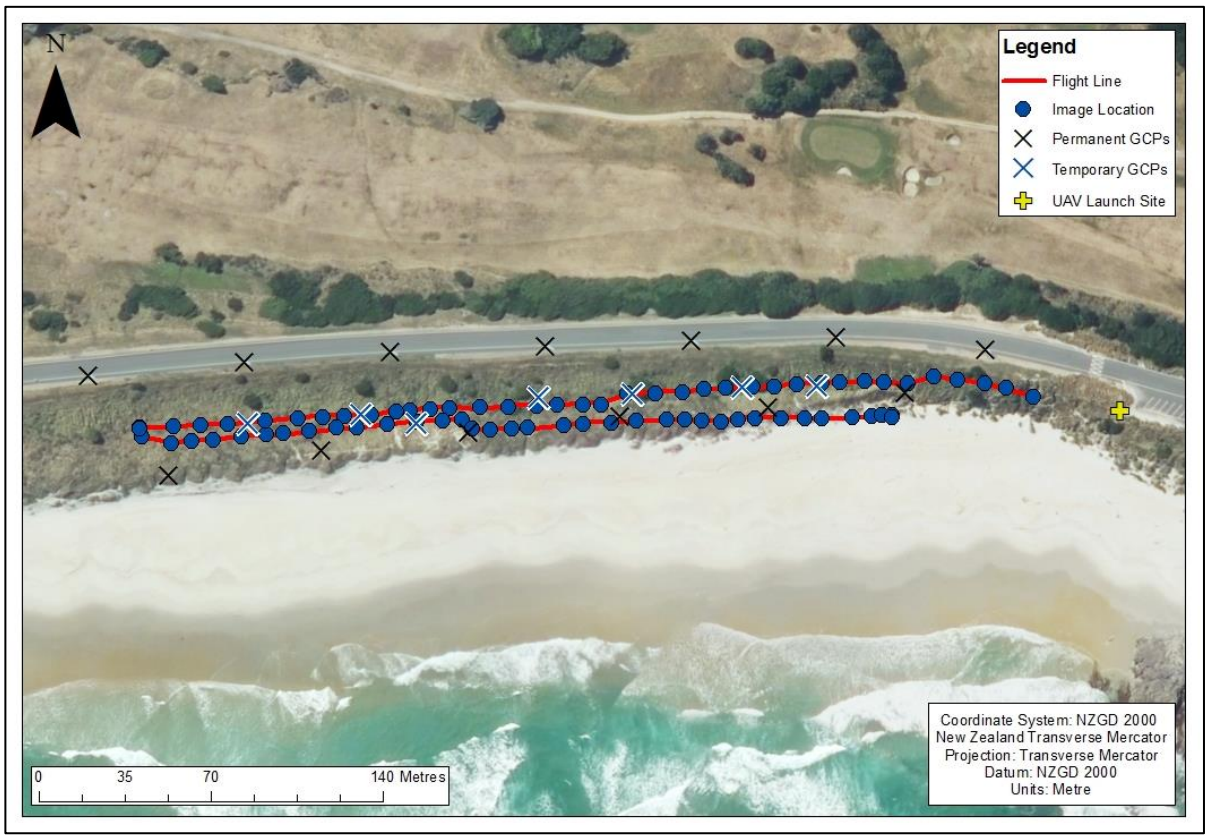

Figure 4.8b: A map showing the Flight 4 path, and the GCP layout. The blue dots represent the location each image was taken, the black crosses are the location of each permanent GCP, and the blue crosses are the temporary GCPs.

Six temporary GCPs were established on the beach for Flight Three, using the RTK-GPS unit with an occupation time of 2 minutes. The temporary points from Flight Three had an average PDOP value of 1.390, an average horizontal precision of 0.010 m, an average vertical precision of 0.017 m, and a RMSE of 0.004 m.

Flight Four did not use beach ground control because the GCPs on the foredune, in the swale and on John Wilson Drive, encapsulated the area in the lee of the notches. The GCPs in the swale of the foredune (wooden pegs hammered into the ground) remained in the ground from Flight 3, and did not need to be resurveyed. White paper plates were placed on top with the nail in the centre. The points in the swale had an average PDOP value of 1.414, an average horizontal precision of 0.013 m, an average vertical precision of 0.017 m, and a RMSE of 0.003 m.

As shown in Figure 4.8a and 4.8b, the parallel flight lines are close together. This is a downfall of manually conducting the survey, as opposed to employing flight planning software. The flight lines should be located further apart, to ensure optimal image overlap and ground coverage. The images were still processed, however, to ensure accurate photogrammetric modelling, it is recommended that the flight lines should be spaced further apart, and a third flight line implemented. The number of flight lines, however, was restricted by the capacity of the RPAS battery.

4.3.5 Pix4D Mapper processing

Data processing within Pix4D Mapper involves three steps, 1) Initial Processing; 2) Point Cloud, Mesh and DSM and; 3) Orthomosaic and Index. Images from each flight were uploaded into Pix4D Mapper for processing. The EXIF metadata is extracted from each image by Pix4D Mapper, and is used to initiate the data processing. The software conducted a BBA, to solve the IOPs (focal length, PPA, radial and tangential distortions) and the EOPs (x, y, z, ω, δ, κ) concurrently. Each image is comprised of a number of 'image rays', referred to as a bundle. A BBA is used to calculate the position and orientation of each image ray, which orientates each image in space. Chapter 2, Section 2.2.4 gives an in-depth explanation of the BBA. Pix4D Mapper reports the results from the BBA in a Quality Report.

Following initial processing, point coordinates for the ground control and check points were uploaded into the software and marked in the images using the *Ray Cloud*. Pix4D Mapper detects the approximate location of the points in the images, and then the user marks the specific location of the points. When marking the point location, the user selects each point as

either a 3D GCP or a check point. The initial processing step is repeated ("re-optimized") when all of the points have been marked, producing a new *Quality Report*. The software uses this data to produce a densified 3D point cloud and textured mesh. Lastly, a DSM, orthomosaic and index map are created.

Flights Two, Three and Four were processed using two different scenarios. The first scenario for all flights have each target marked as a 3D GCP. The DSM produced from this scenario was used to produce the ECS from which volumetric changes could be computed. It was assumed that this fully controlled scenario led to the best representation of reality. The second scenario had every second GCP marked as a "check point". Check points were used as an independent assessment of the quality of the model and were compared to the residuals from the LOOCV for Flight One. The 3D GCP and check point residuals, and the IOPs were recorded for each flight and scenario. The quality of each DSM was assessed using the ME and the root mean square error (RMSE) of the residuals. The RMSE reported assumes a random distribution over the DSM produced with no spatially constructed bias. However, the RMSE is often misleading as systematic bias exists in the surface (Sirguey *et al.*, 2016). This can be particularly sever outside of the confines of the GCPs where departure of the modelled surface from reality can become large, due to suboptimal modelling. Error outside of the GCP configuration is systematic, however, this is not modelled within Pix4D Mapper. Therefore, morphologic change analysis was only conducted in areas within the GCP network. The IOPs were compared between flights and scenarios to investigate the robustness of photogrammetric modelling using a low-cost camera. The residuals and IOP analysis permitted to characterise the morphologic change analyses, and estimate where significant changes could be inferred.

4.3.6 Morphologic change

Elevation and volumetric changes were calculated to describe morphologic changes. The changes have been categorized into short and medium-term changes. Area B was used to assess short-term changes, because it contains two notches expected to facilitate sand deposition at the event-scale. Medium-term changes were assessed in Areas B and C, over a four-month period to assess the overall sand deposition initiated by the notches. Three key epochs were used to assess the short-medium term changes; the May storm event, the September storm event, and the overall study period.

All of the morphologic change analyses were conducted in ArcGIS 10.2. To derive ECSs, the Raster Minus tool from the *3D Analyst* toolbox was used, where the 'before' DSMs

were subtracted from the 'after' DSMs. The net gain, loss and change in volume for each epoch were quantified using the Cut/Fill tool from the *Spatial Analyst* toolbox. The ECS were adjusted for bias based on the ME from the input DSMs, therefore, the ME of the ECSs is 0.

The quadratic formula was used to calculate the precision of the ECS, based on the standard deviation of the input DSMs:

$$SD_{ECS} = \sqrt{{SD_{DSM2}}^2 + {SD_{DSM1}}^2}\,, \tag{4.7}$$

where SD_{DSM1} and SD_{DSM2} are the standard deviation of the input DSMs. A 90% confidence interval was used to identify the areas with statistically insignificant elevation change, namely where:

$$-Z_{\alpha/2} \times SD_{ECS} < ECS < Z_{\alpha/2} \times SD_{ECS}\,, \tag{4.8}$$

where $Z_{\alpha/2}$ = 1.64, and SD_{ECS} is the standard error of the ECS. From this, a map was produced that show the areas of statistically significant elevation change. The areas of gain, loss and no change in sediment in the lee of each notch were mapped and quantified. A 90% confidence interval was then used to determine whether the loss, gain and net change in volume was statistically significant, using equation 4.9.

$$Dv \pm Z_{\alpha/2} \times \frac{A\sigma}{\sqrt{n}}\,, \tag{4.9}$$

where Dv is the total volume change, $Z_{\alpha/2}$ = 1.64, A is the area, σ is the standard deviation n is the number of pixels.

4.4 Results

The purpose of this section is to present the results of this chapter. The results from Flight One are presented first because this flight was employed to test the suitability of the GCP network for subsequent flights. The results produced from the subsequent flights are presented in subsection 4.4.2. The two flight subsections (4.4.1 and 4.4.2) present the residual and lens/sensor robustness assessment. The final subsection (4.4.3) presents the results of the morphologic change analysis, taking into account the error of the photogrammetric model.

4.4.1 Flight One analysis

The first flight took place on the 8th of May 2016. A total of 79 photographs were collected. The GSD was 2.5 cm^2. The 3D densified point cloud produced 7,702,621 3D points. The DSM produced from this flight is presented in Figure 4.9.

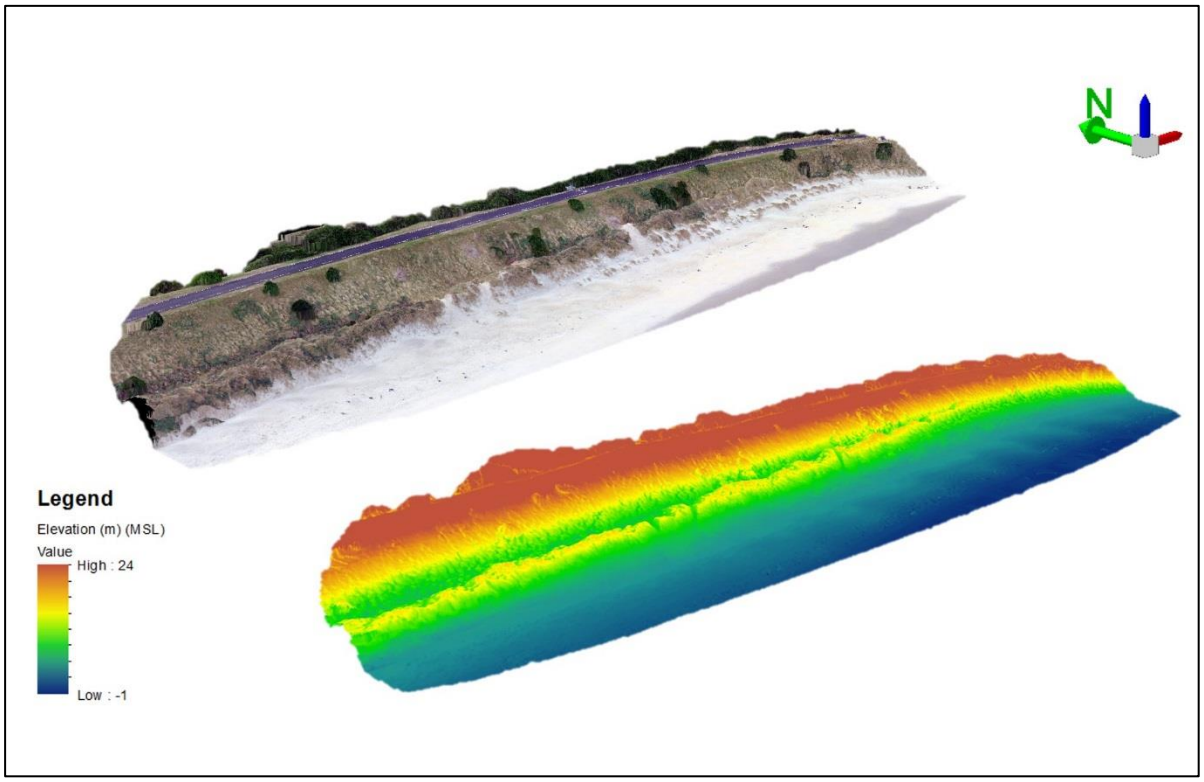

Figure 4.9: The orthomosaic and DSM produced from the Flight One imagery, an example of the outputs produced from the subsequent flights.

The results show the variation between residuals when different GCP configurations are used (Table 4.1a and b). When all of the points are marked as GCP, the residuals decrease because the output surface is controlled by all of the GCPs. Hence, this surface was employed for the subsequent morphologic change analysis. The x, y and z check point residuals from Scenario 2 are all 1 cm lower than the LOOCV check point residuals. The check point residuals from Scenario 3 were relatively higher than the other scenarios, with a z RMSE of 11 cm. This was likely due to the check points being outside of the GCP networks, and therefore, the exposure of the model to systematic error, as opposed to randomly distributed error. This indicates suboptimal photogrammetric modelling. However, Scenario 3 was used to test the GCP layout for Flight Two, where only Area B was of interest. The residuals from Scenario 3

suggest a better GCP layout should be reconsidered for Flight 2. The overall bias of the model, reflected by the ME z of the check point residuals, was 1 cm.

Table 4.1a: *The RMSE from the residual assessment of each Flight One scenario, 1. All GCPs; 2. Half GCP, CP; 3. Flight Two simulation; LOOCV.*

	Ground Control Points				Check Points			
Scenario	No. of Points	RMSE (m)			No. of Points	RMSE (m)		
		x	y	z		x	y	z
1	25	0.045	0.035	0.061	-	-	-	-
2	13	0.046	0.041	0.070	12	0.049	0.025	0.068
3	15	0.030	0.022	0.048	10	0.091	0.054	0.108
LOOCV	-	-	-	-	25	0.058	0.043	0.080

Table 4.1b: *The ME from the residual assessment of each Flight One scenario, 1. All GCPs; 2. Half GCP, CP; 3. Flight Two simulation; LOOCV.*

	Ground Control Points				Check Points			
Scenario	No. of Points	ME (m)			No. of Points	ME (m)		
		x	y	z		x	y	z
1	25	-0.009	-0.005	-0.024	-	-	-	-
2	13	-0.008	-0.003	-0.012	12	0.022	0.007	0.014
3	15	-0.005	-0.002	-0.018	10	-0.081	-0.025	-0.076
LOOCV	-	-	-	-	25	0.003	0.002	0.005

The IOPs from each scenario were compared to investigate the ability of the photogrammetric method to consistently capture the camera characteristics. The tangential lens distortion was negligible, hence, only the radial distortion will be investigated further. The focal length varies between the different Flight One scenarios. The smallest focal length reported was 3.685 mm, from Scenario 4, which is 0.048 mm smaller than the largest focal length (Scenario 2, 3.733 mm). The variation in focal length is likely to be compensated by a variation in the triangulation height from the corresponding scenarios, and hence, shows the relationship between the IOPs and EOPs resulting from the self-calibration. The radial distortion also varies between scenarios (Table 4.2).

Table 4.2: *IOP summary from each Flight One scenario, 1. All GCPs; 2. Half GCP, CP; 3. Flight Two Simulation; LOOCV. Where f is the focal length, PPA x and y are the coordinates of the principal point of autocollimation, and K1, K2, K3 are the radial distortion coefficients.*

Scenario	f (mm)	PPA x (mm)	PPA y (mm)	K1	K2	K3
1	3.714	-0.004	-0.011	-1.38×10^{-3}	8.94×10^{-5}	1.14×10^{-6}
2	3.733	-0.003	-0.010	-1.36×10^{-3}	8.75×10^{-5}	1.11×10^{-6}
3	3.685	-0.004	-0.010	-1.33×10^{-3}	8.68×10^{-5}	1.20×10^{-6}
LOOCV	3.713	-0.004	-0.010	-1.38×10^{-3}	8.94×10^{-5}	1.14×10^{-6}

The radial distortion was plotted to assess the sensitivity of the triangulation (Figure 4.10). The radial distortion curve was the same shape across all scenarios. All of the scenarios follow a negative radial distortion curve between 0.50 mm and 3.61 mm, and then a positive distortion curve, reaching distortion up to 0.024 mm. However, the radial distortion varies between each scenario, the largest difference was 0.003, indicating suboptimal photogrammetric modelling.

Figure 4.10: The radial distortion associated with each Flight One scenario.

4.4.2 Subsequent flights

The second flight was conducted on the 24th of May 2016. The flight captured 58 images, and achieved a GSD of 2.3 cm^2. The 3D densified point cloud consisted of 6,449,964 points. The third flight occurred on the 14th of June 2016, and captured a total of 58 images. The GSD for this flight was also 2.3 cm^2. A total of 5,494,181 3D points were produced. Lastly, Flight Four was conducted on the 10th of September 2016, and obtained a total of 73 images. However, due to saturation in some of the images, only 70 out of 73 of the images could be processed. The GSD was 2.3 cm^2. The point cloud had a total of 6,047,795 3D points.

The DSMs from all three flights (Appendix A) had a RMSE z of 6 cm, based on the independent check points (Table 4.3a). The LOOCV had a RMSE z of 8 cm, two centimetres higher than the error reported by the check points in subsequent flights. All of the surfaces have negative MEs (Table 4.3b). Flights Two, Three and Four reported ME z of -3 cm, -2 cm, and -4 cm, respectively.

Table 4.3a: *The RMSE from the residual assessment of each subsequent flight scenario, 1. All GCPs; 2. Half GCP, CP.*

Flight	Scenario	Ground Control Points				Check Points			
		No. of Points	RMSE (m)			No. of Points	RMSE (m)		
			x	y	z		x	y	z
Two	1	17	0.025	0.023	0.043	-	-	-	-
	2	9	0.021	0.023	0.047	8	0.033	0.033	0.057
Three	1	26	0.034	0.033	0.048	-	-	-	-
	2	13	0.028	0.033	0.048	13	0.040	0.035	0.060
Four	1	18	0.032	0.025	0.035	-	-	-	-
	2	9	0.033	0.019	0.022	9	0.039	0.038	0.058

Table 4.3b: *The ME from the residual assessment of each subsequent flight scenario, 1. All GCPs; 2. Half GCP, CP.*

Flight	Scenario	Ground Control Points				Check Points			
		No. of Points	ME (m)			No. of Points	ME (m)		
			x	y	z		x	y	z
Two	1	17	-0.002	0.004	-0.015	-	-	-	-
	2	9	-0.003	0.003	-0.018	8	0.005	0.022	-0.032
Three	1	26	-0.001	0.003	-0.021	-	-	-	-
	2	13	-0.000	0.006	-0.034	13	-0.001	0.003	-0.020
Four	1	18	-0.005	0.001	-0.015	-	-	-	-
	2	9	-0.007	0.005	-0.009	9	-0.012	0.011	-0.038

The focal length varied between all flights and scenarios, the largest variation is 0.02 mm. The radial distortion also varies between flights, but remains relatively consistent between the scenarios (Table 4.4). However, the radial distortion of the subsequent flights varies greatly from Flight One.

Table 4.4: *IOP summary from each subsequent flight scenario, 1. All GCPs; 2. Half GCP, CP. Where f is the focal length, PPA x and y are the principal points of autocollimation, and K1, K2, K3 are the radial distortion coefficients.*

Flight	Scenario	f (mm)	PPA x (mm)	PPA y (mm)	K1	K2	K3
Two	1	3.661	-0.004	-0.013	-1.34×10^{-3}	8.91×10^{-5}	8.30×10^{-7}
	2	3.668	-0.004	-0.013	-1.34×10^{-3}	9.39×10^{-5}	8.21×10^{-7}
Three	1	3.648	-0.004	-0.014	-1.28×10^{-3}	7.34×10^{-5}	1.69×10^{-6}
	2	3.655	-0.003	-0.014	-1.27×10^{-3}	7.28×10^{-5}	1.67×10^{-6}
Four	1	3.658	-0.004	-0.012	-1.35×10^{-3}	8.38×10^{-5}	1.67×10^{-6}
	2	3.649	-0.004	-0.012	-1.35×10^{-3}	8.46×10^{-5}	1.69×10^{-6}

The radial distortion varies between the flights, suggesting suboptimal triangulation (Figure 4.11). The radial distortion between the flights starts to diverge approximately 2.5 mm away from the image centre, the largest variation in distortion is 0.009 mm, and occurs 4 mm from the image centre. The distortion increases the further from the image centre, indicating that the associated error is systematic, and not randomly distributed as suggested by the RMSE values given by Pix4D Mapper. Hence, caution should be taken when quantifying elevation and change, as areas of change may be artefacts of the photogrammetric model.

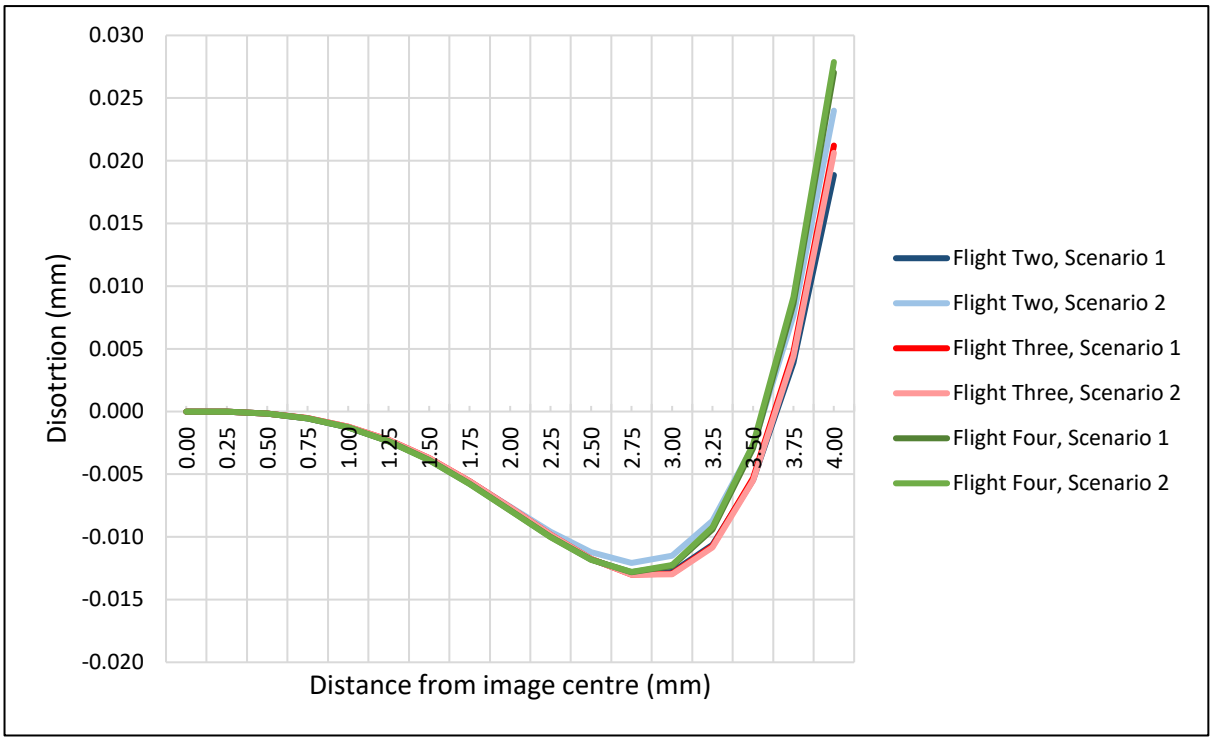

Figure 4.11: The radial distortion associated with each scenario Flight Two, Three and Four scenario.

4.4.3 Morphological change assessment

The results from each flight assessment indicate suboptimal photogrammetric modelling, observed by the variation in IOPs between flights and scenarios. The radial lens distortion assessment indicated an increase in systematic error outside of the GCP network. Therefore, the randomly distributed RMSE may be misleading as it implies the error is spread evenly over the model. The error inside the GCP network, although potentially exposed to systematic patterns due to the suboptimal solution, is expected to be more constrained. The RMSE is assumed to an appropriate measure of the random error affecting the representation of the surface. Due to these findings, the subsequent morphologic change assessment only observed changes within the GCP configuration. The constructed notches were located within the GCP network, and therefore, could be appropriately used for subsequent morphologic change analyses.

A total of six change scenarios were conducted; three to quantify elevation changes and three to quantify volumetric changes. The RMSE was calculated from the input surfaces (Table 4.5).

Table 4.5: *The vertical root mean square error of the morphologic change surfaces, calculated from the input surfaces for each change scenario.*

Morphologic change scenario:	Flight 1 – 2 (8th – 24th May)	Flight 3 – 4 (14th June – 10th September)	Flight 1 – 4 (8th May – 10th September)
RMSE z (m)	0.098	0.083	0.099

At the seaward end of the depositional footprint of Notch B there was a significant increase in elevation (Figure 4.12). The surrounding areas showed a decrease in elevation, and areas with a statistically insignificant elevation change, despite the visible sand deposition in the photographs. The ECS showed a mean elevation change of -12 cm. Notch C portrayed a similar pattern of change, with a small increase in elevation at the seaward end of the depositional footprint, and decreases in elevation shown at the landward end of the depositional footprint. However, a large proportion of the elevation change was statistically insignificant based on the error analysis and confidence interval. The mean change in elevation for the depositional footprint of Notch C was -9 cm.

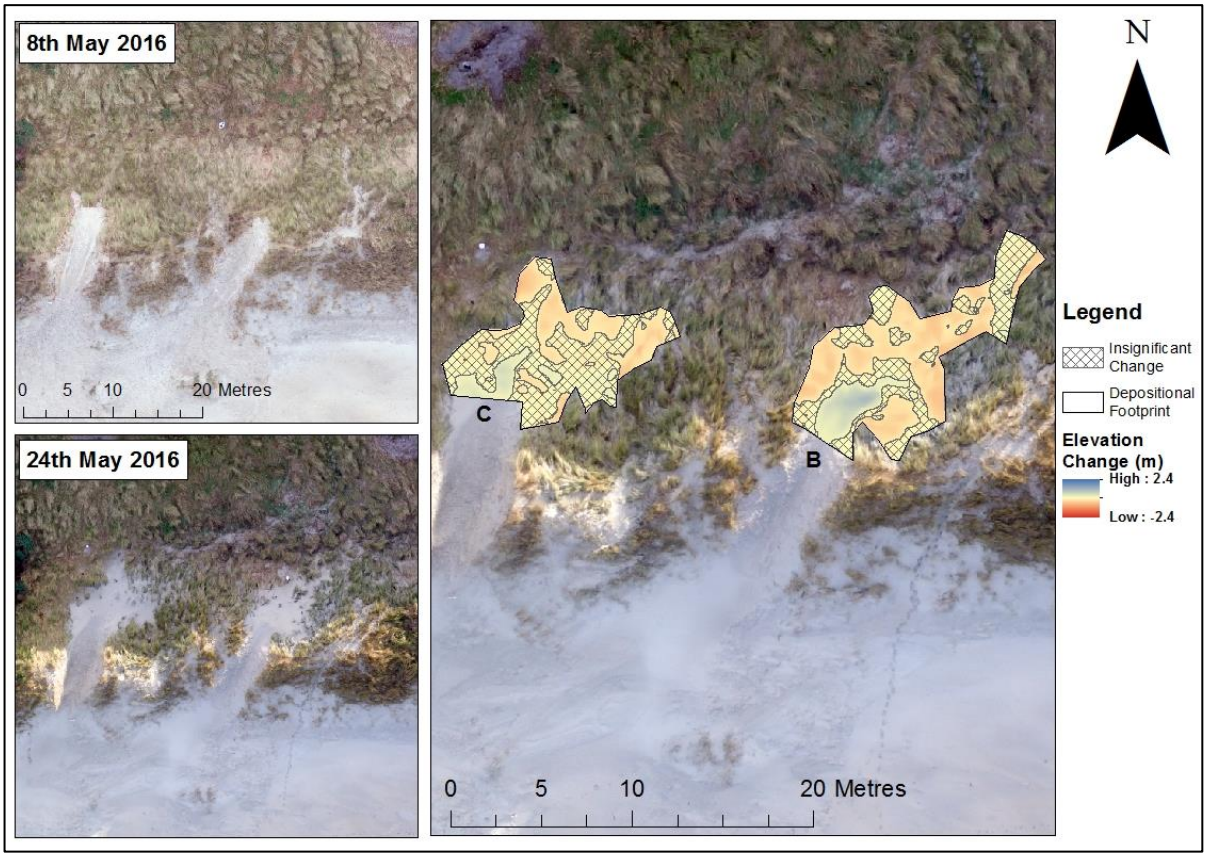

Figure 4.12: The elevation change through Notches B and C, between the 8th and 24th of May.

The volumetric changes of Notch B and C were also analysed. As indicated in Figure 4.12, Notches B and C underwent a net loss in volume between the 8th and 24th of May. The 90% confidence interval calculated for the regions of gain, loss and the net change, do not include zero, indicating that the volumetric changes were statistically significant (Table 4.6).

Table 4.6*: A table summarising the gain, loss and net change through Notches B and C between the 8th and 24th of May. CI refers to confidence interval.*

	Notch B		Notch C	
	Volume (m^3)	90% CI	Volume (m^3)	90% CI
Gain	5.07	(5.05, 5.09)	2.74	(2.72, 2.75)
Loss	12.03	(12.01, 12.06)	6.88	(6.86, 6.90)
Net Change	-6.96	(-6.99, -6.93)	-4.14	(-4.17, -4.11)

The process was repeated to investigate morphologic changes between Flights Three and Four (between the 14th of June and 10th September). The ECS in Figure 4.13 shows little elevation change behind the notches when compared to the change observed in Figure 4.12. There is a small increase in elevation in Notch B, however, the majority of Notches B and C showed little change in elevation.

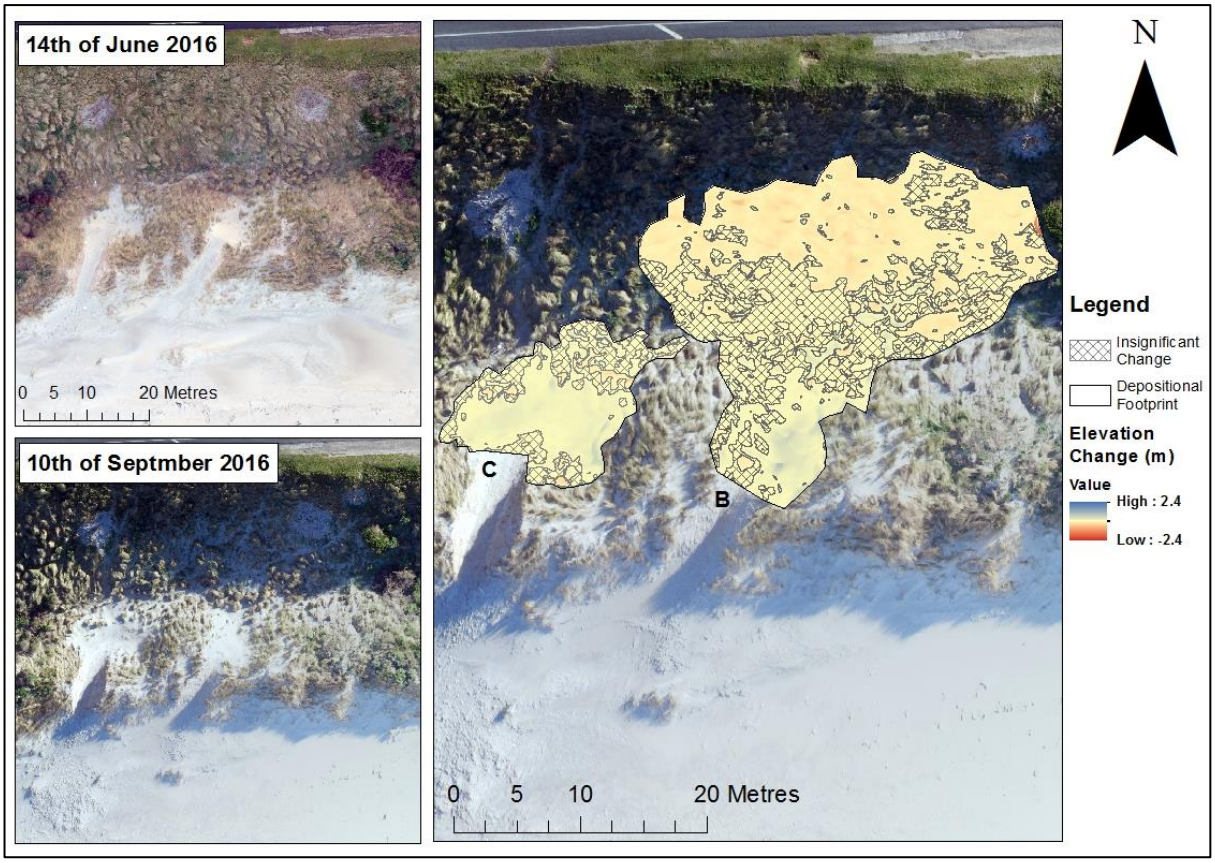

Figure 4.13: The elevation change through Notches B and C, between the 14th of June and the 10th of September.

The volumetric change calculations presented a positive net change in volume of 9.47 m^3 and 8.52 m^3 for Notched B and C, respectively (Table 4.7). The majority of the loss in volume has occurred in areas where the sand was deposited on top of vegetation. The areas that gained volume did not have vegetation present. The 90% confidence intervals do not include zero for the gain, loss or net changes, indicating that the volumetric changes were statistically significant.

Table 4.7: *A table summarising the gain, loss and net change through Notch B and C between the 14th of June and the 10th of September. CI refers to confidence interval.*

	Notch B		Notch C	
	Volume (m^3)	90% CI	Volume (m^3)	90% CI
Gain	9.77	(9.76, 9.80)	8.58	(8.56, 8.60)
Loss	0.30	(0.29, 0.31)	0.06	(0.05, 0.06)
Net Change	9.47	(9.45, 9.50)	8.52	(8.50, 8.54)

The final morphologic change analysis assessed the change over the four month study period (the 8th of May to the 10th of September), through Notches A, B and C. A statistically significant increase in elevation occurred through Notch A along the base of the foredune on the leeward side (Figure 4.14). The eastern side of the depositional footprint exhibits a decrease in elevation. Prior to this study, a tree directly landward of the notch was cut down, and the debris was placed to the east of the notch in the swale and on the bank of John Wilson Drive, this is visible in the 8th of May photograph (Figure 4.14). The debris was subsequently moved further east, as it became apparent that sand was being deflected eastwards, and being deposited on top of the debris. Therefore, the decrease in elevation detected by the elevation change surface was been caused by the movement of tree debris, not a change in the dune morphology due to coastal processes.

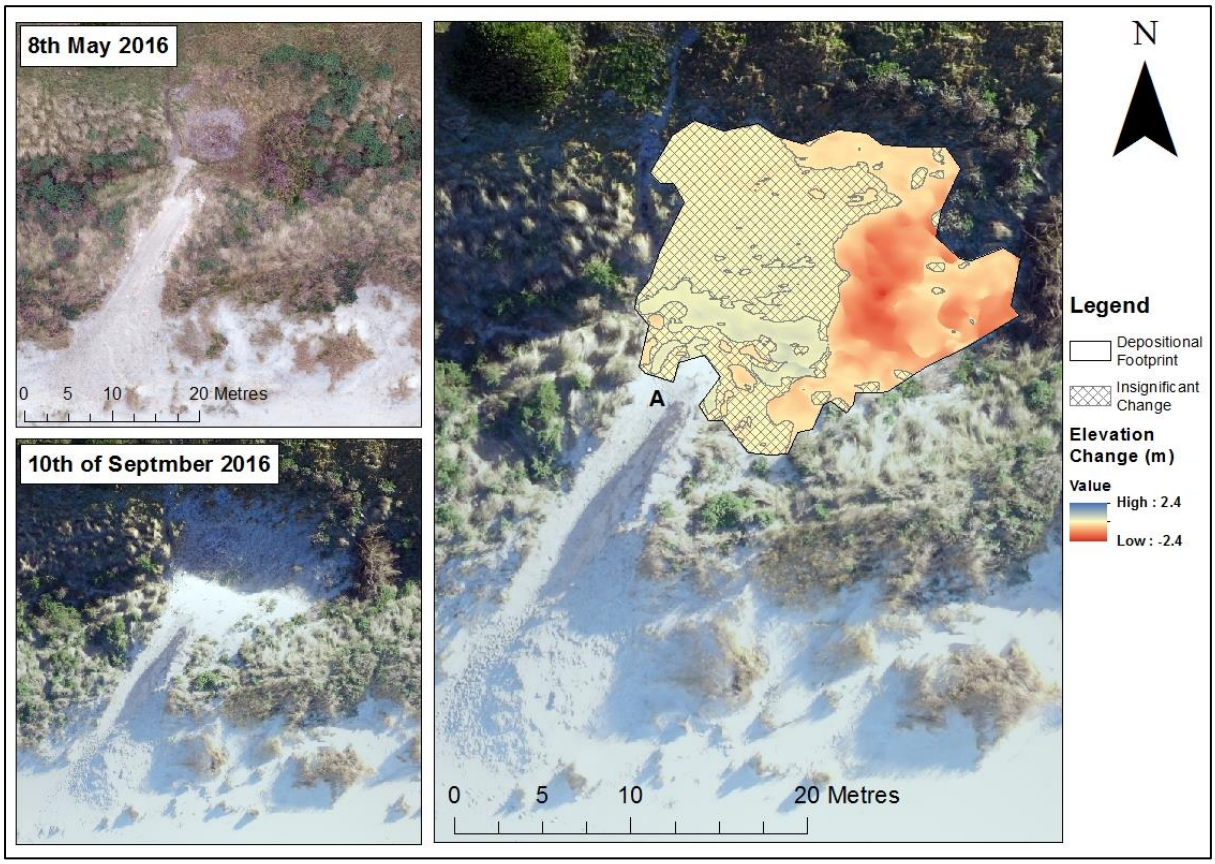

Figure 4.14: The elevation change through Notch A, between the 8th of May and the 10th of September.

Notches B and C both had a stronger increase in elevation at the seaward end of the depositional footprint (Figure 4.15). These areas were the first to have sand deposition over the study period. The majority of elevation change identified in Notches B and C is statistically insignificant, primarily in the areas which were previously vegetated.

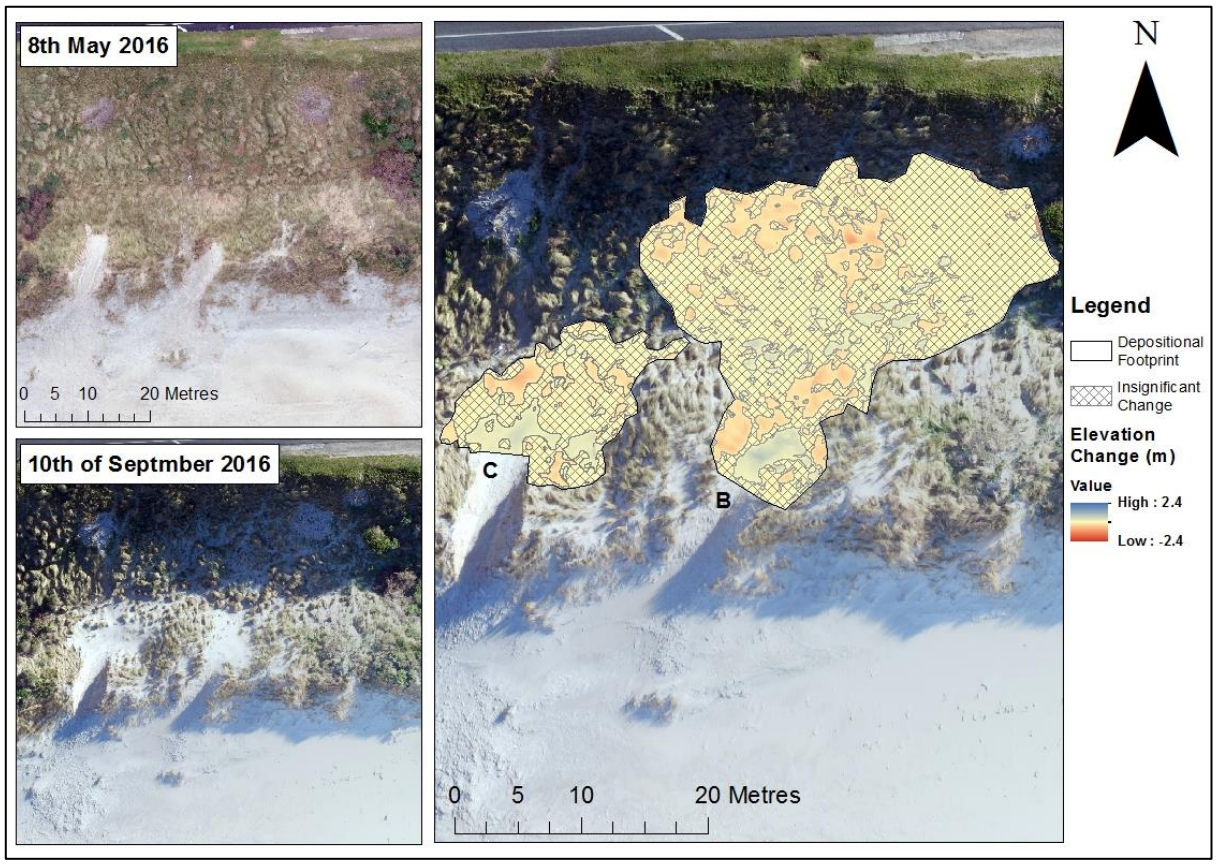

Figure 4.15: The elevation change through Notches B and C, between the 8th of May and the 10th of September.

Over the four month period, Notches A and B exhibited a net loss in volume, with Notch A showing the highest loss of approximately 66 m^3 (Table 4.8). Notch C had an overall net gain in volume, of 0.73 m^3. Notch C, however, had the smallest depositional footprint. All of the notches underwent statistically significant volumetric changes. The ECS indicates that the elevation change over most of the depositional footprint was statistically insignificant, however, this was based on the change in each individual pixel, not the cumulative change suggested by the volumetric calculations.

Table 4.8*: A table summarising the gain, loss and net change through Notch A, B and C between the 8th of May and the 10th of September. CI refers to confidence interval.*

	Notch A		Notch B		Notch C	
	Volume (m^3)	90% CI	Volume (m^3)	90% CI	Volume (m^3)	90% CI
Gain	15.69	(15.65, 15.73)	25.97	(25.91, 26.03)	10.00	(9.67, 10.03)
Loss	81.54	(81.49, 81.59)	38.43	(38.37, 38.49)	9.27	(9.24, 9.30)
Net Change	-65.85	(-65.91, -65.79)	-12.46	(-12.54, -12.38)	0.73	(0.69, 0.77)

The aerial photography shows that each notch has facilitated sand deposition. However, the morphologic analysis conducted using the RPAS imagery only quantified deposition in areas that were bare sand prior to sediment exchange. Vegetated areas with visible deposition exhibited a loss in volume in the morphologic change analysis. This suggests a 'dampening' effect, where sediment that was deposited on vegetated areas, has pushed the vegetation toward the ground. Hence, even though sediment was deposited, the RPAS imagery detected this as a decrease in elevation. This is a result of the RPAS producing a digital surface model opposed to a digital terrain model.

4.4.4 Summary

The results from this study suggest that the photogrammetric method associated with this low-cost RPAS provides inconsistent modelling of the RPAS sensor. There are variations in the solution of the IOPs between flights as well as the scenarios conducted on the imagery from each flight. The parameters with the most variation are focal length and radial distortion. This indicates that the output DSM is influenced by systematic error that is not reported by Pix4D Mapper. The RMSE of the DSMs produced by the photogrammetry software is not accurate outside of the GCP network. Hence, only the areas confined within the GCP configuration were used for subsequent analysis. The morphologic change analysis detected changes in elevation and volume, however, some of the sediment deposition visible in the photographs was calculated as a loss in volume. This is likely a result of the presence of vegetation, and the RPAS imagery creating a DSM rather than a DTM. Hence, RGB RPAS imagery is not suitable for accurate small-scale morphologic change analysis in vegetated areas. However, the dampening effect would be avoided when quantifying large-scale changes, such as foredune erosion, and when quantifying long-term changes.

4.5 Discussion

This aim of this section is to discuss the ability of a low-cost RPAS for quantifying morphologic change of a coastal foredune, based on the results from this study. RPAS technology is a useful tool for coastal geomorphology research, and is available to a wide range of users. However, the photogrammetric method associated with RPAS technology is not as rigorous as traditional photogrammetry methods. Traditionally, photogrammetry was conducted by photogrammetry experts, whereby the interior orientation parameters (IOPs) of the sensor were determined separately to the exterior orientation parameters (EOPs). The six EOPs were solved in the bundle block adjustment (BBA). Conversely, modern RPAS photogrammetry employs a self-calibration of the sensor, where the IOPs are solved simultaneously with the EOPs in the BBA. This requires the BBA to solve for a larger number of unknown parameters with correlation between parameters that may not be well resolved. The BBA rarely finds the optimal solution, which creates systematic errors in the output DSM, unbeknown to the user. This chapter investigates such errors by assessing and comparing the IOPs reported from each flight.

Understanding the patterns and trends relating to morphologic change in coastal dune systems is important for monitoring and managing such environments. RPAS technology is a useful tool for monitoring the morphology of coastal dunes. The technology provides rapid surveys over large areas, which is advantageous for coastal monitoring. Based on insight gained from the sensor and residual assessment, the change in morphology over the four month study period was assessed. The changes in morphology facilitated by the notches were quantified, however, the presence of vegetation impacted the morphology changes detected within the RPAS data. This section will discuss the findings from this chapter to address the second research question.

4.5.1 Flight planning

The RPAS employed in this study was a DJI Phantom-3 Advanced. At the time of this study, flight planning software was unavailable. Flight planning software such as Pix4D Capture enables the user to collect aerial photographs over a defined area with sufficient forward and side-lap for photogrammetric modelling (Nex and Remondino, 2014). Hence, the imagery obtained is guaranteed to sufficiently cover the desired area, and subsequent images maintain the desired overlap. The images captured from Flights Three and Four in this study had suboptimal side-lap, a consequence of manually capturing the imagery (Nex and

Remondino, 2014). Flight planning software would have increased the accuracy of the DSMs produced from these flights. Additional flight lines can also increase the accuracy of the output DSM. A study conducted by Gerke and Przybilla (2016), investigated the influence of cross-flight patterns (Figure 4.16) on the IOPs and residuals reported by the photogrammetry software.

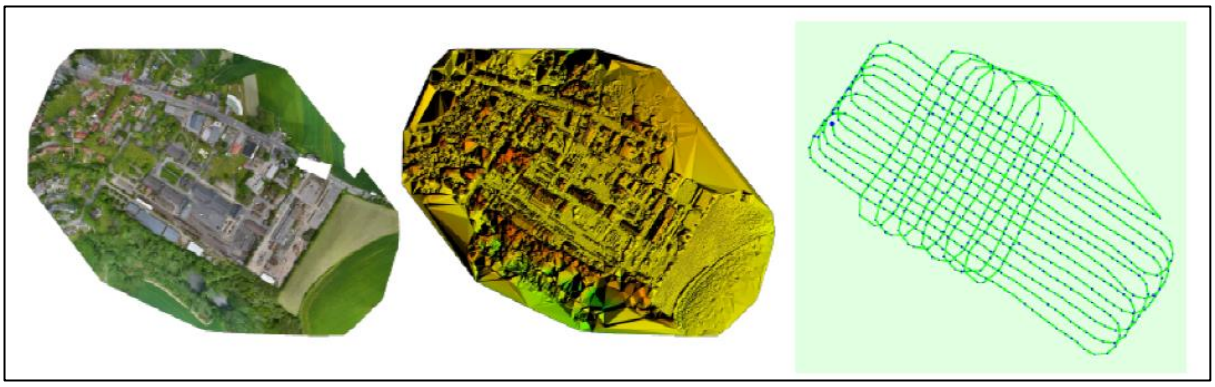

Figure 4.16: An example of a cross-flight pattern Gerke and Przybilla (2016). In addition to a series of parallel flight lines, a second set of flights are employed, perpendicular to the initial flight lines.

The results found an increase in accuracy with the cross-pattern flight line, reflected by the smaller residuals when compared with a parallel flight line mission. It was recognised by Gerke and Przybilla (2016) that an increase in the number of GCPs increases the accuracy of the output. The study also found that the cross-flight pattern is more useful for surveys over flat terrain, as opposed to undulating terrain where there is greater surface variation. However, the RPAS battery capacity can limit the number of flights employed for the survey.

In the current study, the battery capacity was 23 minutes in optimal conditions (DJI, 2015). The total time for each of the flight was 10-12 minutes, and at this point the low battery warning was signalled. The flight endurance is reduced when imagery is captured and the wind speed is higher, as the aircraft uses more energy. Higher quality RPAS have a greater battery capacity, such as the C-Astral Bramor used in a study by Barry and Coakley (2013), which has a 3 hour flight endurance.

4.5.2 Remotely piloted aerial system photogrammetry

RPAS photogrammetry is constantly developing, and is becoming more accessible for coastal and environmental research (Klemas, 2015). The low-cost, 'high' accuracy, and accessibility of such technology is appealing to researchers. The ability to capture photographs

(in addition to conducting surveys) is desirable, because photographs provide a snap shot of the environment at the time of the survey.

Photogrammetry is the process of obtaining measurable data from photographs (Mikhail *et al.*, 2001). The method uses a series of overlapping vertical photographs to derive elevation information. Traditional photography was primarily conducted by photogrammetry experts, however, the development of RPAS has resulted in an increase in non-expert users conducting photogrammetry with low-cost sensors (Sirguey *et al.*, 2016). DSMs can be produced from aerial photography via photogrammetry. A number of steps need to be taken to derive a photogrammetric model from imagery. Firstly, IOPs and EOPs need to be solved to position and orientate the camera and photographs into geographical space. IOPs describe the characteristics of the sensor, such as the focal length, PPA and lens distortion (refer to Chapter 2, Section 2.1.5 for an in-depth explanation of IOPs and EOPs). In traditional photogrammetry, IOPs were calibrated and solved separately to the EOPs. The BBA was only used to solve the six EOPs. However, modern photogrammetry requires self-calibration of the camera, by including IOPs in the BBA (Fryer and Brown, 1986). Hence, the BBA solves the IOPs and EOPs simultaneously, making it more difficult for the process to find the optimal solution (Sirguey *et al.*, 2016).

The errors associated with the self-calibration method have been investigated by Sirguey *et al.* (2016). The results suggest an inability by photogrammetry software to accurately solve the IOPs and EOPs, hence, producing un-modelled error in the output surfaces. The results from the current study coincide with Sirguey *et al.* (2016)'s findings. The IOPs were compared between the models produced from each flight, as well as the different GCP scenarios. Each flight and scenario reported a different focal length, with variations up to 0.02 mm, even though the same sensor was used and the lens was focussed at infinity. The tangential distortion was negligible, however, the radial distortion varied between flights and scenarios. The inconsistencies indicate a suboptimal solution by the photogrammetric model. These errors propagate into the output DSM, but are not modelled. Sirguey *et al.* (2016) concluded that such errors are systematic, rather than randomly distributed. Hence, RMSE can be misleading if interpreted as an error applied equally to all pixels in the DSM. Systematic errors in the surface beyond the RMSE magnitude can yield patterns of change that could be interpreted as a result of a coastal process, despite being an artefact of suboptimal photogrammetric modelling.

The results from Sirguey *et al.* (2016) suggest that the RMSE is only reliable within the confines of the GCP configuration, outside of this network, the model is possibly susceptible to the systematic error caused by the inaccuracies of the sensor. In the current study, the RMSE of the four output DSMs was between 6 and 8 cm. The area within the GCP network includes the foredune, swale, the slope of John Wilson Drive, and the upper beach. Any area outside of this network is not reliable for accurate analysis. The notches used in the morphologic change assessment were within the boundary of the GCPs, and hence, could be used confidently for subsequent analysis based on the RMSE produced by Pix4D Mapper.

4.5.3 Morphologic changes

The DSMs derived from the RPAS imagery were used to quantify the elevation and volumetric changes of the foredune over the study period. Due to the greater potential for systematic error present in the GCP network, only the changes within the GCP network were reported. The morphologic change analyses were concentrated on the areas in the lee of the notches with visible sand deposition, and hence, provided an opportunity to test the RPAS for quantifying this change in morphology.

Three epochs were used to quantify the morphologic changes, two storm events (May and September), and the total change over the course of the study (four months). Morphologic changes were detected in each epoch, however, not all changes were statistically significant. The RPAS did not accurately quantify the sand deposition in the lee of the notches. The RPAS produces a DSM, rather than a DTM. Hence, the RPAS detects the elevation of the top surface of the area surveyed rather than the elevation of the ground surface. The areas in the lee of the notches were initially completely vegetated with *Ammophila arenaria* (marram grass), which can grow to approximately 1 m. The deposition of sand flattened the vegetation, resulting in the RPAS detecting a decrease in elevation. The surfaces that were initially bare sand, or that had sand deposited during the May storm event, reported an increase in elevation and sand volume in the subsequent analysis. Therefore, the ability of the RPAS to detect morphologic changes depends on the surface characteristics, the RMSE, and the timescale of change quantified. Long-term, large scale changes could be sufficiently quantified, however, small scale changes in vegetated areas may not be accurately quantified.

4.6 Conclusions

This study has found that low-cost RPAS technology is capable of detecting morphologic changes in coastal foredunes, however, a number of factors need to be considered.

Firstly, the photogrammetry employed to derive information from RPAS imagery results in potential systematic errors in the photogrammetric model. These errors are contrary to the RMSE reported by RPAS photogrammetry software. As a result, the accuracy of the model has a stronger reliance on the GCP network than traditional photogrammetry. The GCP network must encompass the area of interest, with an establishment of GCPs both throughout the study site and around the perimeter to avoid systematic error in the area of interest. Secondly, sufficient photograph forward and side-lap should be maintained, which can be ensured by employing flight planning software. Vegetation creates an offset in the elevation recorded by the RPAS, and any subsequent deposition of sand will produce a decrease in elevation and volume. Hence, the actual deposition of sand is not well quantified by the RPAS in vegetated areas. However, vegetation presence may be insignificant for large-scale erosion or accretion. RPAS is suitable for quantifying small-scale morphologic change in areas with sparse or no vegetation.

Chapter 5

The impact of vegetation on digital surface models

5.1 Introduction

Surveying the morphology of vegetated environments with RPAS can be problematic. The elevation of an area surveyed with RGB RPAS is based on the visible surface, for example the vegetation canopy (i.e. a DSM is created rather than a DTM) (Whitehead and Hugenholtz, 2014). In areas with dense vegetation, the elevation recorded by the RPAS will be exaggerated, compared to areas with bare sand. Coastal dune systems often exhibit a range of vegetation types and densities. This chapter investigates the elevation offset caused by vegetation in RPAS derived DSMs.

The elevation offset caused by vegetation in RPAS derived DSMs needs to be investigated further. RPAS equipped with RGB cameras have been successfully used to survey coastal areas (for example, Darwin *et al.*, 2014; Gonçalves and Henriques, 2015). In some coastal morphology studies (Gonçalves and Henriques, 2015) the influence of vegetation on the DSM has not been quantified. In other cases (Mancini *et al.*, 2013), the issue is addressed by removing densely vegetated areas from the dataset completely.

The vegetation offset in RPAS DSMs creates inaccuracies when morphologic change is quantified, as found in Chapter 4. Hence, the amount of offset, and where it occurs, needs to be understood to extract accurate elevation data. The discrepancy caused by vegetation in the imagery is determined by the density, the type of vegetation, the flying height of the RPAS, and the quality of the RPAS camera.

This chapter investigates the factors determining the elevation offset in vegetated areas in coastal RPAS surveys. This addresses Research Question 3: *To what degree and how does*

vegetation affect the development of digital terrain models from RPAS photogrammetry? Comparisons are made between foredune surfaces derived from an RPAS and an RTK-GPS survey – that is, between the DSM and DTM of the same area. Four vegetation density classes are selected (dense vegetation, variable, sparse, and no vegetation) to assess the differences in elevation derived from each method. This study assess the hypothesis that the elevation difference between the DTM and DSM, is equal to the height of vegetation. This chapter begins with a description and justification of the study site. The methods employed and the results are then described. Lastly, the findings are discussed in relation to Research Question 3.

5.2 Study Site

The study was conducted on a section of foredune, located at Mason Bay, Stewart Island. The Mason Bay foredune extends approximately 150 m inland and is dominated by *Ammophila arenaria* (marram grass) (Figure 5.1).

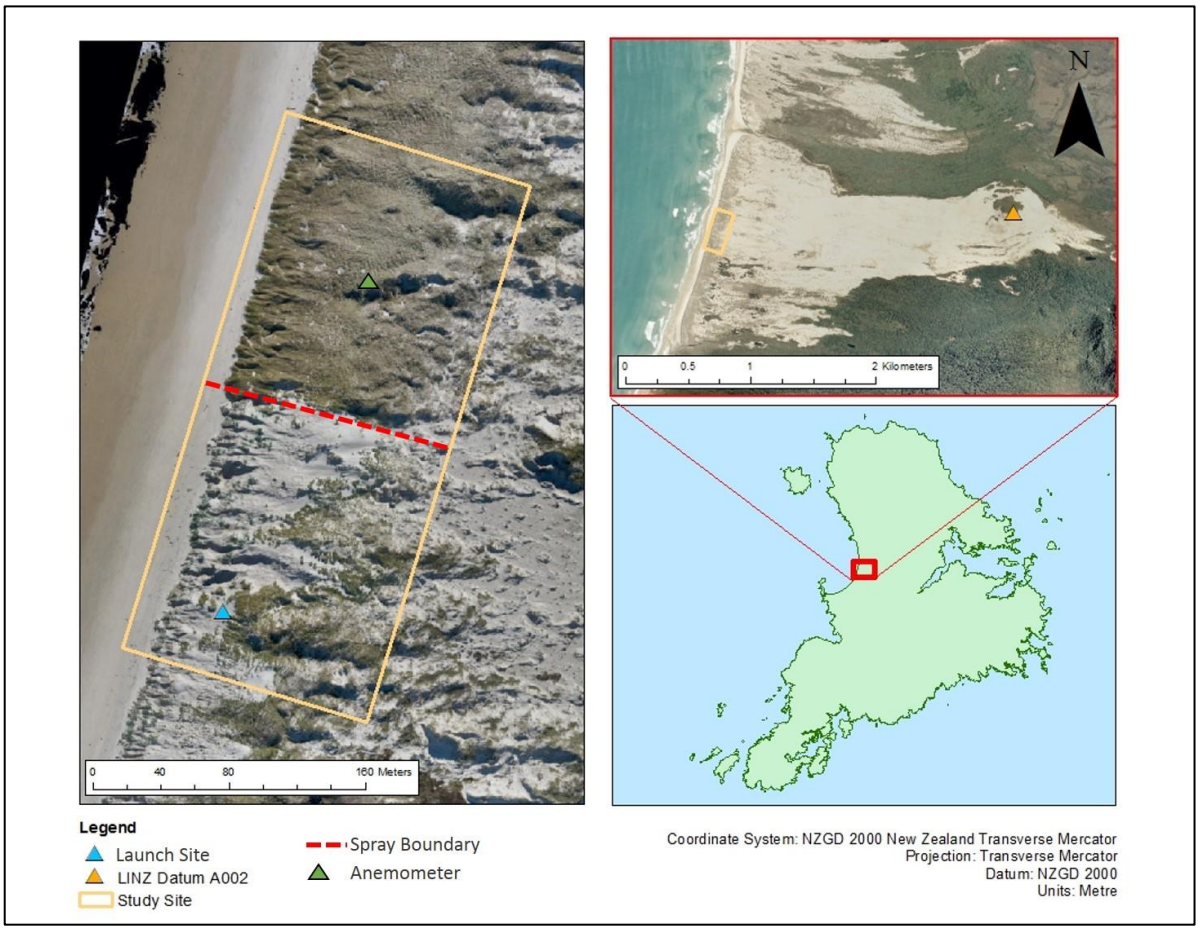

Figure 5.1: The study site, located at Mason Bay, Stewart Island.

The Department of Conservation implemented a long-term *A. arenaria* eradication programme 6 years ago, with an aim to completely remove *A. arenaria* from the dune system (Hilton and Konlechner, 2010). The programme employs different *A. arenaria* spraying methods on different sections of the dune, depending on the distribution. Some of the areas on the foredune that were densely vegetated by *A. arenaria* have been sprayed via helicopter. The backdune has been sprayed with ground-based methods, as *A. arenaria* is less dense in these areas. Variations in the extent of spraying has created different vegetation densities on the foredune. The back of the foredune exhibits a range of species, producing a complex array of vegetation.

The study site includes the boundary between an area that has been sprayed on 5 occasions (the southern half of the study area), and an area that has only been sprayed once (the northern half of the study area) (Figure 5.1). Hence, the variation in vegetation provides an opportunity to test the RPAS on surveying areas with different vegetation densities. Further detail on the Mason Bay dune system is presented in Chapter 1, Section 1.6.3.

5.3 Methods

To assess the elevation offset caused by vegetation in the RPAS DSM, surveys of the same areas were conducted with RTK-GPS and RPAS. The elevation difference between the DTM and DSM was investigated and tested for statistical significance. Within the study site, twelve plots were established which represented different vegetation densities. Four vegetation density classes were defined – Class 1: dense, Class 2: variable, Class 3: sparse, and Class 4: bare sand. Each class had three allocated plots. Ten quadrat samples were obtained from each plot. Samples of the vegetation height, type and approximate cover were obtained from each quadrat. The vegetation surveys were compared with the elevation discrepancies between the RPAS and RTK-GPS. The statistical relationship between the vegetation height and the difference in elevation between the DTM and DSM was investigated using Mann-Whitney U-tests and t-tests. The orthomosaic image of the study area was reclassified to show only the vegetated and non-vegetated area. This was compared with the DTM of difference surface (DoD) to identify the relationship between vegetation cover and the elevation discrepancies. This section will explain, in detail, the methods employed to address Research Question 3.

5.3.1 Vegetation surveys

The study site was divided into twelve vegetation plots, each 5 m^2 in size. Three plots were allocated for each class (Figure 5.2). Class 4 (bare sand) was used as a control site, to test

the error between the elevation recorded by the RTK-GPS and the error recorded by the RPAS, where no vegetation is present. Class 1 plots, on average, had 92% cover in each quadrat which was predominately *A. arenaria*.

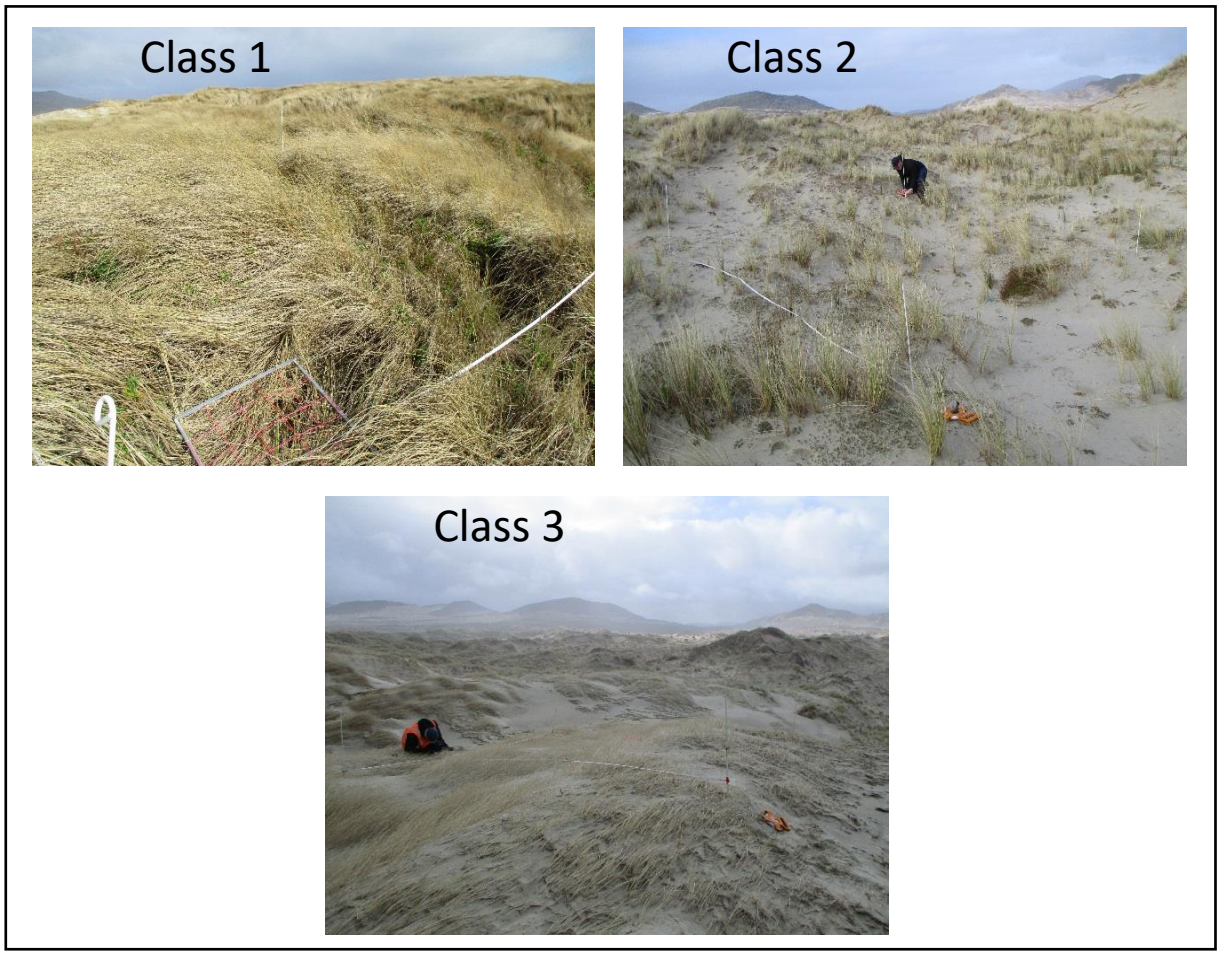

Figure 5.2: Three of the vegetation classes used in this study, Class 1: dense vegetation; Class 2: variable vegetation; Class 3 sparse vegetation.

The Class 1 plots were located on the area of foredune that had only been sprayed once as part of the *A. arenaria* eradication programme (March 2016) (Figure 5.3). The Class 2 plots on average had 38% vegetation cover in each quadrat, which comprised of various species *(Gentiana, Sonchus, Pimelea, Isolepis* and *Coprosma*). These plots were located further inland than Class 1. The Class 3 plots had an average quadrat vegetation cover of 26%, which was primarily dead *A. arenaria*. These plots were in the area of foredune that had been sprayed on five occasions via helicopter.

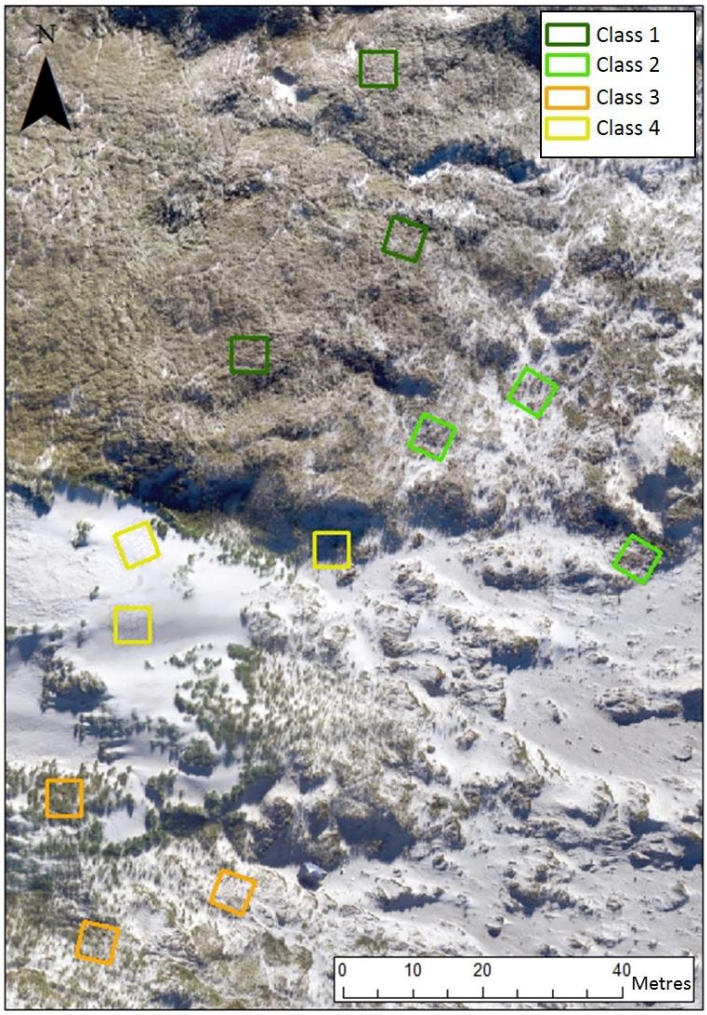

Figure 5.3: The location of each plot on the Mason Bay foredune.

The plots were laid out with a tape measure, and the corners were marked with fibre-glass poles. The poles had bright coloured card on top that were visible in the RPAS imagery. The plant cover was characterised using ten quadrats, located using a random number table. A tape measure was laid out on two edges of the quadrat, one to represent the x axis and the other to represent the y axis.

Each quadrat was divided into 25 squares. The height of vegetation at 9 points in each quadrat was recorded (Figure 5.4). The overall vegetation cover (percentage), number of species present, and the health of the *A. arenaria* (dead or alive) was recorded for each quadrat.

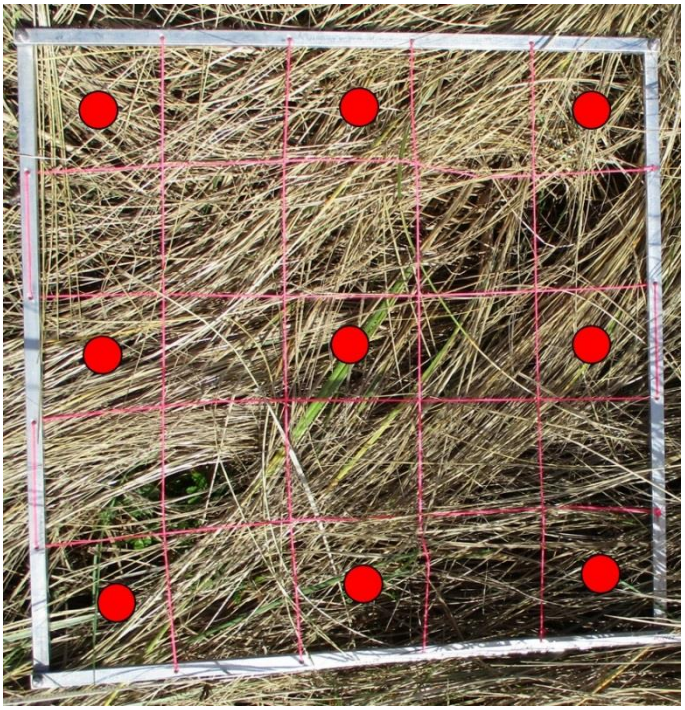

Figure 5.4: The quadrat used to conduct the vegetation surveys. The red dots represent the location of each vegetation height measurement.

Each 5 m^2 plot was surveyed using RTK-GPS. A systematic, stratified, topographic sampling technique was used. Points were recorded by the RTK-GPS every 0.5 m where the terrain was continuous, and more frequently where hummocks were present. This ensured any topographic variations were recorded. The RPAS was flown to obtain imagery over an area (330 m × 150 m) which encompassed all of the plots.

5.3.2 RPAS survey

A DJI Phantom-3 Advanced quadcopter was used for the RPAS survey. A Sony EXMOR 1/2.3" (sensor size 6.17 × 4.55 mm) 12.4 megapixel camera was used, with a field of view of 94° and a 20 mm lens (in 35 mm equivalent) focussed at infinity. The infinity focus prevents the "zoom" from being used, and therefore, keeps the internal image geometry consistent by maintaining the focal length between images. Each image contains 4000 × 3000 pixels. Flight planning software was not employed, and photographs were captured manually during the flight by the operator. The sensor information was used to calculate the 'real' focal length, using the following equation;

$$f_R = \frac{f_{35}\, S_w}{34.6}\,, \tag{5.1}$$

where F_R is the real focal length measured in millimetres, F_{35} is the focal length in the 35 mm equivalent, and S_w is the sensor width. The flying height to obtain a ground sampling distance of 2.5 cm^2 was determined using the following formula;

$$H = \frac{f_R \, n_w \, GSD}{S_w} \tag{5.2}$$

To achieve a ground sample distance of 2.5 cm^2, the height of the aircraft should be at a maximum of 57.8 m. The RPAS flew at 50 m (+/- 0.5 m) above the launch site which was located approximately 10 m above mean sea level. The ground sampling distance achieved, reported by Pix4D, was 2.1 cm^2. The launch site is shown in Figure 5.1, this site was chosen because the area is flat, and slightly sheltered from the sea breeze. This location is also in close proximity to a high point within the foredune, where the operator and the "spotter" could see the entire survey area during the flight.

The image footprint was calculated to determine the distance the RPAS needed to travel between subsequent photographs to obtain a forward image overlap of 85% and side-lap of 70%, believed to be an appropriate compromise to ensure satisfying photogrammetric modelling while being within the RPAS endurance. The approximate dimensions of the rectangular footprint of each image were calculated by multiplying the number of pixels in the width and length of each image by the desired GSD. The minimum distance between pictures to achieve the desired 85% forward overlap was computed as 11.25 m. During image acquisition in the field, photographs were taken approximately every 10 m. Image side-lap was achieved with five flight lines (Figure 5.5).

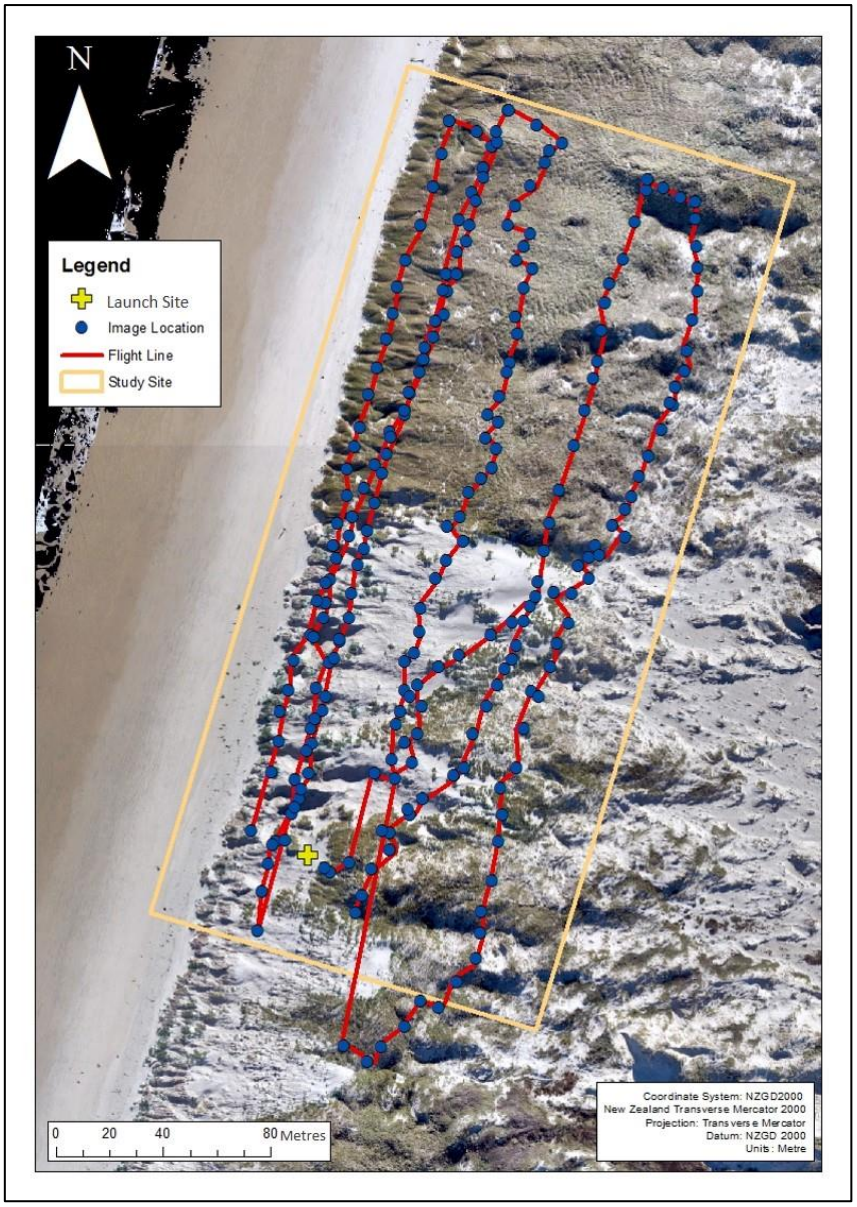

Figure 5.5: The RPAS flight line at Mason Bay. The location of each photograph is represented by blue dots, and the flight path is represented by the red line.

The flight was completed with 5.5 flight lines, and a total of 232 photographs were captured. The aircraft battery was swapped after the second flight line. It was difficult to fly in a direct line across the study area because of the onshore wind (gusts between 1.95 ms^{-1} and 5.65 ms^{-1} were recorded by an anemometer onsite (Figure 5.1)), and without flight planning software. Hence, some sections of the area were initially missed, and were subsequently flown at the end of the survey (Figure 5.5).

A total of 25 GCPs were established across the study area (Figure 5.6). The GCP configuration was selected to ensure the plots were confined within the GCP network, and therefore, were not subject to systematic lens errors (as found in Chapter 4). The GCPs were

surveyed using a Trimble R8 RTK-GPS unit, with an occupation time of 2 minutes. The average PDOP value was 1.413, the average horizontal precision was 0.021 m, and the average vertical precision was 0.026 m. The base station was set-up on LINZ (Land Information New Zealand) datum A002 (4789514.046 N, 1203747.000 E) (Figure 5.1). All of the points were surveyed relative to the New Zealand Transverse Mercator coordinate system, and the elevations were in ellipsoidal height using the New Zealand Geodetic 2000 datum transformation.

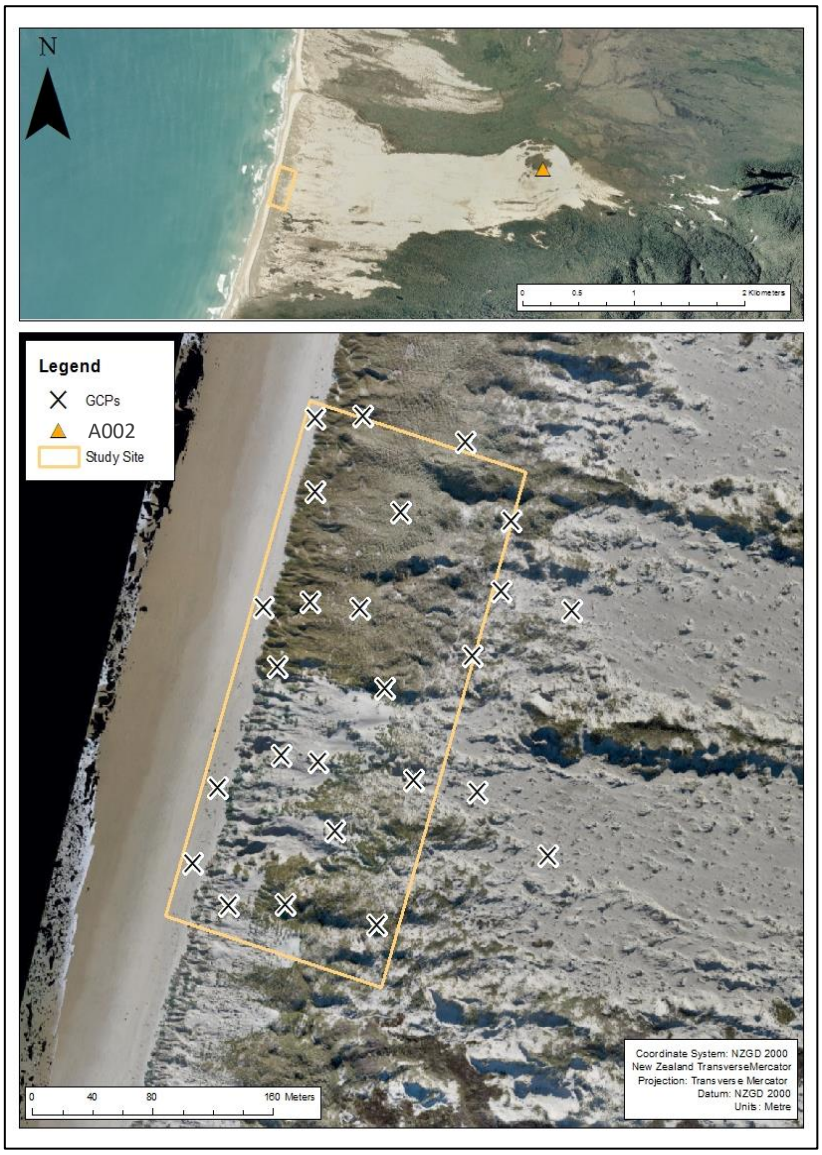

Figure 5.6: The Mason Bay study site ground control point layout. The GCPs were wooden pegs in the ground, with laminated card on top that were visible in the RPAS imagery.

The photographs and GCPs were uploaded into Pix4D Mapper for processing. The photographs were stitched together, and a DSM and orthomosaic were created. The DSM and orthomosaic were imported into ArcGIS. The plots were identified in the DSM using the locations in the orthomosaic, and the RTK-GPS survey points. For further information on Pix4D processing, refer to Chapter 4, Section 4.3.5.

5.3.3 RTK-GPS survey

The RTK-GPS survey was conducted using a Trimble R8 GPS unit. The base station was set-up over the A002 LINZ datum located at the top of 'Big Sand Hill' (4789514.046 N 1203747.000 E), approximately 2.4 km from the study site (Figure 5.5). The area of each plot was surveyed with RTK-GPS. The points were recorded with an occupation time of 5 seconds. The average PDOP of the points was 1.342, the horizontal precision was 0.018 m and the vertical precision was 0.023 m. A systematic, stratified, topographic sampling technique was employed, points were recorded every 0.5 m over consistent terrain, and more often over irregular hummocky ground. This ensured that the DTM created by the points would include any variations in the terrain. The point layout for each plot is presented in Figure 5.7.

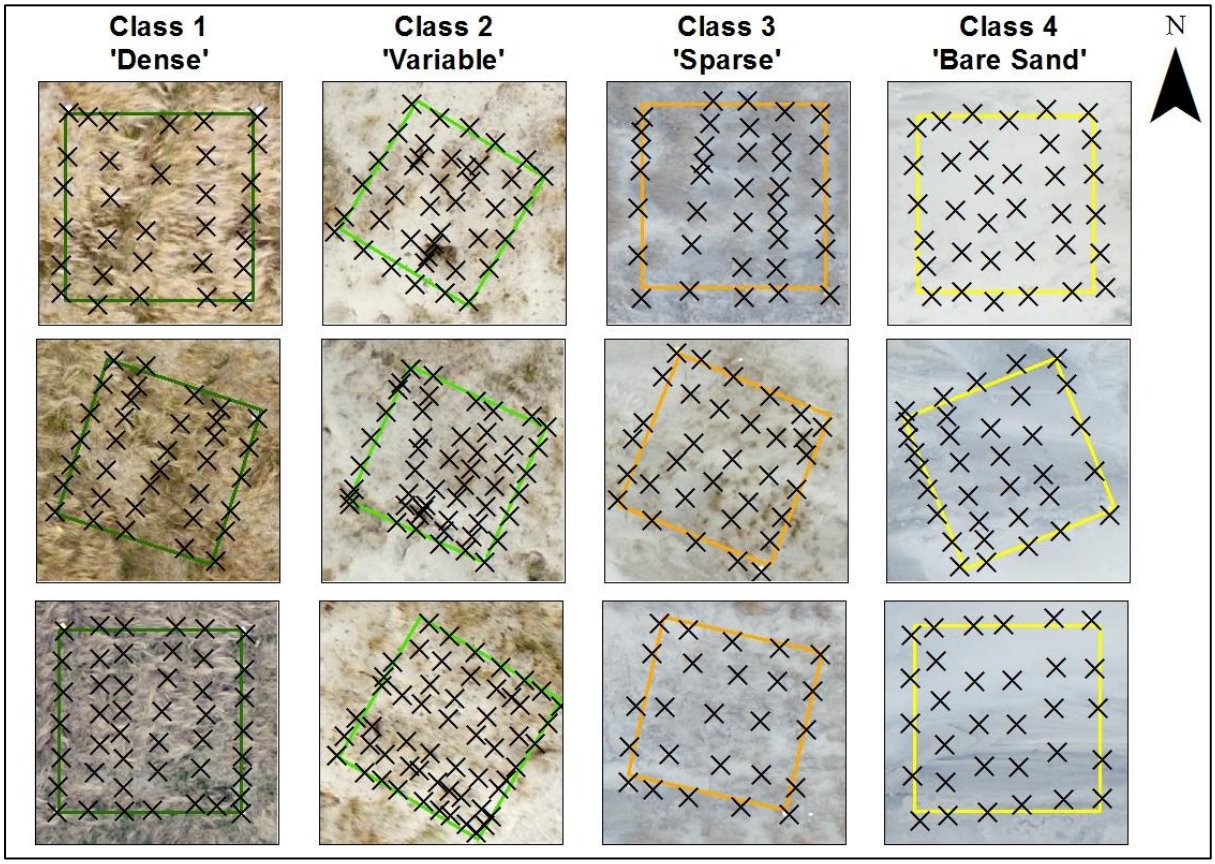

Figure 5.7: The RTK-GPS points recorded in each 5 m^2 plot at Mason Bay, Stewart Island.

The points were recorded relative in New Zealand Transverse Mercator 2000, using the New Zealand Geodetic Datum 2000. The points were uploaded into Trimble Business Centre (TBC), and exported as a Microsoft Excel file. A DTM was generated from the 3D points using ArcGIS, employing a thin plate spline interpolation from the *Geostatistical Analyst* toolbox. The *Geostatistical Analyst* was used to complete a cross-validation to calculate the vertical precision and accuracy of each DTM.

5.3.4 Surface comparison

Two surfaces were created for each plot; one from the RPAS survey, and the other from the RTK-GPS survey. Both surfaces were uploaded to ArcGIS and the 'Minus' tool from the *3D Analyst* toolbox was used to create elevation change surfaces. The RTK-GPS surface was subtracted from the RPAS surface, to determine the elevation difference. For each plot, a significance test was conducted to calculate the statistical significance of the elevation differences. The 'Raster to Point' tool was used to convert the pixels in each surface to points. The point data was then uploaded to excel, and a random number calculator was used to extract 100 points from each surface. The 100 random samples from each surface were tested for equal variances using Minitab 17 statistic software. If the variances were equal, a two sample t-test was conducted between the RTK-GPS sample points and the RPAS sample points. If the variances were not equal, a Mann-Whitney U-test was conducted. The p-values and 95% confidence intervals were used to determine if the elevation differences between the RTK-GPS and RPAS surfaces were significantly different. The null hypothesis is that the difference between the RTK-GPS and RPAS surfaces is not significantly different.

To assess the relevance of vegetation height and cover, the results from the vegetation surveys were compared with the DoDs. The average vegetation height of each plot was compared to the average change in elevation. The 90 vegetation height samples collected from each plot were compared with 90 random samples from the DoDs. A test for equal variances was conducted, to determine which statistical test to use. If the variances were equal, a two sample t-test was used, if the variances were not equal, a Mann-Whitney U-test was conducted. The p-values and 95% confidence intervals were used to assess if the vegetation height and the elevation difference was significantly different. The null hypothesis was that the vegetation height and elevation difference is not significantly different.

A supervised classification was used to reclassify the RPAS orthomosaic to 'vegetated' and 'non-vegetated' areas. 'Training sites' were used to ensure the different types of vegetated

pixels were recognised by the software. The reclassified surface was compared with the elevation difference surface to assess the correlation between vegetation cover and elevation change.

5.3.5 Summary

The ground elevation (surveyed with RTK-GPS) and the surface elevation (RPAS) were compared to assess the discrepancy between the surveying methods. The study site was divided into 12 plots, three for each class. The vegetation surveys were conducted with ten 0.5 m^2 quadrats. The vegetation height and cover were recorded. Statistics were used to compare the RTK-GPS and RPAS surveys, and the vegetation height. The RPAS orthomosaic was reclassified to compare the vegetation cover with the elevation discrepancy.

5.4 Results

This section presents the results from this study. The results from the vegetation surveys are presented as averages per plot and class. Class 1 had the tallest plants and the highest percent plant cover, primarily *A. arenaria*. The height and cover was the lowest in Class 3. There was a statistically significant elevation discrepancy for each class except for the bare sand, indicating the bare sand surfaces derived from the RTK-GPS and the RPAS were statistically equal. Vegetation height was not directly correlated with this discrepancy. The vegetated areas in the reclassified raster correspond with the elevation discrepancies. The RMSE z is less than 10 cm, and ME z is less than 2 cm for both the RTK-GPS and the RPAS surfaces.

5.4.1 Vegetation survey

The average vegetation height per plot was calculated for each vegetation class. On average, the vegetation in the Class 1 plots is higher than the other classes (Table 5.1). Class 1 had the highest vegetation cover and height, which was primarily marram grass. Class 3 had the least number of species, the lowest percent vegetation cover and the lowest *A. arenaria* height. Class 2 had the most species present.

Table 5.1: *The results from the vegetation plot surveys.*

		Average Vegetation Height (cm)	Average Vegetation Cover (%)	Marram Cover (%)	Number of Species Present
Class 1 Dense Vegetation	Plot A	22.18	98.8	87.1	3
	Plot B	27.08	85.0	45.0	6
	Plot C	43.56	94.0	85.7	6
	Class Average	30.94	92.6	72.6	5
Class 2 Variable Vegetation	Plot A	18.25	34.6	17.8	6
	Plot B	23.73	47.0	36.0	7
	Plot C	16.73	32.5	14.6	7
	Class Average	19.72	38.0	22.8	6.7
Class 3 Sparse Vegetation	Plot A	5.70	43.0	43.0	1
	Plot B	4.97	9.0	8.8	2
	Plot C	12.23	26.1	24.1	1
	Class Average	7.56	26.03	25.3	1.3

5.4.2 Digital terrain model and digital surface model comparisons

DTMs and DSMs were produced of each plot from the RTK-GPS and RPAS surveys. The vertical precision and accuracy of each surface is presented in Table 5.2. The RPAS plots were extracted from the DSM of the whole site (Appendix B), the RMSE and ME is, therefore, the same for each plot. The RPAS DSM is more precise for all classes, except for the bare sand. The RPAS surfaces, on average, had a ME of 2 cm. All of the RTK-GPS surfaces had lower vertical ME values, suggesting the RTK-GPS surfaces are less biased. RTK-GPS Class 1, Plot A, had the largest vertical ME (1 cm). The same plot had the highest vertical RMSE (13 cm).

Table 5.2: *The vertical accuracy (mean error) and vertical precision (root mean square error) of each plot surface created from the RTK-GPS and RPAS surveys.*

		RMSE z (m)		Mean Error z (m)	
		RTK-GPS	RPAS	RTK-GPS	RPAS
Class 1 Dense Vegetation	Plot A	0.126	0.034	0.012	-0.018
	Plot B	0.072	0.034	-0.001	-0.018
	Plot C	0.057	0.034	-0.0002	-0.018
Class 2 Variable Vegetation	Plot A	0.074	0.034	-0.002	-0.018
	Plot B	0.078	0.034	0.006	-0.018
	Plot C	0.061	0.034	0.002	-0.018
Class 3 Sparse Vegetation	Plot A	0.073	0.034	-0.005	-0.018
	Plot B	0.053	0.034	0.004	-0.018
	Plot C	0.039	0.034	0.002	-0.018
Class 4 Bare Sand	Plot A	0.014	0.034	-0.002	-0.018
	Plot B	0.030	0.034	0.003	-0.018
	Plot C	0.008	0.034	0.0004	-0.018

The average plot elevation reported by each RTK-GPS and RPAS DSM was compared. The difference in the average elevation between the RTK-GPS and the RPAS surfaces did not exceed 30 cm, and for the bare sand plots the largest difference was 10 cm (Table 5.3).

Table 5.3: *The average elevation for each RTK-GPS and RPAS plot DSM.*

		Average Plot Elevation (m)	
		RTK-GPS	RPAS
Class 1 Dense Vegetation	Plot A	9.6	9.9
	Plot B	7.5	7.6
	Plot C	9.7	10.0
Class 2 Variable Vegetation	Plot A	3.1	3.3
	Plot B	5.1	5.2
	Plot C	3.1	3.3
Class 3 Sparse Vegetation	Plot A	9.8	9.9
	Plot B	5.0	5.2
	Plot C	8.0	8.1
Class 4 Bare Sand	Plot A	4.3	4.3
	Plot B	7.7	7.8
	Plot C	8.5	8.6

A DTM of difference (DoD) was produced for each plot, showing the elevation difference between each corresponding RTK-GPS and RPAS surface. The Class 1 plots have greater elevation differences than the other classes. Class 1, Plot A (Figure 5.8) shows elevation differences between 20 and 60 cm. The elevation difference in Plots B and C range from approximately 20 cm to 75 cm (Figure 5.8).

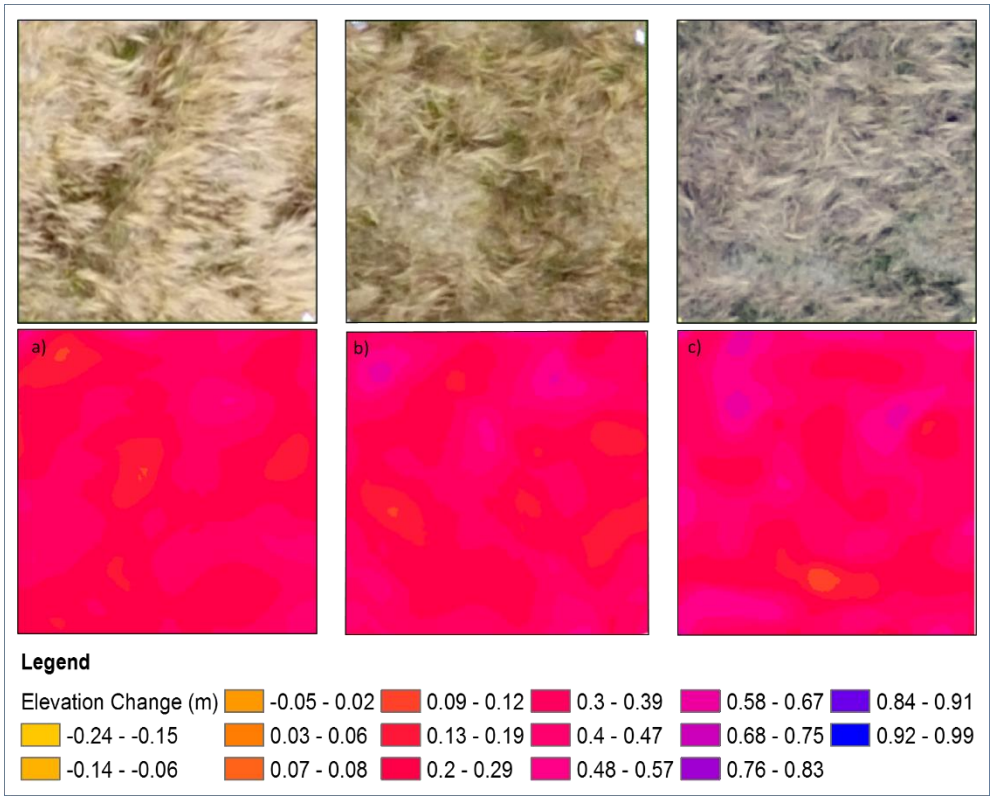

Figure 5.8: The DoDs representing the difference between the RTK-GPS and RPAS surfaces for Class 1 (dense vegetation), and photographs of the corresponding plots.

Class 2 plots have similar elevation differences to the Class 1 plots. However, there are some areas in the Class 2 plots with differences as small as 14 cm. The areas with a negative change in elevation (the orange pixels) correspond with patches of bare sand (Figure 5.9).

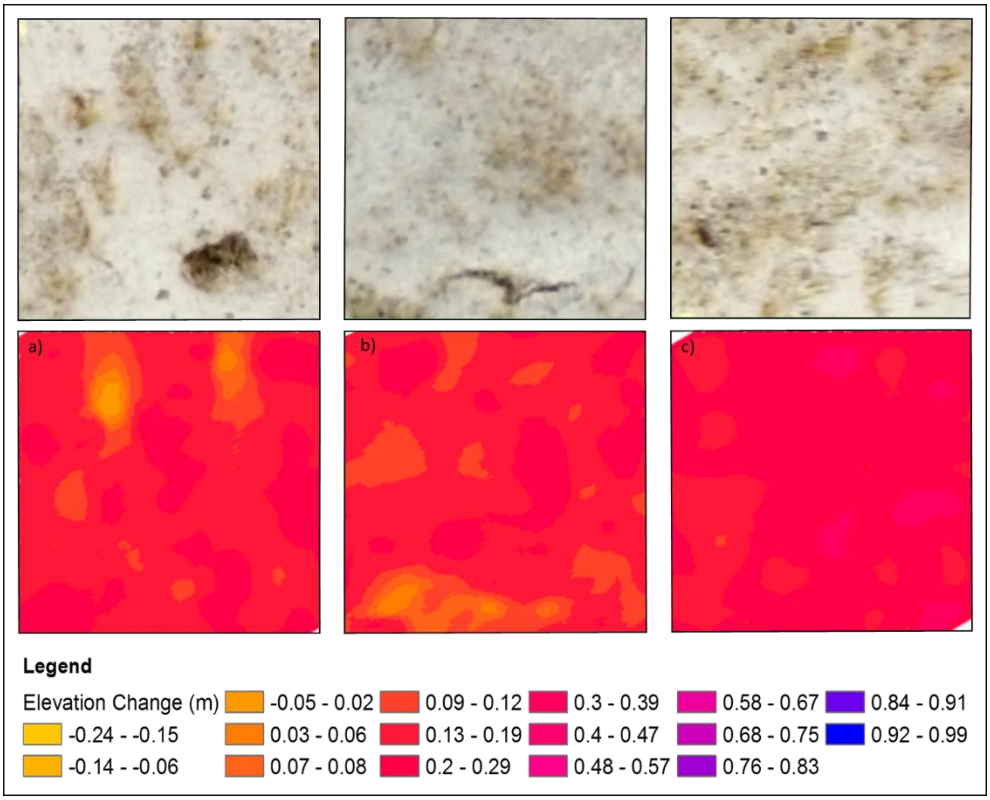

Figure 5.9: The DoD representing the elevational difference between the RTK-GPS and RPAS surfaces for Class 2 ('variable' vegetation), and photographs of the corresponding plots.

The Class 3 plots have smaller elevation differences than Classes 1 and 2. The elevation difference in Plots A and C ranges between -14 cm and 12 cm. Plot B has larger elevation differences, in between 6 cm and 40 cm. The vegetation is Plot B is darker than the other plots, and the individual plants are more clustered. The vegetation in Plots A and C is lighter in colour, and lodged (Figure 5.10).

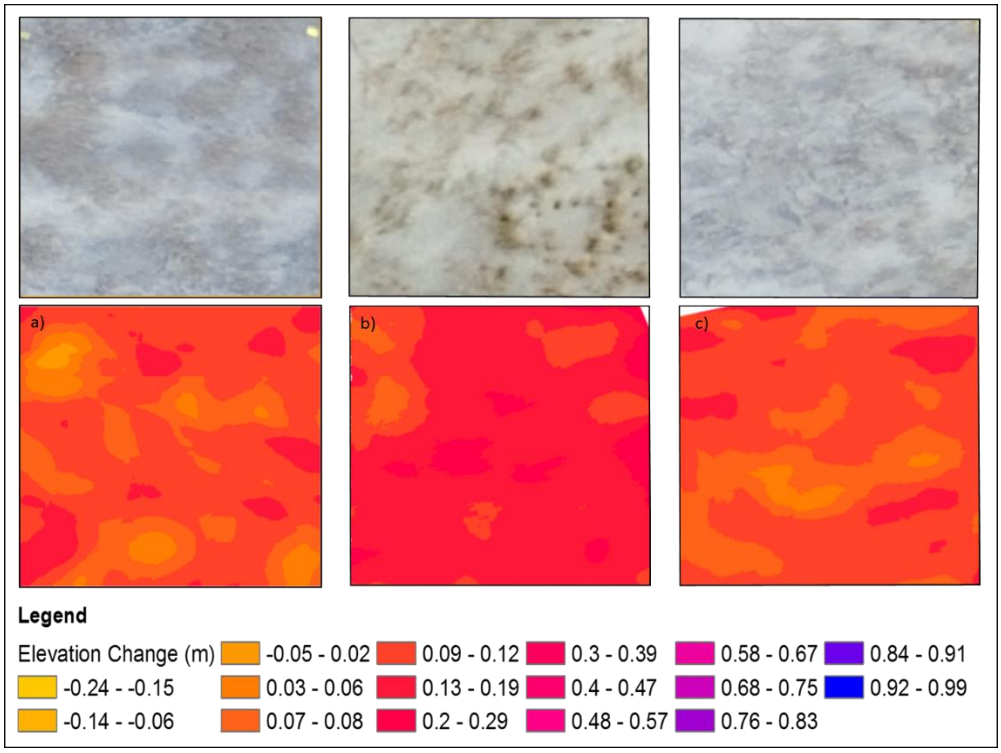

Figure 5.10: The DoDs representing the elevational difference between the RTK-GPS and RPAS surfaces for the Class 3 (sparsely vegetated) plots, and photographs of the corresponding plots.

The Class 4 plots had the smallest elevation discrepancies, ranging between approximately -24 and 20 cm. In the top right corner of all three plots there is a spike in elevation, where the corner marker was included in the RPAS interpolation. The elevation differences in these corners reaches up to 99 cm (Figure 5.11), these values were excluded from the analysis.

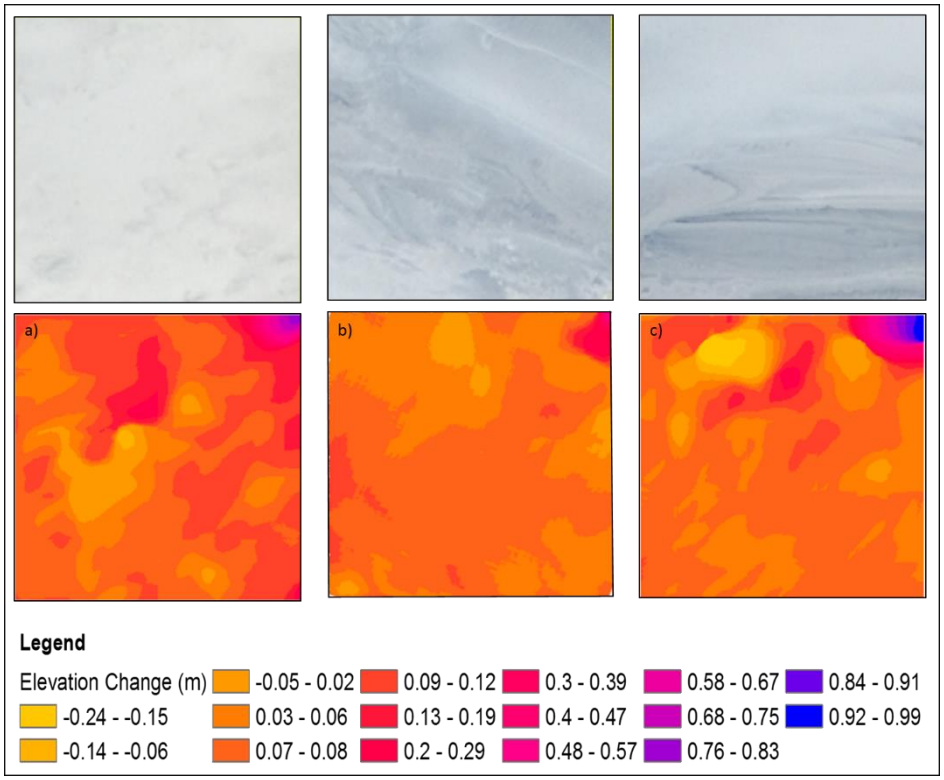

Figure 5.11: The DoDs representing the elevational difference between the RTK-GPS and the RPAS surfaces for Class 4 (bare sand) plots, and photographs of the corresponding plots.

A statistical analysis was undertaken to test the significance of the difference between the elevation of the RTK-GPS and RPAS surfaces (Table 5.4). The differences were tested using a 95% confidence interval.

Table 5.4: *The results from the significance tests, for the difference between the RTK-GPS surfaces and the RPAS surfaces.*

		RTK-GPS vs. RPAS	
		95% Confidence Interval	P-Value
Class 1 Dense Vegetation	Plot 1A	-0.3532, -0.2316	0.000
	Plot B	-0.3917, -0.2490	0.000
	Plot C	-0.1940, -0.0857	0.000
Class 2 Variable Vegetation	Plot A	-0.394, -0.331	0.000
	Plot B	-0.2127, -0.0655	0.000
	Plot C	-0.3199, -0.1839	0.000
Class 3 Sparse Vegetation	Plot A	-0.2202, -0.0676	0.000
	Plot B	-0.2174, -0.0400	0.005
	Plot C	-0.1543, -0.0700	0.000
Class 4 Bare Sand	Plot A	-0.1034, 0.0624	**0.626**
	Plot B	-0.1181, 0.0255	**0.205**
	Plot C	-0.1947, 0.0364	**0.178**

The null hypothesis was that the elevation difference between the RTK-GPS and RPAS surfaces was not significantly different. The null hypothesis was rejected for Classes 1, 2 and 3, because the p-value was below 0.05, and the corresponding confidence intervals did not include 0. Hence, the RTK-GPS and RPAS surface elevations for each plot in Classes 1, 2 and 3 had a statistically significant difference.

All of the plots in Class 4 had p-values above 0.05, and the confidence interval included 0. Hence, the null hypothesis was accepted. This result indicates that the elevation of the RTK-GPS surface and the elevation of the RPAS surface is not significantly different in the bare sand plots, i.e. the elevation of the DSMs is statistically equal.

Significance tests using 95% confidence intervals were conducted to test if the difference in elevation between the DTM and DEM was attributed to vegetation height. The null hypothesis was that the vegetation height and elevation difference was not significantly different. The null hypothesis was rejected for all plots, indicated by the p-values and 95% confidence intervals, except Class 2 Plot A and Class 3 Plot C. The confidence intervals for the majority of the plots did not contain 0 and the p-values are below 0.05; the vegetation height

was not equal to the difference in elevation. Class 2, Plot A, and Class 3, Plot C both had 0 included in the confidence intervals, and retrieved a p-value above 0.05. The null hypothesis was, therefore, accepted for these plots, i.e. the difference between vegetation height and the elevation difference was not statistically significant.

Table 5.5: *The results from the significance test to assess if the height of vegetation and the difference in elevation between the RTK-GPS surfaces and the RPAS surfaces are statistically significant.*

		Vegetation Height vs. Elevation Difference	
		95% Confidence Interval	P-Value
Class 1 Dense Vegetation	Plot A	0.02897, 0.08785	0.0002
	Plot B	0.00953, 0.08219	0.0172
	Plot C	-0.11412, -0.04133	0.0000
Class 2 Variable Vegetation	Plot A	-0.07011, 0.03287	**0.5152**
	Plot B	-0.12299, -0.05799	0.000
	Plot C	0.0281, 0.0878	0.000
Class 3 Sparse Vegetation	Plot A	0.03492, 0.05422	0.000
	Plot B	0.08641, 0.10886	0.000
	Plot C	-0.04376, 0.00154	**0.0815**

The results suggested that the difference in elevation between the two surfaces was not directly related to the height of the vegetation. To investigate the difference further, the cover of vegetation in each plot was calculated, by conducting a vegetation classification on the orthomosaic photograph produced from the RPAS imagery.

The large elevation difference in Class 1 (20–75 cm) is associated with vegetation cover. The patch of sand in Plot C is at the same location as the area of a decrease in elevation in the DoD (Figure 5.12).

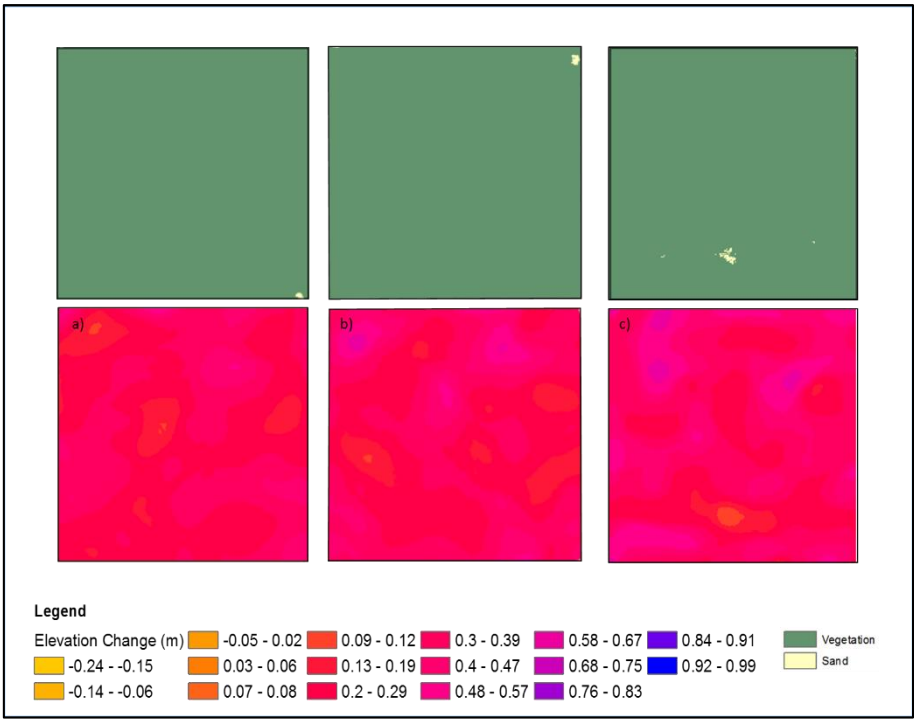

Figure 5.12: The vegetation cover and the DoDs for Class 1 ('dense' vegetation).

Class 2, Plot B has the highest percentage plant cover, however, Figure 5.13 shows that this cover is less homogeneous than the cover in Plot C. The elevation difference between -5 and -8 cm correspond to the areas of bare sand. Plot C, which has more homogeneous vegetation pixels (i.e. is denser), exhibits larger elevation changes.

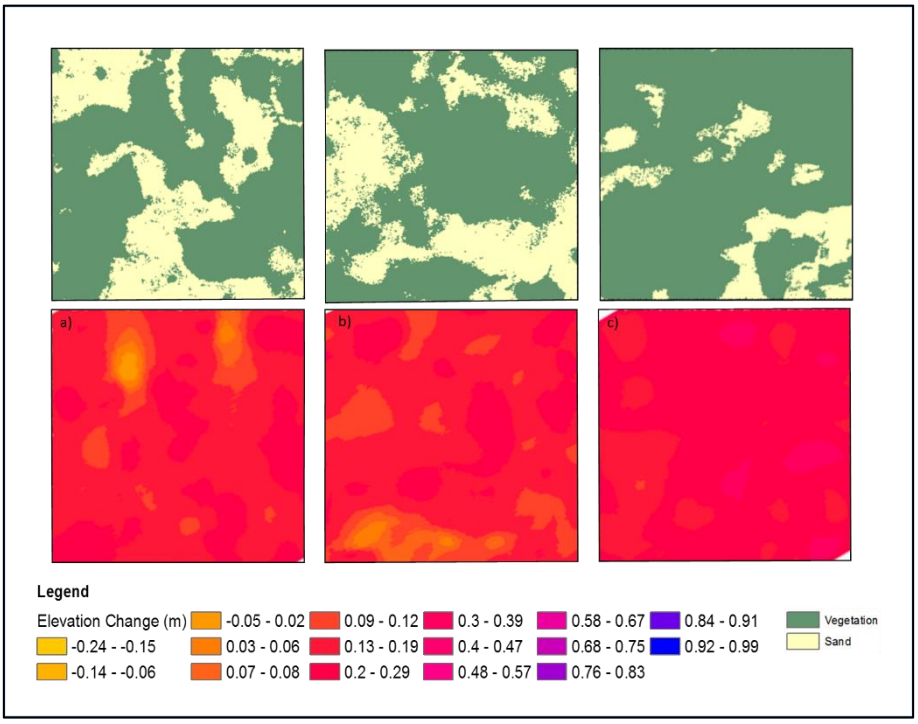

Figure 5.13: The vegetation cover and DoD for Class 2 ('variable' vegetation).

In the Class 3 plots, Plots A and C have the least vegetation cover, and also the smallest difference in elevation between the RTK-GPS and the RPAS DSMs (Figure 5.14). The association between vegetation cover and the elevation difference is clear in the Class 3 plots. Plot C shows areas with increased elevation are the areas where vegetation is presented. Plot B has the most vegetation cover and the largest elevation discrepancies.

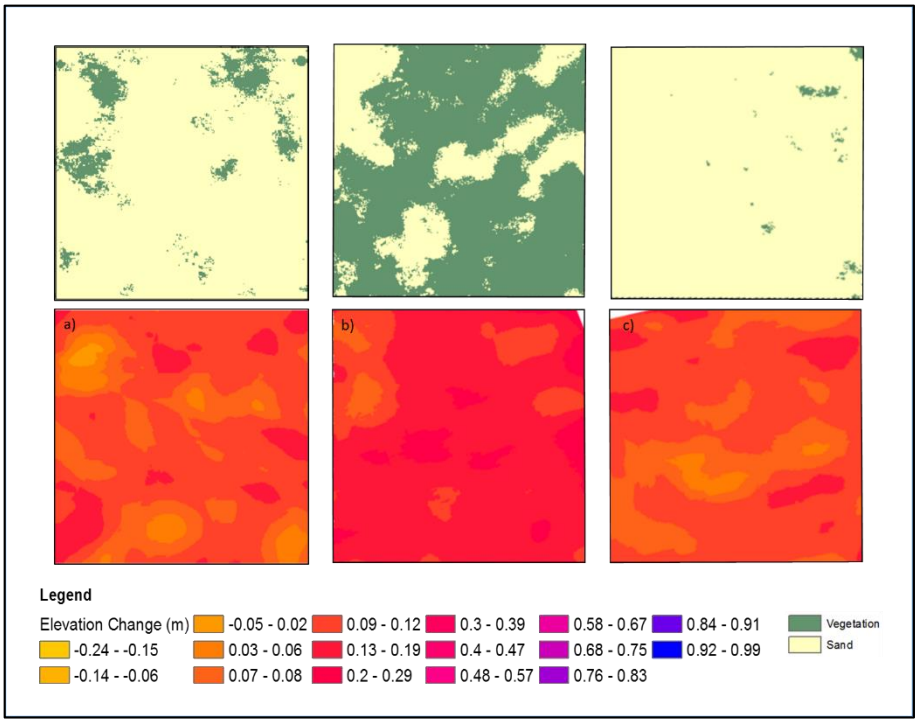

Figure 5.14: The vegetation cover and DoDs for Class 3 (‘sparse’ vegetation).

5.4.3 Summary

The difference in elevation between the surfaces created by the RTK-GPS and RPAS is statistically different, except for the bare sand plots. The discrepancies between the RTK-GPS and RPAS surfaces were greater in the plots containing vegetation. The vegetation height and the elevation discrepancies were statistically unequal. However, the elevation difference corresponded with the vegetation cover.

5.5 Discussion

The difference between the RTK-GPS DTMs and the RPAS DSMs is statistically significant. The height of vegetation does not appear to be a direct cause of the elevation difference. However, it is suggested that the combination of vegetation height and density influences the elevation of the RPAS DSMs. This section will discuss the influence of vegetation height and cover on the elevation recorded by RPAS. Ground filtering algorithms

for deriving DTMs from DSMs, and the impact of spectral properties on elevations derived from RPAS will also be discussed.

5.5.1 Vegetation height and cover

The results suggest there is not a direct link between the elevation discrepancy in the DSM and vegetation height. Four vegetation classes were selected, densely vegetated, variably vegetated (a range of species present), sparsely vegetated, and non-vegetated. The height of *A. arenaria* was greater in the densely vegetated plots. The results of the significance tests indicate that the height of the vegetation and does not in itself correspond to the difference in elevation between the RTK-GPS and RPAS surveys. Hence, the difference between the RTK-GPS DTM and the RPAS DSM is probably not a direct result of vegetation height. Therefore, simply removing the height of vegetation from DSM does not accurately produce a DTM.

The findings from other studies are consistent with the findings from the current study. Li *et al.* (2016) investigated the ability of a low-cost RGB RPAS to estimate the height of maize crops. The study compared the canopy height detected by the RPAS with field measurements using a tape measure. The difference between the heights measured in the field, and the elevation detected by the RPAS was 11 cm. In the current study, the difference between the vegetation heights measured in the field and the discrepancy between the RTK-GPS and RPAS surveys varied between 2.2 cm and 10 cm.

Studies by Harwin and Lucieer (2012), Dufour *et al.* (2013), and Wallace *et al.* (2016) have found that dense and complex vegetation covers (with varying heights, overlapping branches, dead and dry vegetation) are not accurately represented in RPAS point clouds. In the current study, the study site was primarily comprised of *A. arenaria* which has a tussock-like form, and is <1 m high. The underground rhizome system spreads horizontally and vertically. The blades are up to 6 mm wide, and approximately 30 cm long. The blades bend and overlap somewhat inconsistently, creating a complicated vegetation canopy. However, at Mason Bay, *A. arenaria* tends to 'lodge' or lean-over when exposed to the prevailing onshore wind (Hilton and Konlechner, 2010). The lodging directs the blades in the same direction, which can create a dense vegetation cover (Figure 5.15).

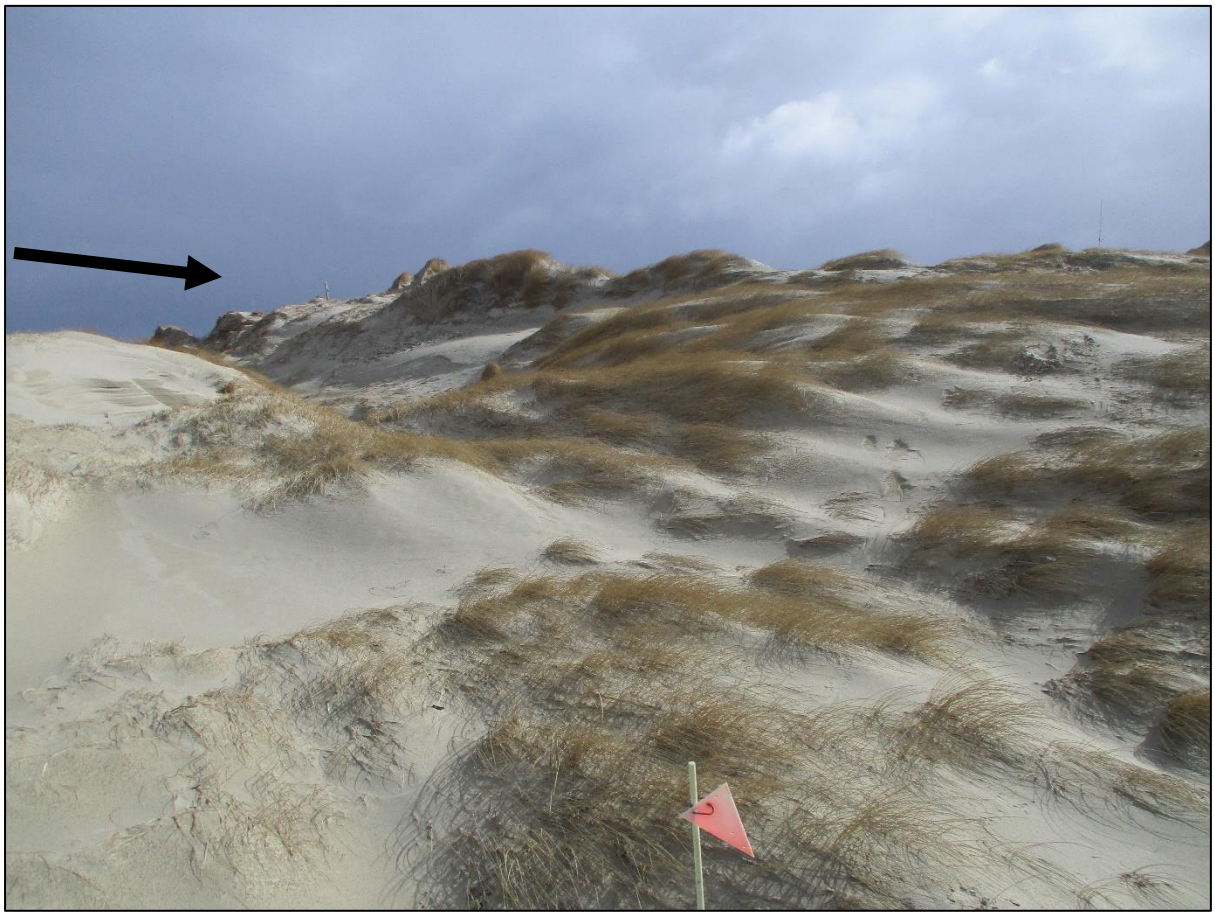

Figure 5.15: Marram grass lodging on the Mason Bay foredune. The black arrow represents the prevailing onshore wind.

The lodged *A. arenaria* creates a dense cover, despite the thin structure of the blades. Vegetation cover also depends on the plant distribution; clusters of individual plants will produce a dense cover. In some areas, the individual plants are sparse, such as the Class 2 and 3 plots, which creates a complicated surface. The representation of vegetated surfaces can also be impacted by the wind. Vegetation on coastal dune systems is largely impacted by wind, which can make image matching difficult, because the position of individual plants can change between subsequent photographs due to the wind (Eltner *et al.*, 2016).

The results from this study suggest that vegetation cover and density have a greater impact on the elevation detected by a RPAS than vegetation height. However, this is largely controlled by the GSD of the imagery. The flight conducted at Mason Bay had an average GSD of 2.1 cm^2, hence, the size of each pixel on the ground is 2.1 cm^2 (Figure 5.16).

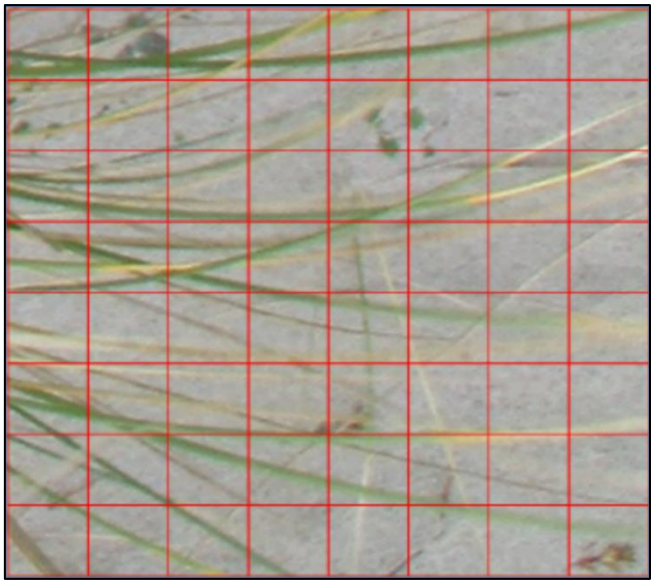

Figure 5.16: Scaled example of the GSD derived from this study. Each grid square is 2.1 cm^2.

The elevation recorded by the RPAS depends on the cover in each 2.1 cm^2 pixel. For example, the cells that are mostly covered in bare sand will record the elevation of the sand. Hence, the smaller the GSD, the more likely the RPAS is to record the ground elevation below patchy or variable *A. aernaria*. The plant structure is, therefore, likely to influence the elevation derived from the RPAS surface.

The effect different plant structures have on RPAS surveys can be observed in the DSMs produced in Chapter 4 at St. Kilda beach, Dunedin. In particular, individual *Coprosma repens* (taupata) and *Lupinus arboreus* (tree lupin) are easily differentiated in the DSMs, compared to *A. arenaria*. *C. repens* is a small tree/shrub that grows between 3-5 m high, and 2-3 m wide. The leaves are dark green, with a surface area of 5–90 mm by 4–60 mm. *L. arboreus* is a shrub that grows 2-3 m high. The shrub is dense, and each branch has multiple light-green leaves that are 15-40 mm x 3-10 mm in size (Figure 5.17).

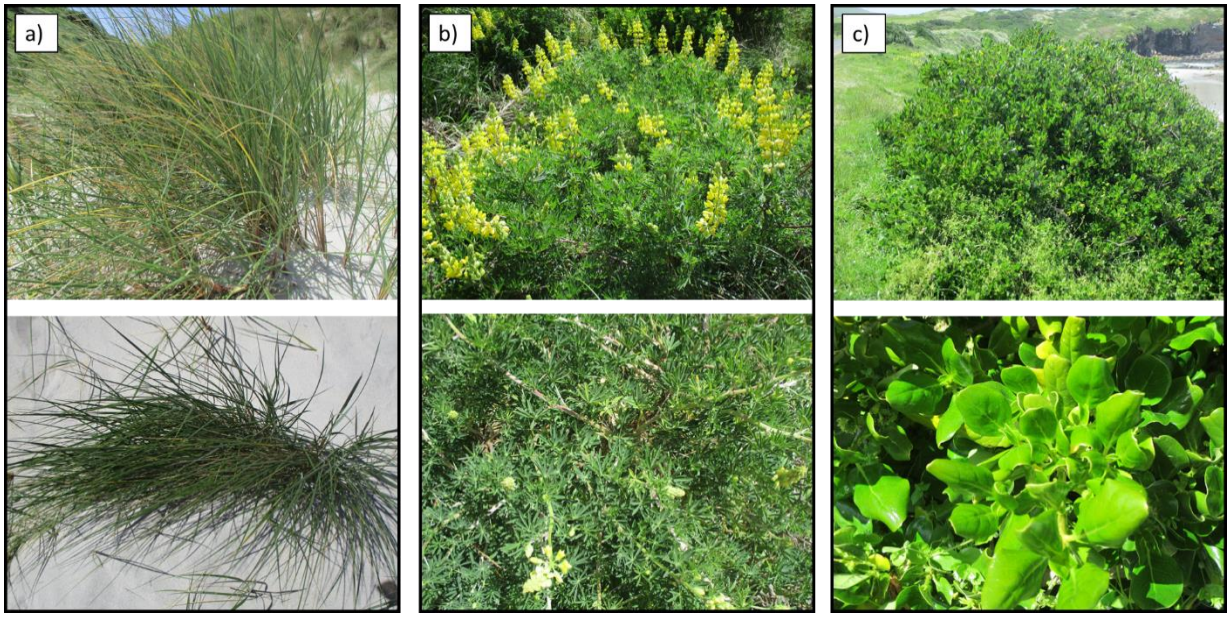

Figure 5.17: Oblique (top) and vertical (bottom) photographs of a) *A. arenaria*, b) *L. arboreus*, and c) *C. repens*.

The individual *C.repens* plants are obvious in the DSM due to the dense leaf and branch structure. Individual plants can be differentiated, even where multiple *C. repens* are located next to each other. Individual *A. arenaria* and *L. arboreus* are easily differentiated on the bank of John Wilson Drive, however, on the foredune where the plants overlap it is difficult to identify the individual plants (Figure 5.18).

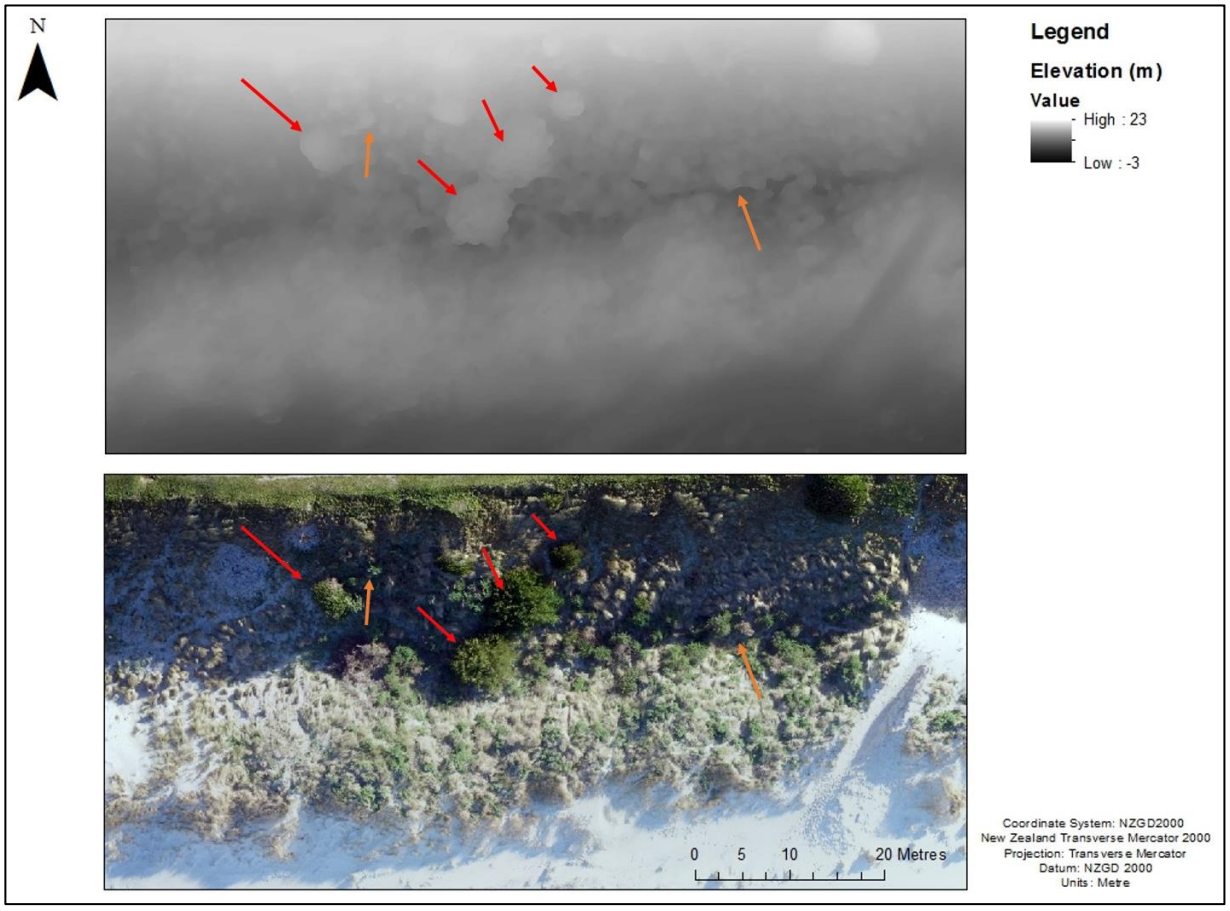

Figure 5.18: A DSM and orthomosaic from Flight Four in Chapter 4 of the St. Kilda foredune. The red arrows point to *C. repens* visible in the DSM, the orange arrows point to *L. arboreus*.

There are three potential explanations for these findings. Firstly, the vegetation is less dense on the bank, therefore, it is more likely that the elevation in-between the plants (i.e. the ground) is recorded. Secondly, the vegetation has a more uniform height on the foredune, making it difficult to differentiate individual plants. Conversely, in the swale, the *L. arboreus* are taller than the *A. arenaria*, allowing individual plants to be differentiated. Lastly, the foredune is more effected by direct sunlight, which creates differences in illumination between the foredune and the swale. Therefore, the plants on the foredune appear brighter and more similar in colour, making the individual plants difficult to interpret.

5.5.2 Ground filtering algorithms

Ground filtering algorithms can be employed to extract digital terrain models from digital surface models (Shaad *et al.*, 2016). The algorithm differentiates 'ground' and 'non-ground' areas, and only uses the areas recognised as 'ground' for the interpolation, hence, generating a DTM not a DSM (Shaad *et al.*, 2016). Ground filtering algorithms are typically used to generate DTMs from LiDAR data (Yilmaz *et al.*, 2016). However, Shaad *et al.* (2016)

and Yilmaz *et al.* (2016) have both explored the issues with ground filtering algorithms on RPAS datasets.

Ground filtering algorithms are used on LiDAR datasets because there are typically a large number of ground points. LiDAR records the first surface the laser reaches, however, the laser often reaches through the gaps in the vegetation (Wallace *et al.*, 2016). RPAS is less likely to detect the ground elevation through gaps in vegetation, depending on the GSD (Dufour *et al.*, 2013). Hence, RPAS data often does not have enough ground data points to successfully apply ground filtering algorithms (Yilmaz *et al.*, 2016).

Ground filtering algorithms may be employed where there is ample ground visible, however, this depends on the sparsity of the vegetation and the vegetation structure. The reclassified plots with 'sparse' and 'variable' vegetation have 'vegetated' and 'non-vegetated' pixels, whereas the 'dense' plots only have 'vegetated' pixels. The applicability of ground filtering algorithms, therefore, depends on the vegetation density.

5.5.3 Spectral resolution

The spectral properties of a surface can influence the processing of aerial imagery for deriving DSMs and orthomosaics (Whitehead and Hugenholtz, 2014). Low-cost RPAS are typically equipped with low-quality sensors These types of sensors can produce artefacts (errors in the output surface caused by inaccurate photogrammetric modelling) in the output DSM (Whitehead and Hugenholtz, 2014). Artefacts are observed in the Mason Bay imagery. Specifically, where incorrect image balancing and blurring is present (Figure 5.19).

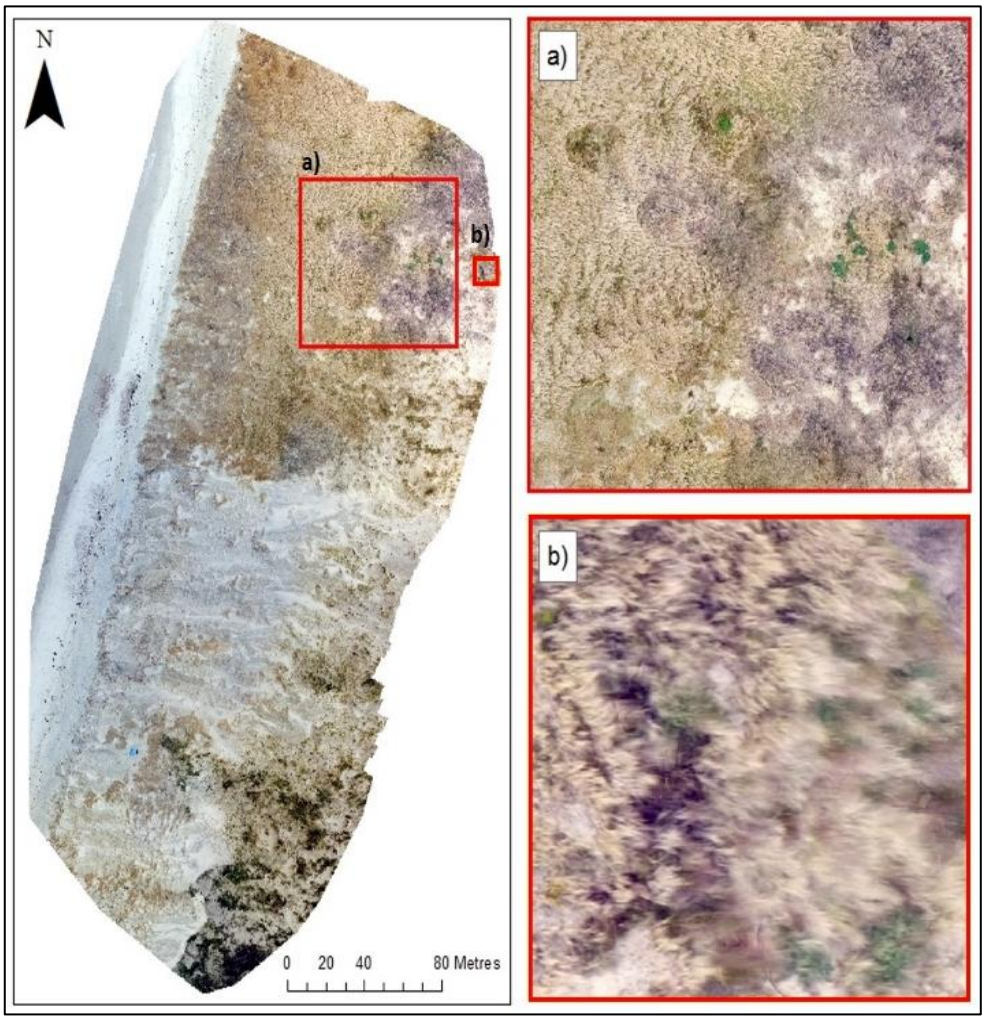

Figure 5.19: Artefacts in the orthomosaic produced from the Mason Bay imagery. a) An example of incorrect colour balancing, b) An example of mosaic blurring.

A. arenaria in the imagery either appears as a dull grey or a bright 'straw' colour, caused by incorrect colour balancing (Figure 5.18). This is likely a result of variation in the cloud cover, which illuminates different areas in subsequent photographs (Whitehead and Hugenholtz, 2014). This variation makes it difficult to recognise plant type based on the plant's spectral properties, and also creates error in the point cloud (Eltner *et al.*, 2016). Image blurring is caused by long exposure time. Blurring reduces the quality of the images, and hence causes inaccuracies in the DSM.

The vegetation is difficult to differentiate from the sand in Class 3, Plots A and C, due to the colour. These plots are located in the section of foredune that has been sprayed for *A. arenaria* on five occasions. *A. arenaria* is present in these areas, however, it is mostly dead and has changed from its healthy green colour to a faded straw-yellow 'straw' colour, similar to sand.

The current study employed a supervised classification to 'training' samples which allowed the software to identify areas of vegetation. 'Training' samples consisted of both the faded and bright marram areas, to avoid an inaccurate reclassification of the orthomosaic. The pixels were categorized as either 'vegetated' or 'non-vegetated'. Clusters of 'vegetated' cells corresponded to the larger elevational discrepancies, opposed to the 'vegetated' cells that were less clustered.

5.5.4 Summary

The results from this study suggest that the elevation recorded by an RPAS is primarily a combination of vegetation height and density. However, the structure of the vegetation also has an influence, whereby the elevation of vegetation with a larger surface area is likely to be detected more accurately by an RPAS than vegetation with a smaller surface area (for example, *A. arenaria*). Vegetation structure also determines the applicability of using ground filtering algorithms to derive DTMs. Last of all, the spectral properties of the surface also contribute to the elevation detected by the RPAS. In this study, the 'sparse' plots contain dead marram plants, similar in colour to the sand. This makes image matching more difficult for the software, because it is difficult to differentiate between the two surfaces.

5.6 Conclusions

This chapter investigated the potential factors causing the elevation offset of RPAS derived DSMs in areas where vegetation is present (Research Question 3). Low-cost RGB RPAS sensors are sensitive to a combination of factors that influence the elevation recorded including, vegetation height; vegetation cover/density; the GSD; the structural properties of the vegetation; and the spectral properties of the surface.

It was initially hypothesized that the difference between the RPAS surface and the ground is equal to the height of vegetation. The results from this study show that vegetation height and the elevation discrepancy between the ground surface and the RPAS derived DSM, are statistically different. Therefore, there are other factors contributing to the elevation discrepancy.

The orthomosaic reclassification showed that the dense vegetation cover was consistent with the areas with larger elevation discrepancies. Therefore, it is clear that the density of vegetation impacts the elevation recorded by the RPAS. The elevation recorded by the RPAS is a combination of the GSD and the structural properties of the vegetation.

Ground filtering algorithms can be used to extract the ground points from the DSM to create a DTM, but they are only useful where there is bare sand visible in the imagery. The reclassification of the densely vegetated plots only identified a few pixels of bare sand. Ground filtering algorithms would, therefore, be inappropriate for datasets that contain dense vegetation.

Lastly, RGB RPAS surveying is sensitive to the spectral properties of the surface. Artefacts such as incorrect colour balancing and image blurring can be present in the resulting orthomosaic. This can be caused by low-quality cameras. This type of method is also impacted by variations in illumination of the surface which can create errors in the point cloud used to create the DSM.

Chapter 6

Synthesis and conclusions

6.1 Introduction

This study evaluates the efficacy of low-cost remotely piloted aerial systems (RPAS) for coastal dune surveying. Coastal dune systems are dynamic environments that are influenced by factors such as sand supply, wind and wave action, human interactions, and vegetation presence (Hesp, 2002). Foredunes act as barriers by absorbing wind and wave energy, and hence, can prevent erosion and inundation of landward features (Bochev-van der Burgh *et al.*, 2011). Foredunes are one of the most seaward dune features and are, consequently, susceptible to changes in morphology caused by wind and waves (Benavente *et al.*, 2013). Therefore, monitoring changes in foredune morphology is important for understanding the vulnerability of the coastline to erosion, and predicting future changes (Saye *et al.*, 2005). Low-cost RPAS are efficient, comparatively inexpensive, and surveys can be conducted at short-notice, which is beneficial for capturing event-scale changes. Low-cost RPAS have the potential to be employed for coastal foredune monitoring (Gonçalves and Henriques, 2015).

The current study investigated the challenges associated with using low-cost RPAS technology. One of the biggest challenges with low-cost RPAS surveying is ensuring the elevation data is accurate, which can depend on the resolution of the camera, the image overlap, and the configuration of GCPs. The process of photogrammetry derives elevation data from the aerial photographs obtained by an RPAS. Prior to the development of RPAS technology, photogrammetry was only conducted by photogrammetry experts. However, the accessibility of RPAS, in conjunction with readily available software, means this technology is employed by a range of non-expert users. Consequently, there is a risk that the method is not employed correctly, and errors in the output model are not identified.

This chapter will discuss the results of Chapters 3, 4 and 5, which were organised to address the following three research questions:

1. How does the accuracy and cost of data collected by low-cost RPAS compare to other coastal surveying methods?
2. Can data collected by a low-cost RPAS be used to quantify morphologic change of a coastal foredune?
3. To what degree and how does vegetation affect the development of digital elevation models from RPAS photogrammetry?

Research Question 1 was addressed by comparing an RPAS survey with three surveying methods widely used in coastal science and management (total station, RTK-GPS, and terrestrial laser scanning). RPAS technology could be employed more widely if the method can provide advantages over other coastal surveying methods. Surveys conducted using each method were compared in relation to the rate of point acquisition (efficiency), the cost of each surveying method, the accuracy of the DSM/DTM produced from each survey, and the limitations imposed on the survey by atmospheric/environmental conditions.

The second research question was addressed by investigating the errors associated with modern RPAS photogrammetry. The photogrammetric method applied to RPAS photogrammetry has been found to produce un-modelled systematic error in the output DSM, typically not identified by RPAS photogrammetry users (Sirguey *et al.*, 2016). This was investigated by assessing the interior orientation parameters of the RPAS used in this study. Secondly, the errors were quantified and used to adjust the DSM, creating unbiased DSMs of the study site. The unbiased DSMs were subsequently used to quantify morphologic changes in the coastal foredune over the four month study period.

Research Question 3 was explored by assessing the DSM produced by the RPAS against a DTM produced by an RTK-GPS survey. RPAS surveying with an RGB camera produces a model based on the elevation of the top surface, hence, vegetation presence can offset the elevation recorded (Whitehead and Hugenholtz, 2014). To examine this offset, areas containing different vegetation densities were compared. Statistical analyses were conducted to investigate the impact of vegetation height on the surface recorded by the low-cost RGB RPAS. An image reclassification was conducted to identify the pixels that contain vegetation,

based on the spectral properties of each pixel. The reclassified image was compared with the elevation difference observed in the DSM/DTM comparison.

6.2 Discussion

6.2.1 Remotely piloted aerial system surveying and photogrammetry

Coastal dune surveys using low-cost RPAS offer advantages over conventional surveying methods. Firstly, low-cost RPAS requires minimal surveying expertise, especially when flight planning software is employed, which largely automates the survey (Nex and Remondino, 2014). Low-cost RPAS surveying does not require a professional pilot, however, civil aviation regulations require a license to fly in certain areas. Civil aviation rules differ between countries. In New Zealand, flights that occur within 4 km of an aerodrome require the pilot to hold a Wings Badge license (CAA, 2015). Conventional surveying methods (such as total stations) do not require a license, however, these methods require more in-depth knowledge of surveying equipment and techniques. RPAS data processing is also mainly autonomous, and only requires a few processing steps to produce a DSM and orthomosaic (Colomina and Molina, 2014). This is beneficial because the method is accessible to a wider range of people (Ivošević *et al.*, 2015). However, it is also problematic because the potential errors in the data are not always identified by non-expert users.

A number of potential errors associated with RPAS photogrammetry may not be recognised by users who do not have background knowledge of photogrammetry (Sirguey *et al.*, 2016). Modern RPAS photogrammetry employs a self-calibration method to solve both the interior and exterior orientation parameters in the bundle block adjustment (BBA), opposed to traditional photogrammetry which solves the interior and exterior parameters separately. The software finds the best solution for all of the parameters, however, it rarely finds the optimal solution. Consequently, un-modelled error is propagated into the output DSM. These errors were investigated in the current study, and the results suggest that the radial lens distortion produces a systematic error in the DSM. The systematic error is contrary to the randomly distributed RMSE reported by the photogrammetric software, Pix4D Mapper. Therefore, RPAS photogrammetry cannot accurately solve the IOPs required for accurate photogrammetric modelling. However, this error is reduced inside the confines of the GCP network (Sirguey *et al.*, 2016).

Accurate RPAS photogrammetry is dependent on the GCP configuration (Sirguey *et al.*, 2016). The GCPs are used to orientate photographs in space (Gonçalves and Henriques,

2015). The GCP configuration needs to extend past the study site to encompass the area of interest, to avoid an increase in systematic error in the photogrammetric model. An even spread of GCPs within the area of interest is also required to produce an accurate photogrammetric model (Linder, 2009). The RMSE value can be assumed 'accurate' if the area of interest is controlled by the GCPs.

A low-cost RPAS is substantially less expensive than conventional surveying instruments. Cost is an important factor; in general, cheaper equipment is more accessible to a wider range of people. An RPAS can be purchased for approximately $1,000 to $100,000. The more expensive models tend to yield better results, however, they also require more expertise to operate. The RPAS in the current study cost approximately $2,000. However, to obtain high accuracy results with RPAS, GCPs must be used. GCPs need to be surveyed with high precision, therefore, RTK-GPS or total station surveys are usually employed to establish a GCP network. High precision surveying equipment increases the cost of an RPAS survey. Photogrammetry software employed to process the imagery can also be expensive; Pix4D Mapper, employed in this study, cost approximately $12,000 for an unlimited licence. However, less expensive software packages are available such as AgiSoft Photoscan, which have also been used to derive DSMs from coastal RPAS surveys (Gonçalves and Henriques, 2015).

Hiring an RPAS surveyor appeared to be the most expensive ($3,000/flight), compared to a total station and RTK-GPS surveyor, which cost $1,500/day. However, the RPAS is capable of surveying large areas in a small amount of time. Hence, if the equivalent survey was conducted with a total station or RTK-GPS, it could take multiple days. As a result, the RPAS survey becomes cost-efficient as the area of the survey increases. For smaller surveys, such as transects, RPAS is less cost efficient.

Rapid surveys are valuable for coastal research (Gonçalves and Henriques, 2015). The dynamic nature of many types of coast can result in major changes in morphology over short time scales. Such changes in morphology are stochastic. Therefore, it is important that surveys can be conducted quickly and at short-notice (Gonçalves and Henriques, 2015). Rapid surveys are especially important when quantifying changes produced from an isolated event, such as storm-forced beach erosion and foredune scarping or coastal inundation. To assess the efficiency of RPAS surveying, the current study compared the time taken to conduct an RPAS survey with the time taken to conduct total station, RTK-GPS and TLS surveys. The RPAS

survey could be completed more rapidly (7 hours faster) than the other methods, including the set-up processing time.

RPAS surveying is, however, more vulnerable to atmospheric conditions than conventional surveying methods. This is primarily a result of the configuration of the aircraft. The size and weight of low-cost aircrafts result in low stability in windy conditions (Nex and Remondino, 2014). Larger RPAS models can withstand higher wind speeds (Aber *et al.*, 2010c). However, during high wind speeds the aircraft uses more power, because the aircraft has to constantly stabilize itself (Nex and Remondino, 2014). The capacity of low-cost RPAS batteries (< 1 hour) is substantially less than other surveying methods (> 2 hours). Therefore, the battery power can deteriorate rapidly in windy conditions. However, RPAS surveying is capable of surveying large areas quickly and, therefore, does not always require an extended battery life.

Precipitation and bright sunlight can also limit RPAS surveys. Low-cost aircrafts, specifically quadcopters, are not waterproof and cannot be operated in the rain. Conversely, bright conditions may create issues with the spectral properties of the imagery. Imagery can become saturated if there is too much illumination. Consequently, imagery may not be able to be processed, as the ground features between adjacent pixels cannot be differentiated. Illumination can also cast shadows over areas of the study site, which can ultimately create errors in the point cloud. Hence, the most optimal conditions for RPAS surveys are low winds (0-5 ms^{-1}), no precipitation, and high cloud cover (diffuse reflection of light). However, because surveys are rapid, it is not difficult to meet the aforementioned conditions (depending on the climate of the area).

In the current study, five flights were undertaken (four at St. Kilda, Dunedin, and one at Mason Bay, Stewart Island). At St. Kilda, flights occurred in the morning, when the wind speed was low. However, the position of the foredune in relation to the sun created variations in illumination during bright conditions. This resulted in colour saturation of some images, which could not be processed, and difficulty identifying the GCP targets in the images. Wind and precipitation at Mason Bay were a major constraint on RPAS surveying, however, a short break in the weather conditions allowed the flight to take place. Variation in illumination can be seen in the orthomosaic as a result of moving cloud cover.

The RPAS DSM was one of the most precise of the four methods compared, because of the dense point cloud. The total station and RTK-GPS were the least precise,

however, each of these surveys contained ~2,000 points. In comparison, the RPAS and TLS retrieved millions of 3D points. Total station and RTK-GPS surveys generally have the highest accuracy and precision, however, the comparatively sparse point cloud makes it difficult for the interpolation to derive a high accuracy DTM.

6.2.2 Vegetation and remotely piloted aerial system surveying

The DSMs derived from the RPAS imagery did not accurately describe dune morphology in vegetated areas. Low-cost RPAS are generally equipped with RGB cameras that are not capable of penetrating vegetation, therefore, the elevation recorded is not necessarily the ground surface (Hugenholtz *et al.*, 2013). In coastal dune environments, this may result in a DSM that describes the elevation of the vegetation canopy, or some elevation between the canopy and the ground. This effect was described in Chapter 3; the RPAS DSM was compared with the DTMs produced from the total station and RTK-GPS data. There were differences of 10 cm to 30 cm between the elevation of the RPAS DSM and the DTMs produced from the other methods in some vegetated areas.

This offset resulted from a number of factors, including vegetation height, vegetation density, the spectral characteristics of the image, and the ground sampling distance (GSD). The GSDs of the flights in this study were approximately 2.5 cm^2 for the St. Kilda flights, and 2.11 cm^2 for the Mason Bay flight. Therefore, the elevation recorded in one pixel will depend on the surface covered by the 2.5 cm^2 and 2.1 cm^2 cells. GSD is a function of flying height. Typically, the lower the altitude of the aircraft, the smaller the GSD. RPAS models will obtain different GSD at different altitudes, depending on the quality of the camera used.

The morphology of the vegetation photographed impacts the elevation model derived from the survey. Grass species such as *Ammophila arenaria* (marram grass), *Spinifex sericeus*, and a sedge, *Ficinia spiralis* (pingao), are dominant New Zealand foredune species. The grasses have thin blades, millimetres in width that lean (lodge) away from the prevailing wind. Hence, the elevation of a single blade will not be detected by a pixel with a GSD of 2.5 cm^2 or 2.1 cm^2, and the pixel will detect the elevation of the surface below. However, the lodging of blades can create a canopy with a larger surface area than an individual blade. Conversely, vegetation with wider leaves, larger surface areas, and uniform canopies, such as *Coprosma repens*, are prominent in DSMs. When leaf surface area is larger than the GSD, the elevation of the leaf surface will be recorded.

Coastal dunes typically have a variety of species present, for example, at St. Kilda beach, Dunedin, there are three main species – *A. arenaria, C. repens,* and *Lupins arboreus*. Different plant species vary in height (Figure 6.1), which may create different elevation offsets. For example, at St. Kilda, *A. arenaria* is typically < 0.5 m high. It tends to be dense of the lee slope of the foredune, and somewhat less dense on the stoss face (because of a history of recent scarping and recovery).

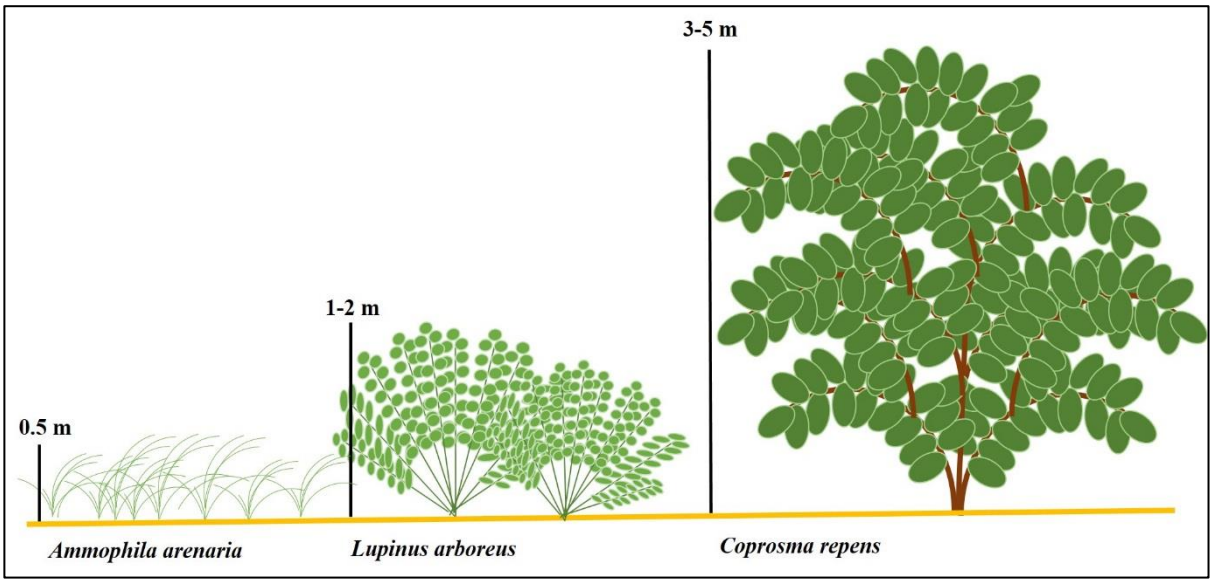

Figure 6.1: Conceptual diagram showing the differences in height and leaf characteristics of *A. arenaria, L. arboreus* and *C. repens*.

Dense *A. arenaria* can cause elevation offsets over larger areas, for example, the dense distribution over the Mason Bay foredune. Conversely, *C. repens* grows as isolated shrubs to a height of approximately 5 m high. Individual *C. repens* can be easily identified in the DSM (Figure 6.2). Therefore, not only does the elevation offset vary between species (due to their leaf characteristics), but it also varies depending on the density of individual plants.

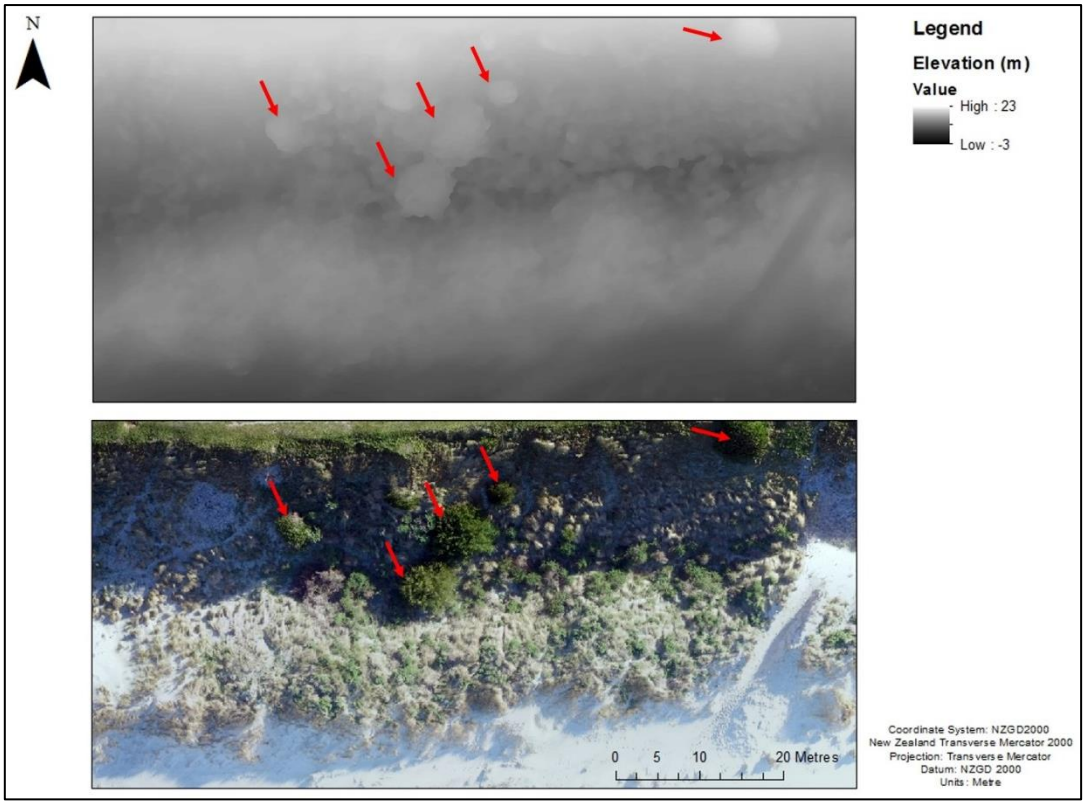

Figure 6.2: Individual *C.repens* visible in the RPAS DSM.

There is considerable variability in the botany of foredunes in New Zealand. The current study has focused on two southern New Zealand coastal dunes – St. Kilda, Dunedin and Mason Bay, Stewart Island (West Coast), which both have foredunes dominated by *A. arenaria*. In contrast, Kokota Spit, located at the very top of the North Island, is dominated by *F. spiralis*. At this site *F. spiralis* forms a relatively patchy cover. The total cover of vegetation is less dense and the height of the canopy is more variable compared to the *A. arenaria* cover at St. Kilda and Mason Bay. The blades of *F. spiralis* are thicker than *A. arenaria*, and are golden in colour. *F. spiralis* forms small coppice dunes throughout the Kokota dune system by trapping sand and extending rhizomes down the face of each coppice dune, which have a convex profile. The Pouto dune system stretches along the West Coast of the Pouto Peninsula on Kaipara harbour, Northland, and is dominated by *S. sericeus*, a native New Zealand dune grass. *S. sericeus* is more erect than *A. arenaria*. *F. spiralis* and *S. sericeus* do not grow as high as *A. arenaria*, and create a sparser cover (Figure 6.3).

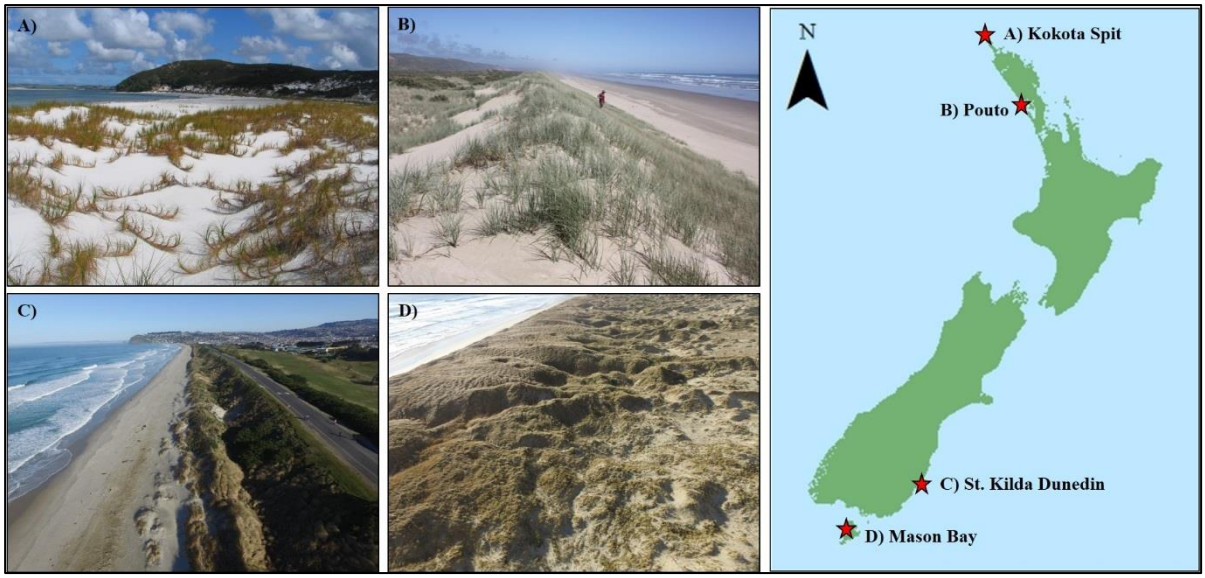

Figure 6.3 Dune vegetation at Kokota Spit, Pouto Peninsula, St. Kilda beach, and Mason Bay, New Zealand.

The vegetation cover of a dune system can be estimated using orthomosaics produced by low-cost RPAS. The current study used an unsupervised pixel reclassification to identify the 'vegetated' and 'non-vegetated' pixels in the orthomosaic. The vegetated pixels matched the pixels that presented an elevation offset. A similar method was used by Konlechner *et al.* (2015) with satellite imagery to quantify vegetation cover ('texture') over a dune system where *A. arenaria* was eradicated. The cover quantified using the reclassification can indicate the type of species present, for example dense cover over large areas is likely to be attributed to invasive species such as *A. arenaria*, whereas sparser covers are typically *F. spiralis* or *S. serius.*

The presence of a variety of species and vegetation densities may make it difficult to accurately survey dune morphology in some situations. The ideal situation would be a sparse, thin-leaved, grass-type cover, where the GSD is capable of surveying the ground. The morphology derived from RPAS surveying is offset by the presence of certain types of vegetation, however, simply removing the height of the vegetation will not produce an accurate DTM of the area (Section 5.4.2), because the elevation is not necessarily directly correlated with vegetation height. Shaad *et al.* (2016) and Yilmaz *et al.* (2016) have suggested ground filtering algorithms, whereby the pixels that correspond to the spectral properties of sand are used for the interpolation, which consequently produces a DTM. However, this does not work in densely vegetated areas, especially with a large GSD. In summary, the morphology derived from RPAS surveys is not always accurate over vegetated areas, depending on the type of vegetation present.

Producing accurate DSMs is important when the data is subsequently used to calculate morphologic change. In the current study, visible sand deposition occurred in the lee of the constructed notches at St. Kilda (Section 4.4.3). However, the deposition had a dampening effect on the *A.arenaria* and the gain in sediment was calculated as a loss. The morphologic change assessment, therefore, could not accurately quantify the amount of sediment deposited in the lee of the foredune. Therefore, low-cost RPAS is not suitable for quantifying small-scale changes when vegetation is present. In such cases, either a sensor capable of penetrating vegetation should be employed, or the elevation offset caused by the vegetation should be quantified.

It is difficult to definitively conclude the elevation offset caused by vegetation, due to the number of influential factors. However, the offset can be estimated based on the results from the current study. Disregarding the GSD and the spectral properties of the surface, the offset is a function of vegetation height and cover. The cover and average height of the vegetation at Kokota and Pouto mimic the 'variable' vegetation class in the current study. On average, the RPAS deviated from the surface by 10–20 cm, and the average vegetation height was approximately 19 cm. Hence, based on the average vegetation height, cover and density present on a foredune, the error associated with RPAS surveying can be estimated.

For many RPAS applications the effect of vegetation is likely to be insignificant. For example, a local authority may wish to determine the volume of sand eroded from a foredune by waves during a storm event. In such circumstances, the presence of vegetation is irrelevant due to the significant loss of sediment. The same applies for long-term changes (years) where the amount of morphologic change dominates the height of the vegetation. For quantifying small-scale changes, such as those exhibited in the current study, low-cost RPAS surveying is less accurate.

6.2.3 Remotely piloted aerial system coastal monitoring

The current study suggests low-cost RPAS surveying is a viable option for monitoring coastal dune systems. The accessibility and flexibility of this type of platform provides benefits over conventional coastal surveying methods. RPAS platforms, especially multirotor models, have the ability to access environments that may be difficult to traverse using ground-based methods such as total stations. Low-cost RPAS platforms are accessible, and can be purchased locally at a low-cost (<$10,000). This type of RPAS platform requires minimal background knowledge of surveying, which provides an opportunity for local authorities to employ this

type of method, as opposed to hiring specialist operators (Ivošević *et al.*, 2015). Low-cost RPAS surveying is ideal for long-term coastal monitoring, because surveys can be easily repeated, given an appropriate GCP network has been established. The survey repeatability is also desirable for quantifying event-scale changes at short-notice.

One of the greatest advantages of the RPAS method over conventional coastal surveying methods is the ability to capture photographs. Obtaining a time series of photographs (both vertical and oblique) can be beneficial for coastal monitoring, as it provides a snapshot of the state of the environment at certain periods in time. Photographs are a useful tool for understanding the coastal processes that have, and are, occurring in that environment. Low-altitude photography enables a unique perspective of the area of interest. Deriving DSMs and orthomosaics of coastal areas incrementally overtime can help identify long-term morphologic trends and the visible changes in the dune system. This type of monitoring could help local authorities identify patterns of change, enable a better understanding of the coastline, and ultimately give insight into future changes.

The biggest disadvantages with employing low-cost RPAS (RGB) technology is the inability to survey through vegetation. This is beneficial in situations where vegetation mapping of the coastal landscape is required, because vegetation type and distribution can be depicted in the imagery. However, when dune morphology is quantified, the elevation is offset by vegetation. New Zealand coastal dune systems typically exhibit a variety of vegetation species, with different structural characteristics and densities. This type of environment can create a complex surface. In such environments, employing sensors such as LiDAR, may be beneficial. Certain LiDAR sensors, such as the Yellow Scan Mapper LiDAR, have the ability to penetrate vegetation, and survey the ground elevation. This type of sensor is typically purchased separately to the aircraft itself. However, non-RGB sensors are typically more expensive, which increases the total price of the survey.

6.2.4 Future remotely piloted aerial system developments

RPAS has been constantly developing over the last decade, and platforms are now highly accessible and inexpensive. Although this technology provides a range of benefits for coastal and environmental monitoring, some aspects could be developed further. Firstly, low-cost RPAS tend to have a short battery life, typically with a capacity of < 1 hour, and in many cases less than 30 minutes. Consequently, the area surveyed in one flight is minimized. This is especially problematic in environments (such as the coast) that are typically windy and in

remote areas when there is a small surveying timeframe. However, compared to total station or RTK-GPS methods, an RPAS can survey large areas rapidly. As RPAS technology evolves, the battery life is likely to increase.

Further development is needed to improve the performance of low-cost RPAS in wind and precipitation. The ability for RPAS to stabilise in windy conditions is especially important for coastal surveys, which are commonly windy environments. Low-cost RPAS are capable of flying in wind speeds up to 10 ms^{-1}, however, such conditions are unlikely to permit aerial photography due to the limited battery power. RPAS performance during precipitation events can also be improved. Photographs are undesirable in heavy precipitation, however, surveys could occur in light precipitation/drizzle if the exterior of low-cost RPAS were more robust (specifically multirotor models).

Lastly, enhancing the ability of sensors on low-cost RPAS to survey through vegetation will be beneficial. LiDAR may be employed instead of RGB sensors, however, this increases the price of the survey. Ground filtering algorithms can be employed where there is ample ground visible, but not in areas with dense vegetation.

6.3 Concluding remarks

This study found that coastal dune systems can be efficiently and accurately surveyed with low-cost RPAS, especially when flight planning software is utilized. However, the systematic errors that are un-modelled by modern photogrammetry need to be understood by RPAS users, to produce accurate photogrammetric models. To avoid the propagation of systematic errors into the photogrammetric model, a GCP configuration needs to be established over the study site, and any surface outside of the GCP perimeter should not be deemed reliable for subsequent morphologic analysis.

RPAS surveying is restricted by the presence of vegetation when an RGB sensor is employed. Low-cost RPAS is only capable of quantifying small-scale morphologic changes when there is a bare surface or sparse vegetation. The elevation offset caused by vegetation presence cannot be fully described by vegetation height, hence, an understanding of the relationship between the GSD, the spectral properties of the surface, vegetation cover/density, and vegetation type is required. The impact of vegetation is insignificant when large-scale changes in morphology occur, such as foredune scarping or long-term accretion.

Low-cost RPAS have the potential to be employed by local authorities for monitoring coastal dunes. Low-cost RPAS technology is accessible, flexible, largely automated, inexpensive, and provides both elevation data and high-detail aerial photography. It is expected that this technology will continue to evolve, and models that can withstand greater wind speeds and precipitation, and have a greater battery capacity, will be developed. The influence of vegetation cover in RPAS derived DSMs needs to be addressed further, however, sensors capable of penetrating vegetation are becoming more accessible for use on multiple RPAS platforms.

References

Aber, J. S., Marzolff, I. & Ries, J. B. (2010a). Introduction to Small-Format Aerial Photography, Chapter 1. *In:* James S. Aber, Marzolff, Irene., Ries, Johannes B. (ed.) *Small-Format Aerial Photography.* Amsterdam: Elsevier.

Aber, J. S., Marzolff, I. & Ries, J. B. (2010b). Lighting and Atmospheric Conditions, Chapter 4. *In:* James S. Aber, Marzolff, Irene., Ries, Johannes B. (ed.) *Small-Format Aerial Photography.* Amsterdam: Elsevier.

Aber, J. S., Marzolff, I. & Ries, J. B. (2010c). Platforms for Small-Format Aerial Photography, Chapter 8. *In:* James S. Aber, Marzolff, Irene., Ries, Johannes B. (ed.) *Small-Format Aerial Photography.* Amsterdam: Elsevier.

Andrews, B., Gares, P. A. & Colby, J. D. (2002). Techniques for GIS modeling of coastal dunes. *Geomorphology,* 48**,** 289-308.

Arbogast, A. F., Shortridge, A. M. & Bigsby, M. E. (2009). Volumetric Estimates of Coastal Sand Dunes in Lower Michigan: Explaining The Geography of Dune Fields. *Physical Geography,* 30**,** 479-500.

Armaroli, C., Grottoli, E., Harley, M. D. & Ciavola, P. (2013). Beach morphodynamics and types of foredune erosion generated by storms along the Emilia-Romagna coastline, Italy. *Geomorphology,* 199**,** 22-35.

Baily, B., Collier, P., Farres, P., Inkpen, R. & Pearson, A. (2003). Comparative assessment of analytical and digital photogrammetric methods in the construction of DEMs of geomorphological forms. *Earth Surface Processes and Landforms,* 28**,** 307-320.

Bangen, S. G., Wheaton, J. M., Bouwes, N., Bouwes, B. & Jordan, C. (2014). A methodological intercomparison of topographic survey techniques for characterizing wadeable streams and rivers. *Geomorphology,* 206**,** 343-361.

Baptista, P., Cunha, T., Matias, A., Gama, C., Bernardes, C. & Ferreira, Ó. (2011). New land-based method for surveying sandy shores and extracting DEMs: the INSHORE system. *Environmental Monitoring and Assessment,* 182**,** 243-257.

Barry, P. & Coakley, R. (2013). Field accuracy test of RPAS photogrammetry. *International Archives of the Photogrammetry, Remote Sensing and Spatial Information Sciences,* 40**,** 1.

Benavente, J., del Río, L., Plomaritis, T. A. & Menapace, W. (2013). Impact of coastal storms in a sandy barrier (Sancti Petri, Spain). *Journal of Coastal Research,* 1**,** 666-671.

Berni, J. A. J., Zarco-Tejada, P. J., Suarez, L. & Fereres, E. (2009). Thermal and Narrowband Multispectral Remote Sensing for Vegetation Monitoring From an Unmanned Aerial Vehicle. *IEEE Transactions on Geoscience and Remote Sensing,* 47**,** 722-738.

Bhattacharya, A., Arora, M. & Sharma, M. (2013). Usefulness of adaptive filtering for improved Digital Elevation Model generation. *Journal of the Geological Society of India,* 82**,** 153-161.

Bochev-van der Burgh, L. M., Wijnberg, K. M. & Hulscher, S. J. M. H. (2011). Decadal-scale morphologic variability of managed coastal dunes. *Coastal Engineering,* 58**,** 927-936.

Brovelli, M. A., Crespi, M., Fratarcangeli, F., Giannone, F. & Realini, E. Accuracy assessment of high resolution satellite imagery by leave-one-out method. Proceedings of the 7th International Symposium on Spatial Accuracy Assessment in Natural Resources and Environmental Sciences, 2006. Citeseer, 533-542.

Brown, D. C. (1966). Decentering distortion of lenses. *Photometric Engineering,* 32**,** 444-462.

CAA (2015). Part 101 CAA Consolidation. *In:* Civil Aviation Authority of New Zealand (ed.).

CAA (2016). The Air Navigation Order 2016 and Regulations. *In:* Civil Aviation Authority of the United Kingdom (ed.).

CASA (2002). Advisory Circular - Unmanned Aircraft and Rockets. *In:* Civil Aviation Safety Authority Australia (ed.). Civil Aviation Safety Authority Australia.

Casella, E., Rovere, A., Pedroncini, A., Mucerino, L., Casella, M., Cusati, L. A., Vacchi, M., Ferrari, M. & Firpo, M. (2014). Study of wave runup using numerical models and low-altitude aerial photogrammetry: A tool for coastal management. *Estuarine, Coastal and Shelf Science,* 149**,** 160-167.

Castelle, B., Le Corre, Y. & Tomlinson, R. (2008). Can the gold coast beaches withstand extreme events? *Geo-Marine Letters,* 28**,** 23-30.

Chari, V. & Veeraraghavan, A. (2014). Lens Distortion, Radial Distortion. *In:* Katsushi Ikeuchi (ed.) *Computer Vision: A Reference Guide.* Boston, MA: Springer US.

Colomina, I. & Molina, P. (2014). Unmanned aerial systems for photogrammetry and remote sensing: A review. *ISPRS Journal of Photogrammetry and Remote Sensing,* 92**,** 79-97.

Dandois, J. P. & Ellis, E. C. (2010). Remote Sensing of Vegetation Structure Using Computer Vision. *Remote Sensing,* 2**,** 1157.

Danzi, M., Di Crescenzo, G., Ramondini, M. & Santo, A. (2012). Use of unmanned aerial vehicles (UAVs) for photogrammetric surveys in rockfall instability studies.

Darwin, N., Ahmad, A. & Zainon, O. (2014). The Potential of Unmanned Aerial Vehicle for Large Scale Mapping of Coastal Area. *IOP Conference Series: Earth and Environmental Science,* 18**,** 012031.

Delacourt, C., Allemand, P., Jaud, M., Grandjean, P., Deschamps, A., Ammann, J., Cuq, V. & Suanez, S. (2009). DRELIO: An Unmanned Helicopter for Imaging Coastal Areas. *Journal of Coastal Research***,** 1489-1493.

Diefenbach, A., Crider, J., Schilling, S. & Dzurisin, D. (2012). Rapid, low-cost photogrammetry to monitor volcanic eruptions: an example from Mount St. Helens, Washington, USA. *Bulletin of Volcanology,* 74**,** 579-587.

Dissanayake, P., Brown, J., Wisse, P. & Karunarathna, H. (2015). Effects of storm clustering on beach/dune evolution. *Marine Geology,* 370**,** 63-75.

DJI (2015). Phantom 3 Advanced User Manual.

DJI (2016a). Mavic Pro User Manual.

DJI (2016b). Phantom 4 User Manual.

Dufour, S., Bernez, I., Betbeder, J., Corgne, S., Hubert-Moy, L., Nabucet, J., Rapinel, S., Sawtschuk, J. & Trollé, C. (2013). Monitoring restored riparian vegetation: how can recent developments in remote sensing sciences help? *Knowl. Managt. Aquatic Ecosyst.***,** 10.

Eamer, J. B. R. & Walker, I. J. (2013). Quantifying spatial and temporal trends in beach–dune volumetric changes using spatial statistics. *Geomorphology,* 191**,** 94-108.

Egels, Y. & Kasser, M. (2003). *Digital photogrammetry,* CRC Press.

El-Ashmawy, K. L. A. (2015). A comparison between analytical aerial photogrammetry, laser scanning, total station and global positioning system surveys for generation of digital terrain model. *Geocarto International,* 30**,** 154-162.

Eltner, A., Kaiser, A., Castillo, C., Rock, G., Neugirg, F. & Abellan, A. (2016). Image-based surface reconstruction in geomorphometry - merits, limits and developments. *Earth Surface Dynamics,* 4**,** 359-389.

Everaerts, J. Unmanned aerial vehicles for photogrammetry and remote sensing. Advances in Photogrammetry, Remote Sensing and Spatial Information Sciences: 2008 ISPRS Congress Book, 2008. CRC Press, 117.

FAA, U. (2016). Summary of small unmanned aircraft rule (Part 107). *In:* Federal Aviation Administration (ed.). Washington, DC: Federal Aviation Administration.

Feagin, R. A., Williams, A. M., Popescu, S., Stukey, J. & Washington-Allen, R. A. (2014). The Use of Terrestrial Laser Scanning (TLS) in Dune Ecosystems: The Lessons Learned. *Journal of Coastal Research,* 30**,** 111-119.

Fisher, P. F. & Tate, N. J. (2006). Causes and consequences of error in digital elevation models. *Progress in Physical Geography,* 30**,** 467-489.

Fraser, R. H., Olthof, I., Lantz, T. C. & Schmitt, C. (2016). UAV photogrammetry for mapping vegetation in the low-Arctic. *Arctic Science,* 2**,** 79-102.

Fryer, J. G. & Brown, D. C. (1986). Lens distortion for close-range photogrammetry. *Photogrammetric engineering and remote sensing,* 52**,** 51-58.

Gallant, D. (2014). Supervised Image Classification. Nova Scotia: Centre of Geographic Sciences.

Gallay, M., Lloyd, C. D., McKinley, J. & Barry, L. (2013). Assessing modern ground survey methods and airborne laser scanning for digital terrain modelling: A case study from the Lake District, England. *Computers & Geosciences,* 51**,** 216-227.

Gares, P. A. & Nordstrom, K. F. (1995). A Cyclic Model of Foredune Blowout Evolution for a Leeward Coast: Island Beach, New Jersey. *Annals of the Association of American Geographers,* 85**,** 1-20.

Gerke, M. & Przybilla, H.-J. (2016). Accuracy Analysis of Photogrammetric UAV Image Blocks: Influence of Onboard RTK-GNSS and Cross Flight Patterns. *Photogrammetrie-Fernerkundung-Geoinformation,* 2016**,** 17-30.

Gonçalves, J. A. & Henriques, R. (2015). UAV photogrammetry for topographic monitoring of coastal areas. *ISPRS Journal of Photogrammetry and Remote Sensing,* 104**,** 101-111.

Gorte, B. (1999). Supervised image classification. *Spatial statistics for remote sensing.* Springer.

Han, S., Gui, Q., Li, G. & Du, Y. (2014). Minimum of PDOP and its applications in inter-satellite links (ISL) establishment of Walker-δ constellation. *Advances in Space Research,* 54**,** 726-733.

Harley, M. D., Turner, I. L., Short, A. D. & Ranasinghe, R. (2011). Assessment and integration of conventional, RTK-GPS and image-derived beach survey methods for daily to decadal coastal monitoring. *Coastal Engineering,* 58**,** 194-205.

Harwin, S. & Lucieer, A. (2012). Assessing the Accuracy of Georeferenced Point Clouds Produced via Multi-View Stereopsis from Unmanned Aerial Vehicle (UAV) Imagery. *Remote Sensing,* 4**,** 1573.

Hesp, P. (2002). Foredunes and blowouts: initiation, geomorphology and dynamics. *Geomorphology,* 48**,** 245-268.

Higgins, L. S. (1933). Coastal Changes in South Wales—The Excavation of an Old Beach.

High, R. (2006). Smart surveying. *International Construction,* 45**,** 51-56.

Hilary, F. S., Asbury, H. S., Jr., Jeffrey, H. L. & Rob, A. H. (2002). Estimation of Shoreline Position and Change Using Airborne Topographic Lidar Data. *Journal of Coastal Research,* 18**,** 502-513.

Hilton, M. (2010). The Geomorphology of the Ocean Beach Dune System–Implications for Future Management of Ocean Beach Domain.

Hilton, M., Duncan, M. & Jul, A. (2005). Processes of Ammophila arenaria (Marram Grass) Invasion and Indigenous Species Displacement, Stewart Island, New Zealand. *Journal of Coastal Research,* 21**,** 175-185.

Hilton, M. J., Hatcher, S. V., Wakes, S. J. & Konlechner, T. M. (2016). Flow Deflection and Deceleration Across a Simple Foredune. *Journal of Coastal Research***,** 293-297.

Hilton, M. J. & Konlechner, T. M. A review of the marram grass eradication program (1999–2009), Stewart Island, New Zealand. Proceedings, the New Zealand plant protection society inc. and the council of Australasian weed societies Inc.—17th Australasian weeds conference, 2010. 26-30.

Hugenholtz, C. H., Whitehead, K., Brown, O. W., Barchyn, T. E., Moorman, B. J., LeClair, A., Riddell, K. & Hamilton, T. (2013). Geomorphological mapping with a small unmanned aircraft system (sUAS): Feature detection and accuracy assessment of a photogrammetrically-derived digital terrain model. *Geomorphology,* 194**,** 16-24.

Hugenholtz, C. H., Wolfe, S. A. & Moorman, B. J. (2008). Effects of sand supply on the morphodynamics and stratigraphy of active parabolic dunes, Bigstick Sand Hills, southwestern Saskatchewan. *Canadian Journal of Earth Sciences,* 45**,** 321-335.

Ierodiaconou, D., Schimel, A. C. & Kennedy, D. M. (2016). A new perspective of storm bite on sandy beaches using Unmanned Aerial Vehicles. *Zeitschrift für Geomorphologie, Supplementary Issues*.

Ivošević, B., Han, Y.-G., Cho, Y. & Kwon, O. (2015). The use of conservation drones in ecology and wildlife research.

Kaneko, K. & Nohara, S. (2014). Review of Effective Vegetation Mapping Using the UAV (Unmanned Aerial Vehicle) Method. *Journal of Geographic Information System,* Vol.06No.06**,** 10.

Kidson, C., Collin, R. L. & Chisholm, N. W. T. (1989). Surveying a Major Dune System: Braunton Burrows, North-West Devon. *The Geographical Journal,* 155**,** 94-105.

Klemas, V. V. (2015). Coastal and Environmental Remote Sensing from Unmanned Aerial Vehicles: An Overview. *Journal of Coastal Research,* 31**,** 1260-1267.

Konlechner, T. M., Buckley, E. E. C. B., Hilton, M. J. & Wakes, S. J. (2016). Downwind dune dynamics following Ammophila arenaria invasion. *Journal of Coastal Research,* 75**,** 298-302.

Konlechner, T. M., Ryu, W., Hilton, M. J. & Sherman, D. J. (2015). Evolution of foredune texture following dynamic restoration, Doughboy Bay, Stewart Island, New Zealand. *Aeolian Research,* 19, Part B**,** 203-214.

Langley, R. B. (1998). Rtk gps. *GPS World,* 9**,** 70-76.

Lee, J.-M., Park, J.-Y. & Choi, J.-Y. (2013). Evaluation of Sub-aerial Topographic Surveying Techniques Using Total Station and RTK-GPS for Applications in Macrotidal Sand Beach Environment. *Journal of Coastal Research***,** 535-540.

Lemmon, T. R. & Gerdan, G. P. (1999). The Influence of the Number of Satellites on the Accuracy of RTK GPS Positions. *Australian Surveyor,* 44**,** 64-70.

Levin, N., Ben-Dor, E. & Karnieli, A. (2004). Topographic information of sand dunes as extracted from shading effects using Landsat images. *Remote Sensing of Environment,* 90**,** 190-209.

Li, J. & Heap, A. D. (2008). A review of spatial interpolation methods for environmental scientists.

Li, R., Di, K. & Ma, R. (2003). 3-D Shoreline Extraction from IKONOS Satellite Imagery. *Marine Geodesy,* 26**,** 107-115.

Li, W., Niu, Z., Chen, H., Li, D., Wu, M. & Zhao, W. (2016). Remote estimation of canopy height and aboveground biomass of maize using high-resolution stereo images from a low-cost unmanned aerial vehicle system. *Ecological Indicators,* 67**,** 637-648.

Linder, W. (2009). *Digital photogrammetry*, Springer.

Lisle, R. J. (2006). Google Earth: a new geological resource. *Geology Today,* 22**,** 29-32.

Liu, X. (2011). Accuracy Assessment of Lidar Elevation Data Using Survey Marks. *Survey Review,* 43**,** 80-93.

Mancini, F., Dubbini, M., Gattelli, M., Stecchi, F., Fabbri, S. & Gabbianelli, G. (2013). Using Unmanned Aerial Vehicles (UAV) for High-Resolution Reconstruction of Topography: The Structure from Motion Approach on Coastal Environments. *Remote Sensing,* 5**,** 6880-6898.

Martinez, M. L., Gallego-Fernandez, J. B., Garcia-Franco, J. G., Moctezuma, C. & Jimenez, C. D. (2006). Assessment of coastal dune vulnerability to natural and anthropogenic disturbances along the Gulf of Mexico. *Environmental Conservation,* 33**,** 109-117.

Mathew, S., Davidson-Arnott, R. G. D. & Ollerhead, J. (2010). Evolution of a beach–dune system following a catastrophic storm overwash event: Greenwich Dunes, Prince Edward Island, 1936–2005. *Canadian Journal of Earth Sciences,* 47**,** 273-290.

McConachie, M. (2015). *Random forest learning-based classification of ultra-high resolution imagery of coastal dunes at Mason Bay, Stewart Island.* Master of Applied Science, University of Otago.

Mikhail, E. M., Bethel, J. S. & McGlone, J. C. (2001). *Introduction to Modern Photogrammetry*, John Wiley & Sons Australia, Limited.

Morton, R. A., Mark, P. L., Jeffrey, G. P. & Michael, A. C. (1993). Monitoring Beach Changes Using GPS Surveying Techniques. *Journal of Coastal Research,* 9**,** 702-720.

Nagihara, S., Mulligan, K. R. & Xiong, W. (2004). Use of a three-dimensional laser scanner to digitally capture the topography of sand dunes in high spatial resolution. *Earth Surface Processes and Landforms,* 29**,** 391-398.

Nelson, A., Reuter, H. I. & Gessler, P. (2009). Chapter 3 DEM Production Methods and Sources. *In:* Hengl Tomislav & I. Reuter Hannes (eds.) *Developments in Soil Science.* Elsevier.

Nex, F. & Remondino, F. (2014). UAV for 3D mapping applications: a review. *Applied Geomatics,* 6**,** 1-15.

Noernberg, M. A., Fournier, J., Dubois, S. & Populus, J. (2010). Using airborne laser altimetry to estimate Sabellaria alveolata (Polychaeta: Sabellariidae) reefs volume in tidal flat environments. *Estuarine, Coastal and Shelf Science,* 90**,** 93-102.

O'Shea, M. & Murphy, J. (2013). Predicting and Monitoring the Evolution of a Coastal Barrier Dune System Postbreaching. *Journal of Coastal Research,* 38-50.

Omran, M. G., Engelbrecht, A. P. & Salman, A. Differential evolution methods for unsupervised image classification. 2005 IEEE Congress on Evolutionary Computation, 2005. IEEE, 966-973.

Papakonstantinou, A., Topouzelis, K. & Pavlogeorgatos, G. (2016). Coastline Zones Identification and 3D Coastal Mapping Using UAV Spatial Data. *ISPRS International Journal of Geo-Information,* 5**,** 75.

Pardo-Pascual, J. E., Garc, xed, a-Asenjo, L., Palomar, V., xe, zquez, J. & Garrigues-Talens, P. (2005). New Methods and Tools to analyze beach-dune system evolution using a Real-Time Kinematic Global Positioning System and Geographic Information Systems. *Journal of Coastal Research,* 34-39.

Park, H., Salah, M. & Lim, S. (2011). Accuracy of 3D models derived from aerial laser scanning and aerial ortho-imagery. *Survey Review,* 43**,** 109-122.

Pereira, E., Bencatel, R., Correia, J., xe, lix, L., Gon, xe, alves, G., Morgado, J. & Sousa, J. (2009). Unmanned Air Vehicles for Coastal and Environmental Research. *Journal of Coastal Research,* 1557-1561.

Pix4D (2016). Pix4D Mapper User Manual. Lausanne, Switzerland: Pix4D.

Psuty, N. P. (1993). Foredune morphology and sediment budget, Perdido Key, Florida, USA. *Geological Society, London, Special Publications,* 72**,** 145-157.

Reid, A., Ramos, F. & Sukkarieh, S. Multi-class classification of vegetation in natural environments using an Unmanned Aerial system. Robotics and Automation (ICRA), 2011 IEEE International Conference on, 9-13 May 2011 2011. 2953-2959.

Remondino, F., Barazzetti, L., Nex, F., Scaioni, M. & Sarazzi, D. (2011). UAV photogrammetry for mapping and 3d modeling–current status and future perspectives. *International Archives of the Photogrammetry, Remote Sensing and Spatial Information Sciences,* 38**,** C22.

Rozé, F. & Lemauviel, S. (2004). Sand Dune Restoration in North Brittany, France: A 10-Year Monitoring Study. *Restoration Ecology,* 12**,** 29-35.

Sallenger, A. H., Krabill, W., Brock, J., Swift, R., Jansen, M., Manizade, S., Richmond, B., Hampton, M. & Eslinger, D. (1999). Airborne laser study quantifies El Ni˜ o-induced Coastal Change. *EOS, Transactions American Geophysical Union,* 80**,** 89-92.

Sanz-Ablanedo, E., Chandler, J. H. & Wackrow, R. (2012). Parameterising internal camera geometry with focusing distance. *The Photogrammetric Record,* 27**,** 210-226.

Saye, S. E., van der Wal, D., Pye, K. & Blott, S. J. (2005). Beach–dune morphological relationships and erosion/accretion: An investigation at five sites in England and Wales using LIDAR data. *Geomorphology,* 72**,** 128-155.

Scarelli, F. M., Cantelli, L., Barboza, E. G., Rosa, M. L. C. C. & Gabbianelli, G. (2016). Natural and Anthropogenic Coastal System Comparison Using DSM from a Low Cost UAV Survey (Capão Novo, RS/Brazil). *Journal of Coastal Research,* 75**,** 1232-1236.

Schenk, T. (1999). *Digital photogrammetry: Vol. I: Background, fundamentals, automatic orientation produceres,* TerraScience.

Schiefer, E. & Gilbert, R. (2007). Reconstructing morphometric change in a proglacial landscape using historical aerial photography and automated DEM generation. *Geomorphology,* 88**,** 167-178.

Seeliger, U., Sar, V. C., Sar, P. L. O. & Marcus, S. (2000). Long-Term Changes of Coastal Foredunes in the Southwest Atlantic. *Journal of Coastal Research,* 16**,** 1068-1072.

Shaad, K., Ninsalam, Y., Padawangi, R. & Burlando, P. (2016). Towards high resolution and cost-effective terrain mapping for urban hydrodynamic modelling in densely settled river-corridors. *Sustainable Cities and Society*, 20**,** 168-179.

Sirguey, P., Boeuf, J., Cambridge, R. & Mills, S. (2016). Evidences of Sub-Optimal Photogrammetric Modelling In RPAS-based Aerial Surveys.

Sirguey, P. & Cullen, N. J. (2014). A Century of Photogrammetry on Kilimanjaro. *FIG Congress*. Kuala Lumpur, Malaysia.

Smith, R. K. & Bryan, K. R. (2007). Monitoring Beach Face Volume with a Combination of Intermittent Profiling and Video Imagery. *Journal of Coastal Research***,** 892-898.

Stewart, M. & Rizos, C. (2002). *GPS projects: Some planning issues*, Taylor & Francis, London and New York.

Tahar, K. N., Ahmad, A., Akib, W. & Mohd, W. Aerial mapping using autonomous fixed-wing unmanned aerial vehicle. Signal Processing and its Applications (CSPA), 2012 IEEE 8th International Colloquium on, 23-25 March 2012 2012. 164-168.

Taylor, E. B., Gibeaut, J. C., Yoskowitz, D. W. & Starek, M. J. (2015). Assessment and Monetary Valuation of the Storm Protection Function of Beaches and Foredunes on the Texas Coast. *Journal of Coastal Research,* 31**,** 1205-1216.

Teng, Y. & Wang, J. (2016). Some Remarks on PDOP and TDOP for Multi-GNSS Constellations. *The Journal of Navigation,* 69**,** 145-155.

Theuerkauf, E. J. & Rodriguez, A. B. (2012). Impacts of Transect Location and Variations in Along-Beach Morphology on Measuring Volume Change. *Journal of Coastal Research***,** 707-718.

Thom, B. & Hall, W. (1991). Behaviour of beach profiles during accretion and erosion dominated periods. *Earth Surface Processes and Landforms,* 16**,** 113-127.

Tomczak, M. (1998). Spatial interpolation and its uncertainty using automated anisotropic inverse distance weighting (IDW)-cross-validation/jackknife approach. *Journal of Geographic Information and Decision Analysis,* 2**,** 18-30.

Torres-Sánchez, J., Peña, J. M., de Castro, A. I. & López-Granados, F. (2014). Multi-temporal mapping of the vegetation fraction in early-season wheat fields using images from UAV. *Computers and Electronics in Agriculture,* 103**,** 104-113.

Toutin, T. & Chénier, R. GCP requirement for high resolution satellite mapping. Proceedings International Society for Photogrammetry and Remote Sensing Congress, Istanbul, 2004. 836-839.

Trimble (2004). Trimble R8 GNSS System Datasheet *In:* Trimble Navigation Limited (ed.).

Trimble (2012). Trimble TX5 3D Laser Scanner. California U.S.A: Trimble Navigation Limited.

Trimble (2013). Trimble Access Release Notes. California, U.S.A: Trimble Navigation Limited.

Turner, D., Lucieer, A. & Watson, C. Development of an Unmanned Aerial Vehicle (UAV) for hyper resolution vineyard mapping based on visible, multispectral, and thermal imagery. Proceedings of 34th International symposium on remote sensing of environment, 2011. 4.

Turner, I. L., Harley, M. D. & Drummond, C. D. (2016). UAVs for coastal surveying. *Coastal Engineering,* 114**,** 19-24.

Vousdoukas, M., Pennucci, G., Holman, R. & Conley, D. (2011). A semi automatic technique for Rapid Environmental Assessment in the coastal zone using Small Unmanned Aerial Vehicles (SUAV). *Journal of Coastal Research,* 64**,** 1755-1759.

Wallace, L., Lucieer, A., Malenovský, Z., Turner, D. & Vopěnka, P. (2016). Assessment of Forest Structure Using Two UAV Techniques: A Comparison of Airborne Laser Scanning and Structure from Motion (SfM) Point Clouds. *Forests,* 7**,** 62.

Wallace, L., Lucieer, A., Watson, C. & Turner, D. (2012). Development of a UAV-LiDAR System with Application to Forest Inventory. *Remote Sensing,* 4**,** 1519.

Weng, J., Cohen, P. & Herniou, M. (1992). Camera calibration with distortion models and accuracy evaluation. *IEEE Transactions on pattern analysis and machine intelligence,* 14**,** 965-980.

Whitehead, K. & Hugenholtz, C. H. (2014). Remote sensing of the environment with small unmanned aircraft systems (UASs), part 1: a review of progress and challenges. *Journal of Unmanned Vehicle Systems,* 02**,** 69-85.

Whitlow, R. (1986). Mapping erosion in Zimbabwe: a methodology for rapid survey using aerial photographs. *Applied Geography,* 6**,** 149-162.

Yang, J., Seo, D., Lim, H. & Choi, C. (2010). An analysis of coastal topography and land cover changes at Haeundae Beach, South Korea. *Acta Astronautica,* 67**,** 1280-1288.

Yilmaz, V., Konakoglu, B., Serifoglu, C., Gungor, O. & Gökalp, E. (2016). Image classification-based ground filtering of point clouds extracted from UAV-based aerial photos. *Geocarto International***,** 1-29.

You, Z. & Nielsen, P. (2013). Extreme Coastal Waves, Ocean Surges and Wave Runup. *Coastal Hazards.* Springer.

Yuneec (2015). Typhoon Q500 4K Instruction Manual.

Zhou, G. & Xie, M. (2009). Coastal 3-D Morphological Change Analysis Using LiDAR Series Data: A Case Study of Assateague Island National Seashore. *Journal of Coastal Research***,** 435-447.

Appendix A

St. Kilda digital surface models and orthomosaics

Appendix A contains the DSMs and orthomosaic images of the St. Kilda foredune for Flights Two, Three and Four produced from the RPAS. All of the elevation measurements are relative to mean sea level.

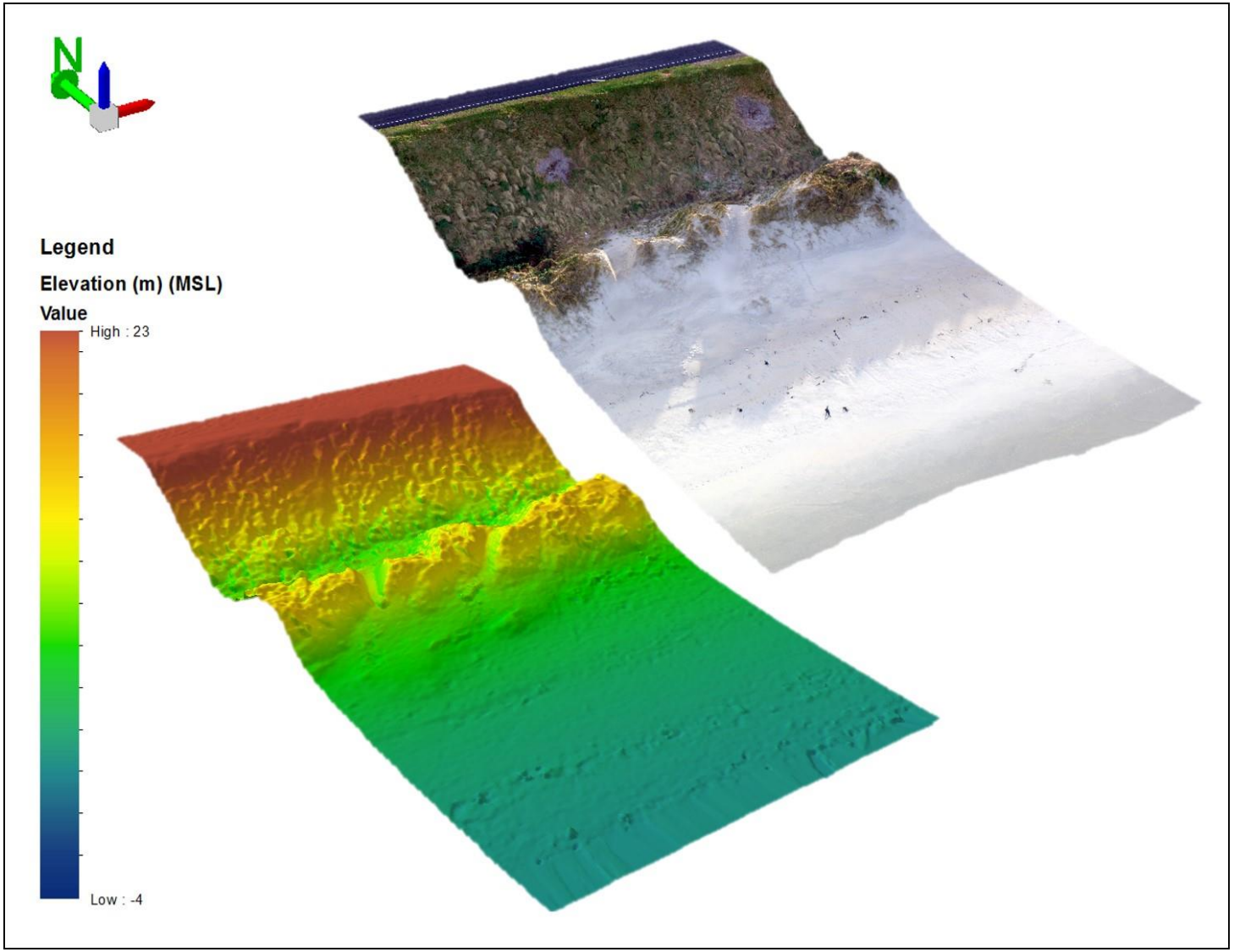

Figure A.1: DSM and orthomosaic of Area B, on the 24th of May, 2016.

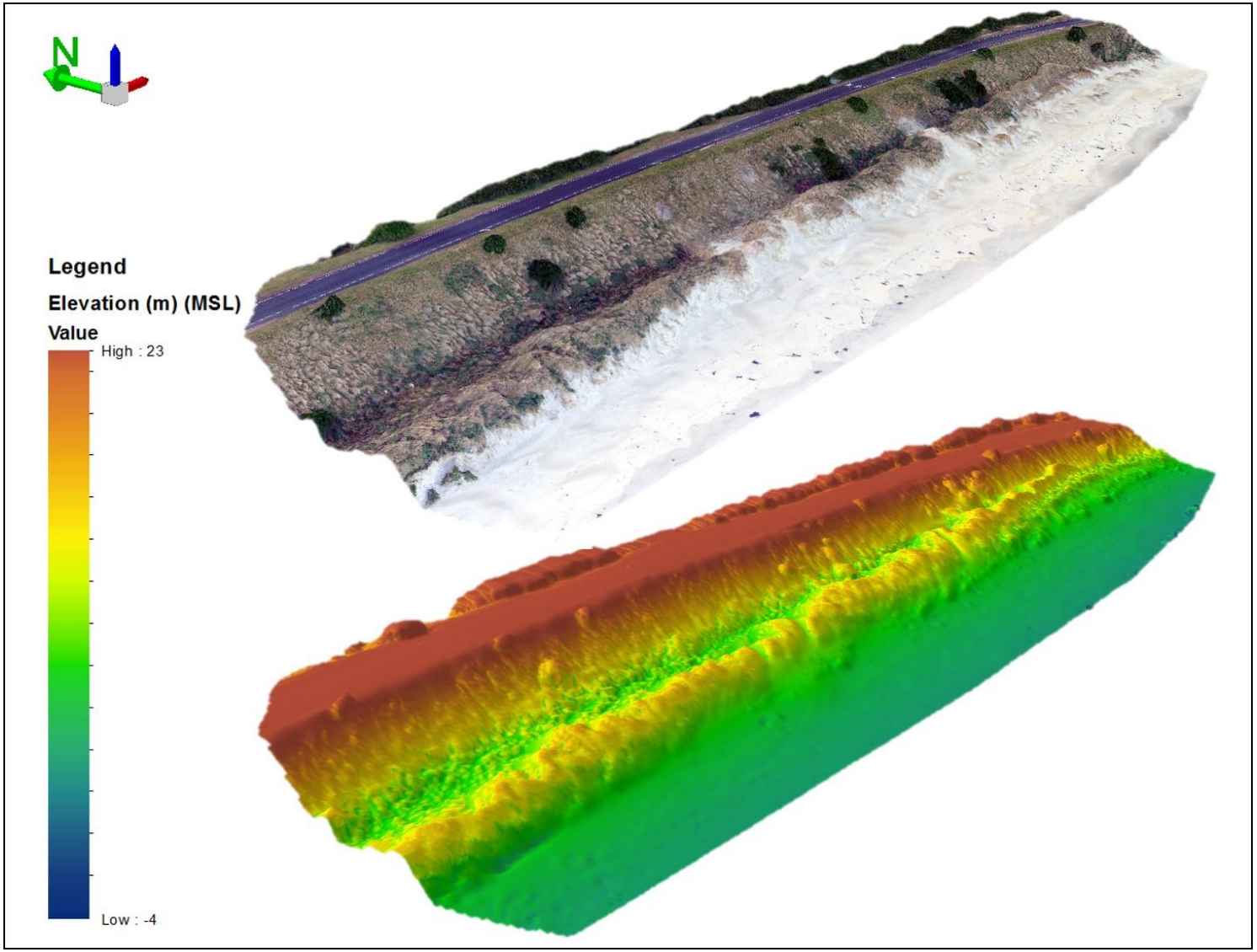

Figure A.2: DSM and orthomosaic of Area A, on the 14th of June, 2016.

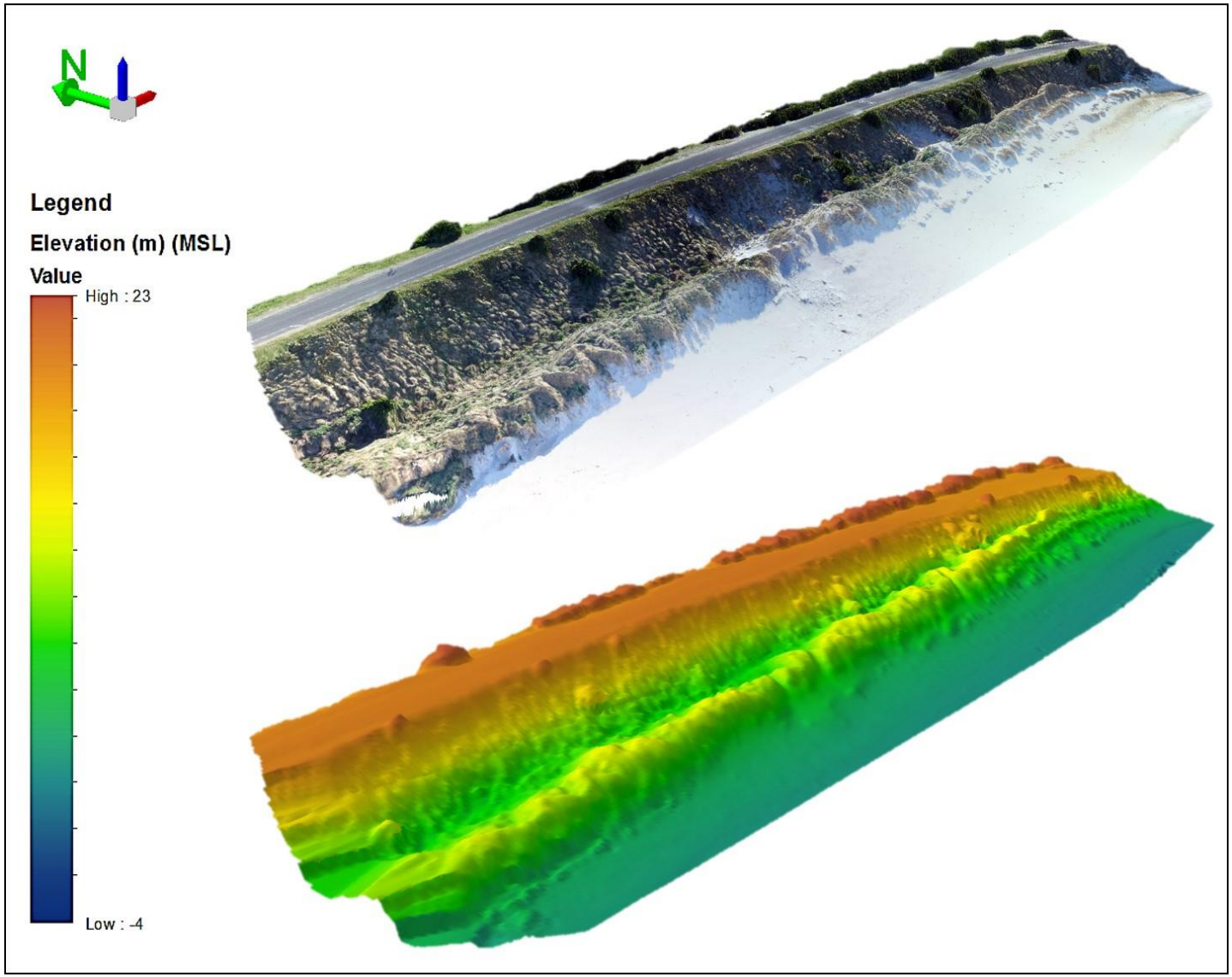

Figure A.3: DSM and orthomosaic of Area A, on the 10th of September, 2016.

Appendix B

Mason Bay digital surface model and orthomosaic

Appendix B contains the DSM and orthomosaic image of the Mason Bay produced from the RPAS, on September 1st, 2016. The elevation is relative to mean sea level.

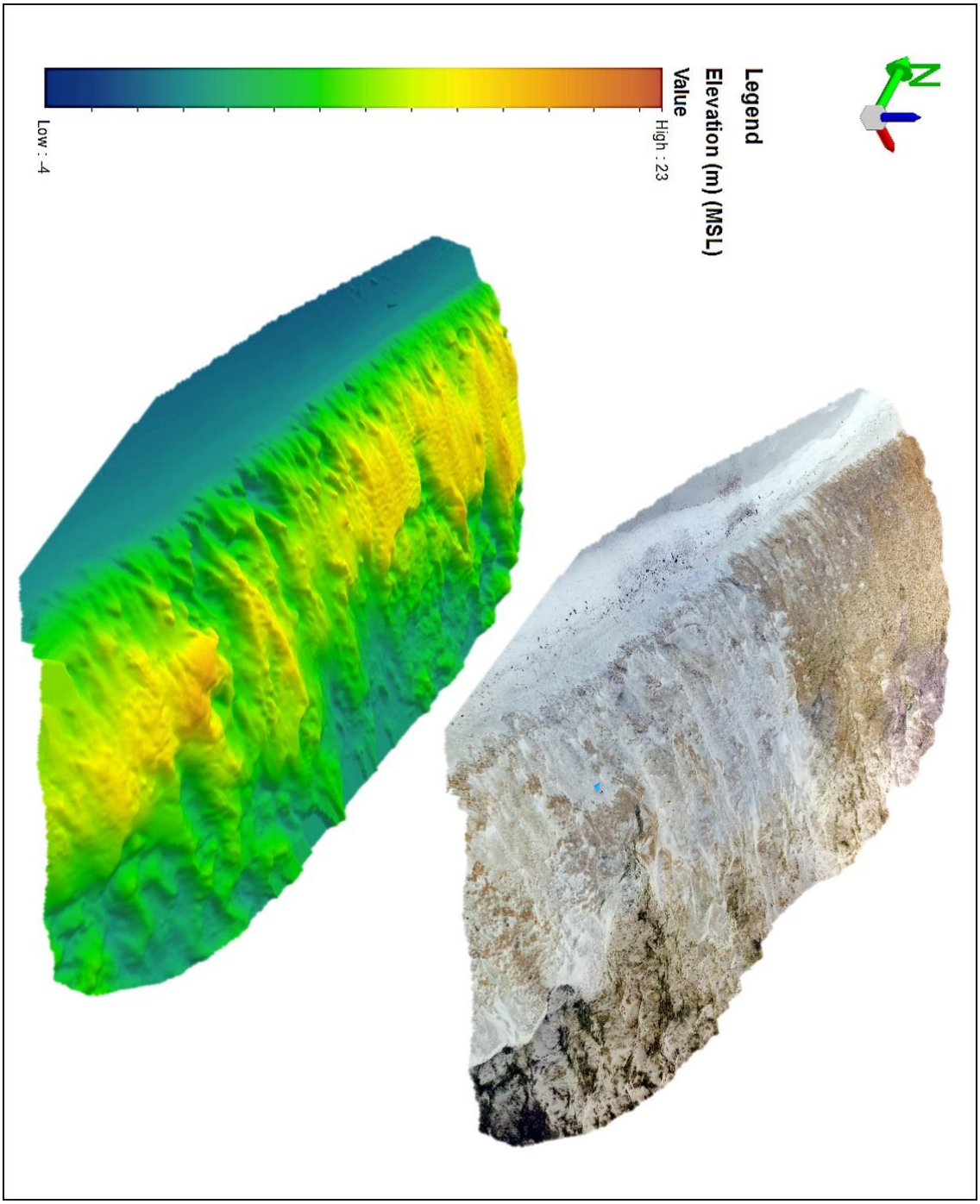

Figure B.1: DSM and orthomosaic of the Mason Bay foredune on the 1st of September, 2016.